Ghent University

Faculty of Engineering

Department of Flow, Heat and Combustion

Academic Year 2011-2012

Practical Application of Validated Computer Models for Fire Hazard Analysis in Nuclear Power Plants

Hernán Butafuoco

Promoter: Bart Merci

Master thesis submitted in the Erasmus Mundus Study Programme

International Master of Science in Fire Safety Engineering

DISCLAIMER

This thesis is submitted in partial fulfilment of the requirements for the degree of *The International Master of Science in Fire Safety Engineering (IMFSE)*. This thesis has never been submitted for any degree or examination to any other University/programme. The author(s) declare(s) that this thesis is original work except where stated. This declaration constitutes an assertion that full and accurate references and citations have been included for all material, directly included and indirectly contributing to the thesis.

This document may contain confidential information which falls under the restrictions set by the OECD PRISME project. Therefore, nothing may be made public in any way without the prior permission of the PRISME management board. The PRISME Management Board (MB) deliberated that the Project data be kept confidential for a period of three years following the completion of the Project. This would not preclude that publication of the main test results be made in e.g. conferences or technical literature during the course of the Project, as requested by several partners. These publications would however require the MB approval, which can be requested by e-mail via the NEA secretariat. In the frame of the PRISME agreement, Bel V and Tractebel Engineering are responsible for the project deliverables in Belgium. It is therefore strictly forbidden to publish, cite or make public in any way this document or any part thereof without the express written permission of Bel V and the MB. Under no circumstance this document may be communicated to or put at the disposal of third parties; photocopying or duplicating it in any other way is strictly prohibited. Disregarding the confidential nature of this document may cause irremediable damage.

The restrictions set above expire on the 1st of July 2014 as the PRISME project was ended in June 2011. Nevertheless, the PRISME MB can one-sided decide to alter this term. Further, the author gives permission to make this master dissertation available for consultation and to copy parts of this master dissertation for personal use. In the case of any other use, the restrictions set above have to be respected. In addition, the limitations of the copyright have to be respected, in particular with regard to the obligation to state expressly the source when quoting results from this master dissertation. The thesis supervisor must be informed when data or results are used.

Hernán Butafuoco

30th of April of 2012

Abstract

The increasing use of performance-based design makes the computer fire modelling a useful tool in fire safety engineering. This approach has started to be used in new field such as nuclear power plants. Since it is also a relatively new tool much investigation is required.

The objective of this master thesis is to simulate real fire scenarios of Nuclear Power Plants (NPP) in a reliable way. In order to achieve this goal, the thesis is separated into three sections: a comparison with experimental data part, a blind simulation part and the simulation of real scenarios.

In comparison with experimental data part, a test of the PRISME programme is simulated taking into account the most important variables that were measured during the test.

In the blind simulation part, a scenario of the NUREG-1824 is calculated and compared with the test.

In the last part, real configurations are assessed and the worst credible scenarios are simulated. A sensitivity analysis is performed to the most relevant variables in order to have an idea of the reliability of the solutions.

Contents

1. List of abbreviations

CFAST	Consolidated Model of Fire and Smoke Transport (NIST)
CFD	Computational Fluid Dynamics
DIVA	Dispositif Incendie, Ventilation et Aérocontamination (Research Device for Fire, Ventilation and Aero-contamination)
EBU	Eddy Break-up Model
EDM	Eddy Dissipation Model
FDS	Fire Dynamics Simulator (NIST)
FVM	Finite Volume Method
IRSN	Institut de Radioprotection et de Sûreté Nucléaire (France) (Institute for radioprotection and the nuclear safety)
ISIS	Incendie Simulé pour la Sûreté
INTI	Instituto Nacional de tecnología Industrial (Argentina) (National Institute of industrial technology)
NFPA	National Fire Protection Association (USA)
NIST	National Institute of Standards and Technology (USA)
NPP	Nuclear Power Plant
OC	Oxygen Concentration
PRISME	French acronym for “Fire Propagation in Elementary Multi-room Scenarios”
RTE	Radiative Transfer Equation
SFPE	Society of Fire Protection Engineers
SC	Species Concentration
THF	Total Heat Flux
TPH	Hydrogenated tetra-propylene
USNRC	United States Nuclear Regulatory Commission
V&V	Verification and Validation

2. List of tables and figures

3. Introduction & Objectives

The Performance-Based Design is more and more used in order to achieve better and/or more economical solutions in fire safety engineering. This approach requires reliable tools to solve the new challenges that it has to face. Fire modelling simulations have evolved from simple equations model for hand calculation or for spreadsheets, passing through zone modelling, to the Computational Fluid Dynamics (CFD) programs. The CFD programs solve a simplified form of the Navier-Stokes equations and have several sub-models (turbulence, combustion, etc) to calculate parts of the problem that cannot be resolved directly with the conservation equations. This makes the programs very complex. Because of the complexity of the model, the verification and validation of the software and the expertise of the user are required to reach reliable outcomes.

In the past, Nuclear Power Plants (NPPs) were built using prescriptive based design, in the area of fire safety, leading to conservative solutions. With the advance of the technology and the knowledge, the performance based design is gaining space within the fire safety assessment of NPPs. In this sense, the use of CFD software to assess different fire scenario in this field is growing and the importance of obtaining trustable results is even more significant.

The topic of this thesis was proposed by BEL V that is a subsidiary of the FANC (Federal Agency for Nuclear Control) who makes the regulatory controls in nuclear installations in Belgium. BELV conducts research in the area of fire modelling and was interesting in enhancing their knowledge in this area.

Several CFD programs are available for this purpose. The one that was chosen for performing this work is ISIS, a CFD code develop by IRSN ("Institute de Radioprotection et de Sûreté Nucléaire") [18]. ISIS is a Reynolds-Averaged Navier-Stokes (RANS) code that uses different physical models for solving the flow turbulence, combustion, soot production and heat transfers in order to calculate the development of a fire. One of the important features of this programme is its capability of computing fire scenarios in closed rooms with mechanical ventilation, like the ones that can be found commonly in NPPs.

The main objective of this thesis is to assess the fire safety in real scenarios of NPPs by means of validated fire simulation programs. The simulations of these scenarios have to be conducted in such a way that the results are trustable for taking action in order to improve fire safety. In order to achieve this objective, this work is divided in three parts:

- Validation of the software and the user by mean of a comparison between simulations and fire test;
- Validation of the user through a blind simulation;
- Assessment of real fire scenario.

Each stage has a different degree in complexity and a particular way of approaching the results. In all the stages the program selected for the simulations is ISIS.

4. Software description

4.1 Governing equations

There are several fire models ranging from simple one line equation model to complex computational models such as Computational Fluid Dynamics (CFD). CFD is a tool used to model the transport of mass and energy through solving the fundamental equations. The geometry is divided in small cell where these equations are applied. The fundamental equations solve by these models are:

- Conservation of mass;
- Conservation of momentum;
- Conservation of energy;
- Conservation of chemical species

The conservation of mass states that the rate of change of mass in a control volume (CV) is equal to the mass that enters the volume minus the mass that goes out of the volume. This is represented by the equation:

$$\frac{\partial \rho}{\partial t} + \nabla \cdot (\rho \vec{v}) = S_m$$

Where ρ is the density of the fluid, t is the time, $\vec{v}$ is the velocity in all the directions and S_m is the mass added to the continuous phase. The first term in the left hand side is the rate of change of mass within the fluid element in time and the second represents the difference between the mass that enters to the CV and the mass that goes out of the CV.

The conservation of momentum law states that the sums of the forces acting in a fluid element are equal to the rate of change of momentum. This law can be written as:

$$\frac{\partial \rho \vec{v}}{\partial t} + \nabla \cdot (\rho \vec{v} \vec{v}) = -\nabla p + \nabla \cdot (\bar{\bar{\tau}}) + \rho \vec{g} + \vec{F}$$

Where p is the static pressure, $\bar{\bar{\tau}}$ is the stress tensor, $\rho \vec{g}$ is the gravitational force and $\vec{F}$ is the external forces. The first term in the left part of the equation is the change of momentum with time and the second is the change of momentum in the space.

The conservation of energy states that the rate of change of energy within the control volume is equal to the net rate of heat added to the CV, plus the net rate of work done on the CV, plus the net rate of heat added by the source to the CV. This law in the enthalpy form is:

$$\frac{\partial (\rho h)}{\partial t} + \nabla \cdot (\rho h \vec{v}) = \nabla \cdot \left(\frac{k_t}{c_p} \right) + S_h$$

Where h is the enthalpy, k_t is the turbulent thermal conductivity; c_p is the specific heat and S_h is the source term. The enthalpy is defined as:

$$h = E + \frac{p}{\rho}$$

Where E is the internal energy.

The law of conservation of species states that the rate of change of species in the CV is equal to the net rate of species added to the CV plus the net rate of creation of species within the CV. This can be expressed with the convection diffusion equation for i-th species as:

$$\frac{(\rho Y_i)}{\partial t} + \nabla \cdot (\rho Y_i \vec{v}) = \nabla \cdot \vec{J}_i + S_i$$

Where Y_i is the local mass fraction of each specie, S_i is the net production of specie i and $\vec{J}_i$ is the diffusion of component i.

4.2 Reynolds-Averaged Navier-Stokes

The Reynolds-Average Navier-Stokes approach does not compute the turbulence of the fluid through the fundamental equations; it separates the fluctuating part and the mean part of variables and uses a model for solving the turbulence. This can be expressed as:

$$\phi = \overline{\phi} + \phi'$$

Where $\overline{\phi}$ represents the time average of the quantity ϕ and ϕ' the fluctuating part of this quantity. Reynolds average is not used by ISIS, it uses the Favre average or density-weighted average that produces simpler averaged governing equations. All the variables except the pressure and the density (averaged using Reynolds average) are calculated as:

$$\phi = \widetilde{\phi} + \phi''$$

Where $\widetilde{\phi} = \phi\rho / \overline{\rho}$ and $\rho\phi'' = 0$. Using this weighted average in the Navier-stokes equations, the Favre-averaged Navier-Stokes system (FANS) is obtained. This system reduces the amount of stresses to the Reynolds and scalar terms, making the computation simpler. The governing equations for mass and momentum, after substituting the averaged terms, are:

$$\frac{\partial \overline{\rho}}{\partial t} + \nabla \cdot \left(\overline{\rho}\widetilde{v}\right) = 0$$

$$\frac{\partial \overline{\rho}\widetilde{v}}{\partial t} + \nabla \cdot \left(\rho\widetilde{v} \otimes \widetilde{v}\right) = -\nabla \overline{p} + \nabla \cdot \left(\overline{\tau} - \overline{\rho v'' \otimes v''}\right) + \left(\overline{\rho} - \overline{\rho}_0\right)\overline{g}$$

Where the viscous stress tensor is:

$$\overline{\tau} = \mu\left(\nabla\widetilde{v} + \nabla^t\widetilde{v} - \frac{2}{3}\left(\nabla \cdot \widetilde{v}\right)I\right)$$

And the turbulent stress must be modelled. This model uses the turbulent viscosity concept (Boussinesq) to link the shear stresses to the mean velocity gradient, as:

$$\overline{\rho v'' \otimes v''} = \mu_t\left(\nabla\widetilde{v} + \nabla^t\widetilde{v}\right) - \frac{2}{3}\left(\mu_t \nabla \cdot \widetilde{v} + \rho k\right)I$$

Where μ_t is the turbulent viscosity and k is the mean turbulent kinetic energy [m²/s²] defined by:

$$k = \sum_i \widetilde{u}_i''^2$$

And the system is described by the equations:

$$\frac{\partial \overline{\rho}}{\partial t} + \nabla \cdot \left(\overline{\rho} \tilde{v} \right) = 0$$

$$\frac{\partial \overline{\rho} \tilde{v}}{\partial t} + \nabla \cdot \left(\rho \tilde{v} \otimes \tilde{v} \right) = -\nabla \overline{p} + \nabla \cdot \left(2 \mu_e \overline{S} \right) + \left(\overline{\rho} - \overline{\rho}_0 \right) \overline{g}$$

Where $\overline{S} = \frac{1}{2} \left(\nabla \tilde{v} + \nabla^{t} \tilde{v} \right)$ is the mean stress tensor and $\overline{p}' = \overline{p} + \frac{2}{3} \left(\mu_e \nabla \cdot \tilde{v} + \overline{\rho} k \right)$ is the modified pressure. The transport equation for the quantity ϕ is:

$$\frac{\partial \left(\overline{\rho} \tilde{\phi} \right)}{\partial t} + \nabla \cdot \left(\rho \tilde{v} \tilde{\phi} \right) = \nabla \cdot \left(\overline{\rho} D_{\phi} \nabla \tilde{\phi} - \overline{\rho v'' \phi''} \right)$$

Where $\overline{\rho v'' \phi''}$ must be modelled.

4.3 Models

4.3.1 Turbulence model

There are two turbulence models available in ISIS: the standard k-ε and the RNG k- ε. Generally, the complexity of turbulence excludes the use of a one equation model. Thus, both available models consist of two turbulent transport equations models that provide closure to the Favre Averaged Navier-Stokes system. To satisfy dimensional requirements, at least two scaling parameters are required to relate the Reynolds stresses to the rate of eddy deformation.

4.3.1.1 Standard k- ε model

A choice for the closure of the FANS system can be: the turbulent kinetic energy k [m²/s²] and the rate of dissipation of kinetic energy ε [m²/s³]. The transport equation for these variables can be described as:

$$\frac{\partial(\bar{\rho}k)}{\partial t} + \nabla \cdot (\rho k \tilde{v}) = \nabla \cdot \left(\mu + \frac{\mu_t}{\sigma_k} \right) + P_k + P_{kb} - \bar{\rho}\varepsilon$$

$$\frac{\partial(\bar{\rho}\varepsilon)}{\partial t} + \nabla \cdot (\rho \varepsilon \tilde{v}) = \nabla \cdot \left[\left(\mu + \frac{\mu_t}{\sigma_\varepsilon} \right) \nabla \varepsilon \right] + \frac{\varepsilon}{k} \left(c_{1\varepsilon} P_k + c_{3\varepsilon} P_{\varepsilon b} - c_{2\varepsilon} \rho \varepsilon \right)$$

Where the first terms in the left hand side are the local rate of change of the quantity (k or ε) and the second is the transport of the quantity by advection. In the right hand side, the first terms are the transport of k or ε by diffusion and the rest of the terms are source terms. P_k is the production of turbulence kinetic energy due to the mean velocity gradients and P_{kb} is the production of the turbulence kinetic energy due to buoyancy. σ_k and σ_ε are the turbulent Prandtl for k and ε, respectively.

The characteristic velocity and the characteristic length are defined as: $v_t = \sqrt{k}$ and $l = \frac{k^{3/2}}{\varepsilon}$. And the viscosity is:

$$\mu_t = c\rho v_t l = c\rho \frac{k^2}{\varepsilon}$$

Where c is an empirical constant.

4.3.1.2 RNG k- ε model

The Renormalization Group method is very similar to the standard model but it has an additional production term which is important for rapid distortion and gives a lower effective viscosity than the standard k- ε model.

Near the wall, where the viscous effects are dominant, neither of these models is valid because they are high Reynolds number models. Wall functions are used in the interface between the boundary and the fluid.

4.3.2 Combustion model: Eddy Break Up (EBU) model

The combustion is a very complex process because it involves physical and chemical processes at different time and space scale. The combustion models simplify this process in order to predict the HRR, the position of the flame, the species concentration and the soot concentration.

The EBU model is based on the conserved scalar approach and assumes fast chemistry. This means that the oxidant and the fuel cannot coexist except where reaction takes place, within an infinitely thin flame sheet. This reaction is a single-step, irreversible and infinitely fast reaction.

The burning is controlled by the turbulent mixing of fuel and oxygen. This is reasonable because the scale of mixing is lower than the chemical reaction scale. Species mass fraction are inferred from the mixture mass fraction ($\tilde{z}$) and from the fuel mass fraction (Y_F). Other species mass fractions and temperatures are functions of these two variables. The governing transport equations for these variables are:

$$\frac{\partial(\overline{\rho}\tilde{z})}{\partial t}+\nabla\cdot(\rho\tilde{v}\tilde{z})=\nabla\cdot\left(\frac{\mu_e}{\sigma_\phi}\nabla\tilde{z}\right)$$

And

$$\frac{\partial(\overline{\rho}\tilde{Y}_F)}{\partial t}+\nabla\cdot(\rho\tilde{v}\tilde{Y}_F)=\nabla\cdot\left(\frac{\mu_e}{\sigma_\phi}\nabla\tilde{Y}_F\right)+\overline{\dot{\omega}}_F$$

The fuel burning rate is calculated as:

$$\overline{\dot{\omega}}_F=-C_R\overline{\rho}\frac{\varepsilon}{k}\min\left(\tilde{Y}_F,\frac{\tilde{Y}_O}{s}\right)$$

Where C_R is a dimensionless constant, s is the stoichiometric ratio for oxygen and $\tilde{Y}_O$ is the mass fraction of oxidizer.

4.3.3 Radiation model: Finite Volume Method

Radiation exchanges plays and important role in the energy transport in the case of fire, particularly in large scale fire. The radiation process is very complex because it involves the transfer of heat by electromagnetic waves. The radiation transport will depend on the absorption, transmission and reflexion of the different media (gases, boundary conditions, etc) and the different behaviour at different wavelength. It also depends of the temperature and material of the emitter.

The absorption and emission of the combustion products are modelled in different ways in ISIS:

- Constant value
- Product mass fraction dependent function
- Temperature dependent function
- Gray-medium assumption

The first model propose a constant absorption coefficient for the media, the second one makes the absorption dependent of the amount of each specie in the media, the third one set the absorption through a function that depends on the temperature of the media and the last one define the absorption in every cell with the formula:

$$k_{gas} = \frac{-1}{L_m}\ln(1-\varepsilon)$$

Where $L_m = 3.6\frac{\Delta V}{\Delta S}$ is the mean beam length and ε is the emissivity of the gas.

The effect of the soot on the absorption coefficient is accounted for adding the absorption coefficient of the soot to the one of the other products (water vapour, carbon dioxide and carbon monoxide).

The governing equation for radiative transfer of energy (RTE) is:

$$\frac{dI_\lambda(r,s)}{ds} + (k+\sigma_{\lambda s})I_\lambda(r,s) = kI_{\lambda b}(r,s) + \frac{\sigma_{\lambda s}}{4\pi}\int_{4\pi} I_\lambda(r,s')\phi(\lambda,s,s')d\Omega'$$

Where: r is a position in the spatial domain, s is the unit vector along a direction of propagation of radiation, Ω' is the scattering solid angle, k is the absorption coefficient, $\sigma_{\lambda s}$ is the scattering coefficient, $I_{\lambda b}(r,s)$ is the Planck function describing the spectral intensity of blackbody radiation and ϕ is a phase function defined as the ratio of the scattered intensity in a given direction with the intensity for isotropic scattering.
The blackbody spectral intensity, describing spontaneous emission, is assumed to be proportional to σT^4, where σ is the Stefan-Boltzmann constant.

The Finite Volume method discretizes the total set of admissible direction of propagation in a finite set of control angles characterized by the angular coordinates of its direction. The RTE is express as:

$$\frac{dI(r,\theta,\phi)}{ds} + kI(r,\theta,\phi) = \frac{k\sigma}{\pi} T^4$$

and integrated over control volumes and control angles. The radiative source term involved in the energy balance is:

$$-\nabla \cdot q_r = kG - 4k\sigma T^4$$

Where the incident radiation is:

$$G = \int_{4\pi} I(r,s) d\Omega$$

4.3.4 Soot model

Soot is a product of incomplete combustion. It is very difficult to model due to the fact that its formation is a complex phenomenon. In ISIS, there are several models for this purpose, like:

- Fixed soot fraction
- Khan model
- Moss model

The **Fixed soot fraction** approach uses a fixed value of the soot fraction and therefore, no equation is solved for this value. The soot is computed using the soot conversion factor in the one step reaction equation for combustion:

$$C_n H_m + \left(n + \frac{m}{4} - v_s \right) O_2 \rightarrow (n - v_s) CO_2 + \frac{m}{2} H_2O + v_s C$$

The soot conversion factor v_s is used for accounting the amount of carbon that is not becoming CO_2, incomplete combustion. This means that for each molecule of fuel that is burnt, there will be v_s times the molecules of carbon in the products. The soot conversion factor is calculated as:

$$v_s = Y_s \left(\frac{W_{fuel}}{W_C} \right)$$

Where Y_s is the soot yield, W_{fuel} is the molar mass of fuel and W_C is the molar mass of carbon.

The **Khan model** is a one equation approach where the mass fraction of soot is the unknown. It satisfies the advection-diffusion equation:

$$\frac{\partial(\rho Y_S)}{\partial t} + \nabla \cdot (\rho \upsilon Y_S) = \nabla \cdot \left(\frac{\mu_e}{\sigma_\phi} \nabla Y_S \right) + \omega_{s,f} - \omega_{s,c}$$

Where the diffusion coefficient depends on the effective viscosity and the turbulent Prandtl number and the source term are divided in two parts: soot formation and soot combustion.

The **Moss model** is a two equations approach where the soot mass fraction and the soot particle concentration are the unknowns. This model takes into account the processes of nucleation, surface growth and coagulation. The equations for this model are:

$$\frac{\partial(\rho Y_S)}{\partial t} + \nabla \cdot (\rho \upsilon Y_S) = \nabla \cdot \left(\frac{\mu_e}{\sigma_\phi} \nabla Y_S \right) + \omega_s - \nabla \cdot \left(\rho v^{th} Y_S \right)$$

$$\frac{\partial(\rho X_n)}{\partial t} + \nabla \cdot (\rho \upsilon X_n) = \nabla \cdot \left(\frac{\mu_e}{\sigma_\phi} \nabla X_n \right) + \omega_n - \nabla \cdot \left(\rho v^{th} X_n \right)$$

Where X_n is the soot particle concentration and the source term for Y_S is:

$$\omega_S = C_\delta C_\alpha \rho^2 T^{1/2} \chi_f e^{-T_\alpha / T} + C_\gamma \rho T^{1/2} n \chi_f e^{-T\gamma / T} - \left(36\pi n \frac{\rho^2}{{\rho_s}^2} \right)^{1/3} \tau_{ox} {Y_s}^{2/3}$$

with	C_δ	[kg]	(default value = 144)
	C_α	nucleation constant	depends on the fuel
	T_α	activation temperature for nucleation	(default value = 46100)
	χ_f	fuel mole fraction	
	C_γ	surface growth constant [m]	depends on the fuel
	$T\gamma$	activation temperature for surface growth	(default value = 12600)
	τ_{ox}	oxidation rate	several models.

The first term in the right hand side part of the equation is the nucleation term, the second one is the surface growth term and the last is the oxidation term.

For χ_n the source term is:

$$\omega_n = C_\alpha \rho^2 T^{1/2} \chi_f e^{-T_\alpha / T} - C_\beta \rho^2 T^{1/2} n \chi_n{}^2$$

Where the first term in the right hand side part of the equation is the nucleation term and the second one is the coagulation term. C_β is the coagulation constant and the thermodiffusion velocity is defined by:

$$\left(v^{th}\right)_j = -0.54 \frac{\mu}{\rho} \frac{\partial}{\partial x_j} \left(\ln T\right) = -0.54 \frac{\mu}{\rho} \frac{1}{T} \frac{\partial T}{\partial x_j}$$

For the oxidation rate there are two models available: Nagle-Strickland-constable (NSC) and Lee-Thring-Beer (LTB).

4.3.5 Walls boundary conditions

4.3.5.1 Standard wall function

In the region near the wall, where viscous effects are dominants, the high Reynolds number model does not apply. For this reason, a standard wall function is used which provides give boundary conditions for the kinetic energy, its dissipation and the wall shear stresses. The wall functions are established by neglecting the convection, the volume force and the pressure gradient against the viscous terms for a steady flow on a plane plate. The boundary Γ is supposed to be at a distance δ of the wall as it is depicted in Figure 1.

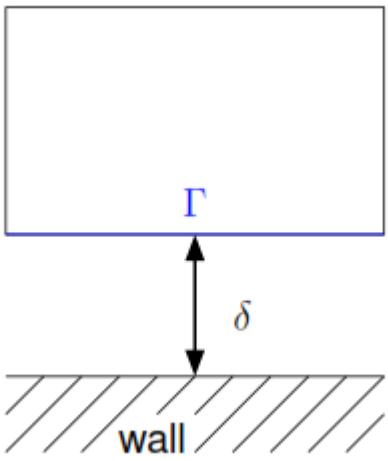

Figure 1: Configuration for wall law [6]

A normalized velocity and distance are defined by:

$$u^+ = \frac{v_t(y)}{u_\tau} \quad \text{and} \quad y^+ = \frac{\rho u_\tau y}{\mu}$$

Where v_t is the tangential velocity at y and u_τ is the friction velocity. The wall function is separated in two parts, the linear sub layer and the log-law layer. In the first the viscous effects are dominant, whereas in the second the turbulent effects are preponderant:

- Linear sub layer: $$y^+ = u^+$$
- Log-law layer: $$u^+ = \frac{1}{k}\ln\left(Ey^+\right)$$

Where k and E are model's constants

4.3.5.2 Boundary conditions: Wall conduction

The heat flux from the fluid is calculated as:

$$-\lambda\frac{\partial T}{\partial n} = h_c\left(T_f - T_i\right)$$

The convective heat transfer is specified by the user or determined by the log-law for enthalpy:

$$h_c = \frac{\rho c_p u_\tau}{T^+}$$

Where T^+ is:

$$T^+ = \frac{T - T_i}{T_\tau} \quad \text{with} \quad T_\tau = \frac{Q_w}{\rho c_p u_\tau}$$

Remark: if the laminar and the turbulent Prandtl numbers are equal ($p_r = p_{rt}$), then the transition value is the same as for the velocity:

$$y^+_{trans,T} = y^+_{trans}$$

5. Study of comparison with experimental data

5.1 Methodology

5.1.1 Test characteristics

This stage comprises a comparison between a fire test and a simulation. The fire test selected for this purpose is a PRISME SOURCE test conducted by IRSN [9]. The denomination of this test is PRS_SI_D6 and consists of a room of 6m long, 5m wide and 4m high, as shown in figure 2.

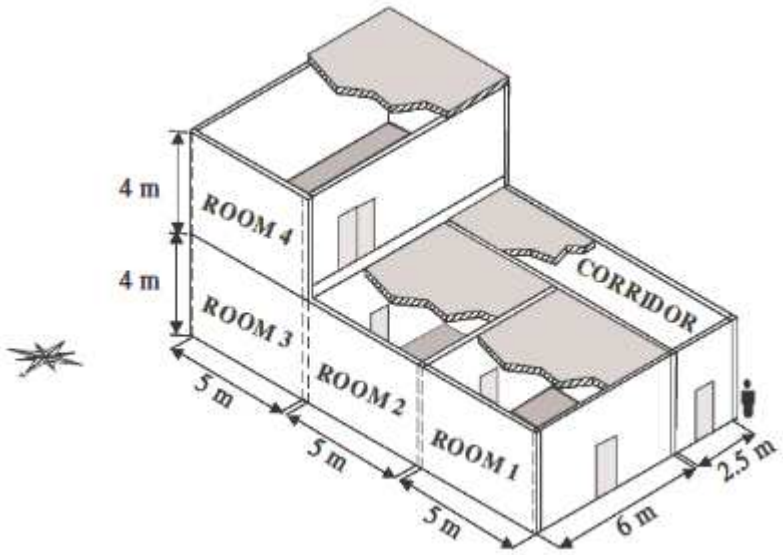

Figure 2: Perspective view of the DIVA facility inside the JUPITER [19]

Room Characteristics

The room that was used is "ROOM 2" of the DIVA facility which is dedicated for the performance of fire test in contained and ventilated multi-room configurations. It is included in the JUPITER facility which has a volume of 2630m³ and comprises three rooms of 120m³, one corridor of 150m³ and one room of 170m³ in the first floor. It was closed and there was mechanical ventilation. There was an exhaust point near the ceiling and a two intake point, one near the ceiling and the other near the floor, as shown in figure 3. The area of the ventilation grids is 0.18m² (0.3m x 0.6m) and the area of the ducts is 0.16m² (0.4m x 0.4m). The walls, floor and ceiling are made of concrete and the ceiling is isolated with 5cm Rockwool, so that the real size of the room is 6m x 5m x 3.95m. The thickness of the walls is 30cm.

The characteristic of the materials can be seen in the table 1.

Material	Thermal Conductivity [W/m.K]	Heat Capacity [J/kg.K]	Emissivity	Density [kg/m³]
Concrete	1.5	736	0.7	2430
Rock Wool	0.102	840	0.95	140

Table 1: Characteristics of the room's materials [19]

Ventilation characteristics

The ventilation system consists of an intake of air at 0.65m height from the floor and an exhaust of air at 0.75m from the ceiling. The air change rate is 4.7 volumes per hour; that is 560m³/h. The pressure of the room was measured before starting the test and it was 117Pa above the atmospheric.

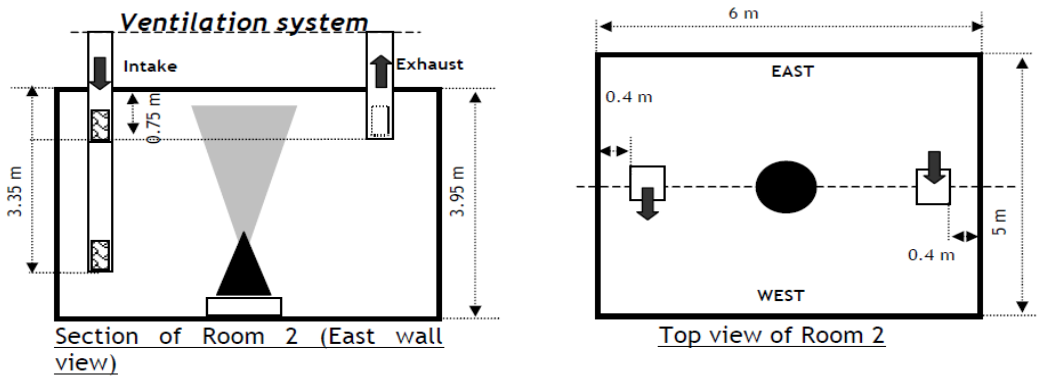

Figure 3: Position of intake and exhaust openings in Room 2 [19].

Fire source characteristics

This source is a circular pool fire of 0.4m², full with hydrogenated tetra-propylene. The tank depth is 10cm and it was placed 40cm above the floor in the centre of the room. The pan was filled with 5cm of fuel; this corresponds to 15.9kg. The characteristics of the fuel can be seen in Table 2.

Properties	Temperature	Values	Test Conditions	Uncertainties
Molar mass[g/mol]	-	170	-	-
Density[kg/m³]	20°C	758	NF ISO 1675	±0.2%
Thermal conductivity[W/m.K]	290-470K	0.186-0.1791 10^{-3}	-	-
Viscosity[kg/m.s]	20°C	1.235 10^{-3}	-	±1%
Kinematic Viscosity[m²/s]	20°C	1.629 10^{-6}	NF ISO 3104	±1%
Specific Heat[J/kg.K]	23°C	2163	ISO/DIS11 357-4	±4%
Boiling point[°C]	-	188	-	-
Flashpoint[°C]	-	53.5	NF ISO13736	-
Auto-ignition temp.[°C]	-	240	ISO 5660-1	-
Heat of Combustion[MJ/kg]	-	40-48	PRISME SOURCE free atmosphere	-

Table 2: hydrogenated tetra-propylene properties [13]

Measurements points

The coordinate system, for the measurement points on the walls, is as follows: a plane where "x" is the horizontal direction and "z" the vertical. For the measurements not on the walls, the

centre of the system is in the centre of the room and (x_NS, x_EW, Z) are the coordinates. The coordinate x_NS is in horizontal direction and is measured between North and South wall. The same is true for x_EW between East and West walls. The next tables show the different variables that are analyzed. The first one contains the thermocouples in the North wall and a thermocouple tree.

Variable	Reference	Location	Unit
Temperature	TP_L2_N355	L2 ; North Walls (Z=3.55 m ; X=1.5 m)	°C
Temperature	TP_L2_N260	L2 ; North Walls (Z=2.60 m ; X=1.5 m)	°C
Temperature	TP_L2_N155	L2 ; North Walls (Z=1.55 m ; X=1.5 m)	°C
Temperature	TP_L2_N030	L2 ; North Walls (Z=0.30 m ; X=1.5 m)	°C
Temperature	TGL2_SE_XXX	L2 (x_NS=1.5 m ; x_EW=-1.25m ; Z=X[1])	°C

Table 3: Temperature measures [8]

Table 4 contains the position of the equipments for measuring species and heat fluxes. The heat fluxes are measured in each wall at a height 2.6m and near the north wall at four heights. The species are determined near the ceiling, at height 3.3m and close to the floor, at height 0.8m.

Variable	Reference	Location	Unit
Oxygen	O2L1_HAUT	L2 (Z=3.3 m ; x_NS=1.5 m ; x_EW=-1.25m)	%
Oxygen	O2L1_BAS	L2 (Z=0.8 m ; x_NS=1.5 m ; x_EW=-1.25m)	%
CO	COL1_HAUT	L2 (Z=3.3 m ; x_NS=1.5 m ; x_EW=-1.25m)	%
CO	COL1_BAS	L2 (Z=0.8 m ; x_NS=1.5 m ; x_EW=-1.25m)	%
CO2	CO2L1_HAUT	L2 (Z=3.3 m ; x_NS=1.5 m ; x_EW=-1.25m)	%
CO2	CO2L1_BAS	L2 (Z=0.8 m ; x_NS=1.5 m ; x_EW=-1.25m)	%
Heat flux	FLR_L2_N355	L2 ; North Walls (Z=3.55 m ; X=1.5 m)	W/m²
Heat flux	FLR_L2_N260	L2 ; North Walls (Z=2.6 m ; X=1.5 m)	W/m²
Heat flux	FLR_L2_N155	L2 ; North Walls (Z=1.55 m ; X=1.5 m)	W/m²
Heat flux	FLR_L2_N030	L2 ; North Walls (Z=0.3 m ; X=1.5 m)	W/m²
Heat flux	FLT_L2_WC260	L2 ; West Walls (Z=2.6 m ; X=0.0 m)	W/m²
Heat flux	FLT_L2_EC260	L2 ; East Walls (Z=2.6 m ; X=0.0 m)	W/m²
Heat flux	FLT_L2_SC260	L2 ; South Walls (Z=2.6 m ; X=0.0 m)	W/m²
Heat flux	FLT_L2_NC260	L2 ; North Walls (Z=2.6 m ; X=0.0 m)	W/m²

Table 4: heat flux and species concentration measures [8]

[1] *Thermocouples tree with thermocouples in z every 5 cm.

5.1.2 Simulation parameters

In Table 5, the different models of ISIS and the selected parameters of these models are shown:

Model	Parameter	Value
Time management	Initial time	-20
	Final Time	2500
	Time step	Automatic_time_step: velocity prediction
	Time order	Order1
Meshing	Geometry	Cartesian_3D
	Type	Structured_mesh
	Space discretization	Finite_volumes
	Type	Gambit_meshing
Physical modelling	Navier-Stokes	Low_mach
	Energy_balance	Enabled
	Turbulence_model	k_ ε
	Combustion model	EBU
	Radiation model	FVM
	Soot model	Moss_model
Boundary conditions Walls	Type	Wall
	Velocity	Wall_law
	Temperature	Wall_conduction
Boundary conditions Ventilation	Type	Pipe_junction
	Velocity	Pipe_mass_flow_rate
Boundary condition fire source	Type	inflow
	Velocity	Fixed_mass_flow_rate (from file)
Turbulence	Wall_law type	Log_law

Table 5: Simulation models

In the table 6, the values of the different variables of the simulation can be seen:

Properties	Variable	Value
Air properties	Laminar Viscosity	1.7x 10^{-5}kg/(m.s)
	Specific Heat Capacity	1020J/kg.K
	Reference Temperature	298K
	Turbulent Prandtl	0.7
	Turbulent Schimidt	0.7
	Absorption coefficient	0.1m^{-1}
	Reference Density	1.2kg/m^3
	External Pressure in Pipes	in: 101131pa out: 100310pa
	Resistance in the Pipes	R_{in}=8880 R_{out}=20022
Fuel	Heat of combustion	4.2x10^7J/kg
	Boiling point	461 K
	Formula	$C_{12}H_{26}$
	Soot Coefficient	s= 2.125
Initial Conditions	Velocity	0.0 0.0 0.0 m/s
	Initial Temperature	298 K
	Pressure	98384Pa
	Turbulence Kinetic Energy	1 x 10^{-6} m^2/s^2
	Dissipation Rate of Turbulent Kinetic Energy	1 x 10^{-9} m^2/s^3
	Mixture Fraction	0.0
	Fuel Fraction	0.0

Table 6: Simulation values

The simulation was stated 20 second before the fire starts, in order to have steady state conditions for the ventilation flows as it was in the experiment. The time step in the program was chosen as automatic and calculated with velocity prediction model using the fixed target approach. This model compares the predicted and the final velocity of the Navier-Stokes equations. The time step is adjusted for a difference of 10%. The minimal time step was set to 0.001s and the maximal to 0.5s.

The external pressure in the pipes was set as measured in the experiment the total pressure in the inlet is P_{in}= 101131pa and the total pressure in the outlet is P_{out}=100310pa.

The resistance was calculated with:

$$R = \frac{1}{\rho Q_v^2}\left(P + \frac{1}{2}\rho v^2\right)$$

Where: Q_v is the volumetric caudal of air in the pipe.

ρ is the density of the air

P is the pressure difference between the room and the pipe

v is the velocity of the air in the pipe

The results for the resistance are R_{in}=8880m^{-4} and R_{out}=20022m^{-4}.

The soot coefficient was calculated with the formula:

$$s = y_s \frac{W_{fuel}}{W_c}$$

Where: y_s is the soot yield choose as 0.15 from the SFPE handbook [2]

W_{fuel} is the molar weight of the fuel molecule

W_c is the molar weight of the carbon molecule

The Mass Loss Rate was measure during the experiment using a scale under the fuel pan and with and oxygen consumption calorimeter. The first one was chosen as input for the program. The curve of the MLR as measured is depicted in Figure 4.

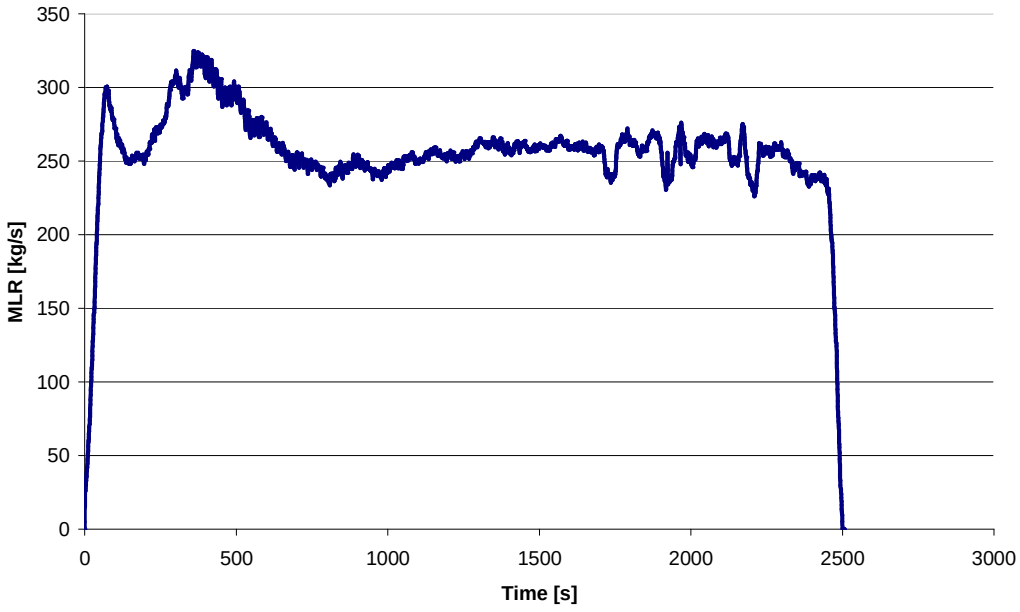

Figure 4: Mass loss rate [kg/s] measured in the experiment vs. time [s] [8]

In figure 5, the geometry for this scenario can be seen. It was calculated with a structured mesh with cells of 10cm x 10cm x 10cm. the boundary conditions defined in the room are the walls, the exhaust of air, the two inlets of air and the pool fire.

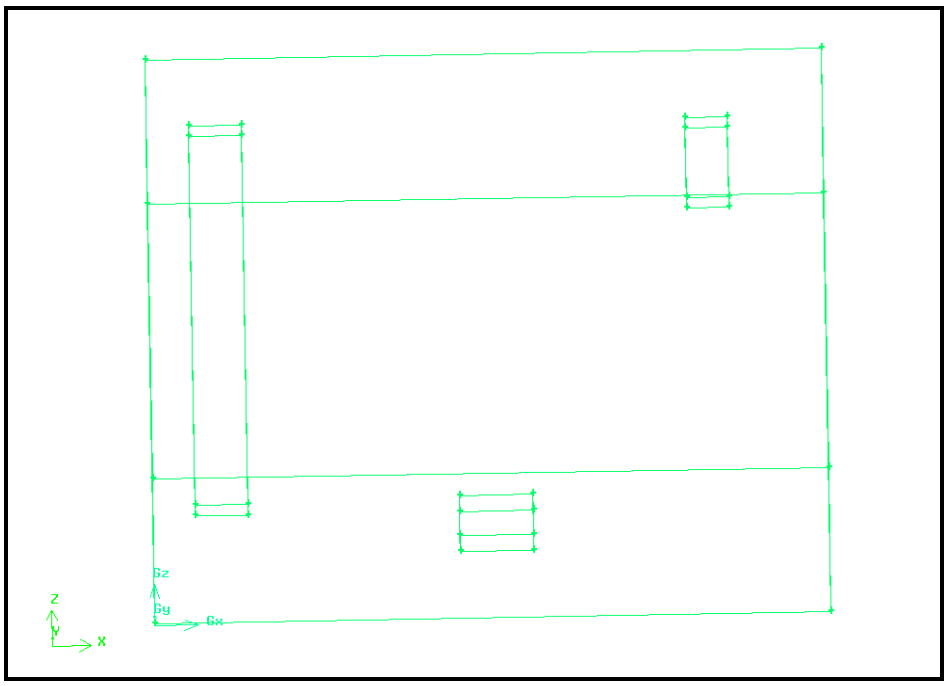

Figure 5: Geometry of the first scenario

5.2 Results

5.2.1 Computational time

The mesh used for this simulation is a structured mesh with cells of 10cm in each side and it has:

- Number of vertices: 153077
- Number of cells: 144096

The simulation was run on 12 processors during 27:33:36.3 h:m:s and the mean time step was 0.4968s, determined by the automatic time step.

5.2.2 Oxygen Concentration (OC)

The distribution of the oxygen concentration at 1200s is shown in the figure 6. Most of the room has an oxygen concentration around 12% except in the plume, where it is lower, and near the floor where it is higher. The oxygen concentration is lower in the plume because the fuel reacts with the oxygen in this zone, consuming the oxygen available in this region. There is a bigger amount of oxygen near the floor because the fresh air has a bigger density and tends to travel to the lower region of the room due to the buoyancy effect. Near the plume there is a higher concentration of oxygen too, this is because the fresh air is sucked by the fire. The entrainment of fresh air is not shown in this picture.

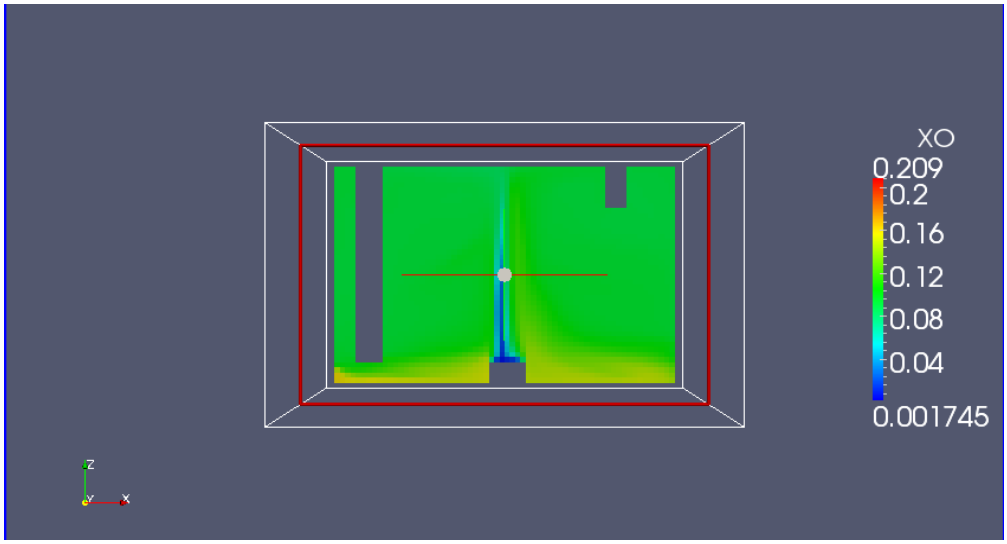

Figure 6: oxygen concentration at 1200s in the Y=2.5m plane

In figure 7, the comparison between the experiment oxygen concentration and the simulation is shown. The two curves agree very well.

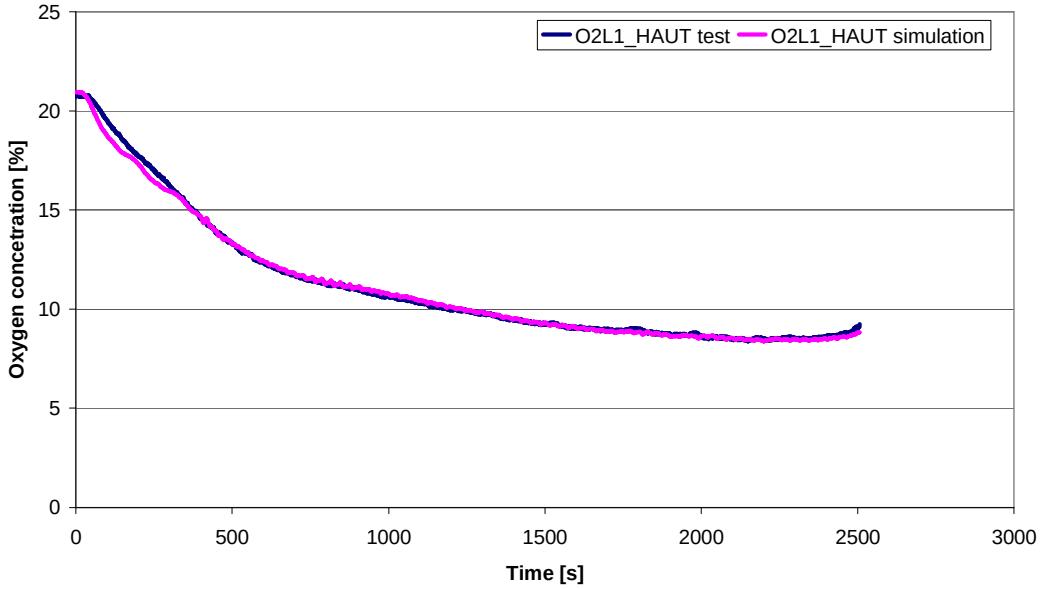

Figure 7: Comparison of the oxygen concentration between the simulation and the experiment in the upper sensor vs. time [s]

Figure 8 reveals that the relative error between the two curves is below 10% at all times and it is between -/+ 4% for the steady state. This good agreement is achieve because the MLR used is the one measured in the test. The ventilation parameters are an average of the ones measured in the test. The heat of combustion was tuned for achieving these results in the oxygen concentration.

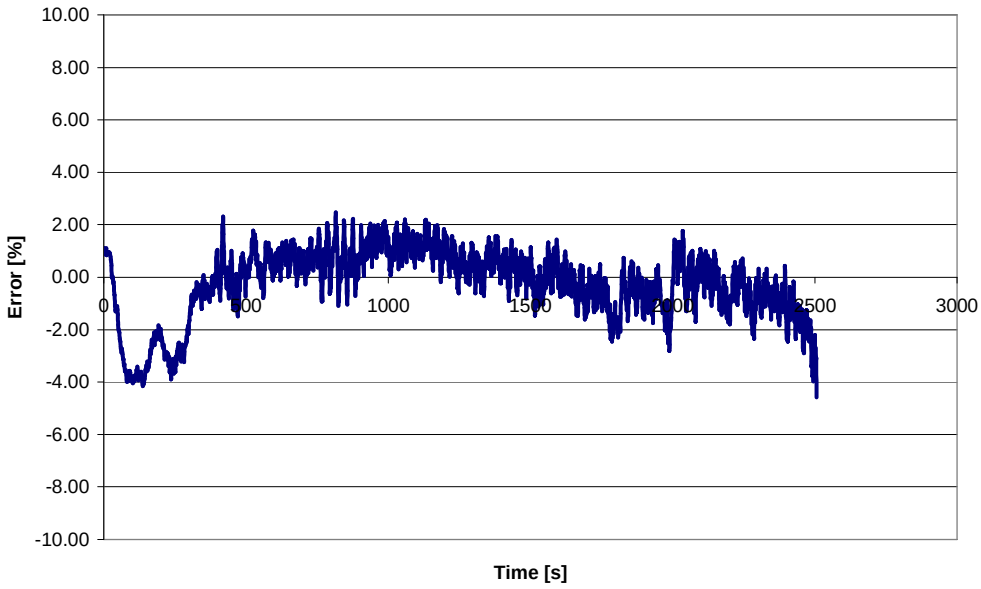

Figure 8: Relative error between the simulation and the test OC vs. time [s]

Figure 9 shows the curve of OC for the sensor placed at height 80cm from the floor. For this case, the difference between the two variables increases with time. In the test, the OC reaches a plateau, but it continues to decrease in the simulation. This means that the simulation underestimates the OC values at this point. The reason for this disparity can be linked with a bad representation in the different variables near the floor.

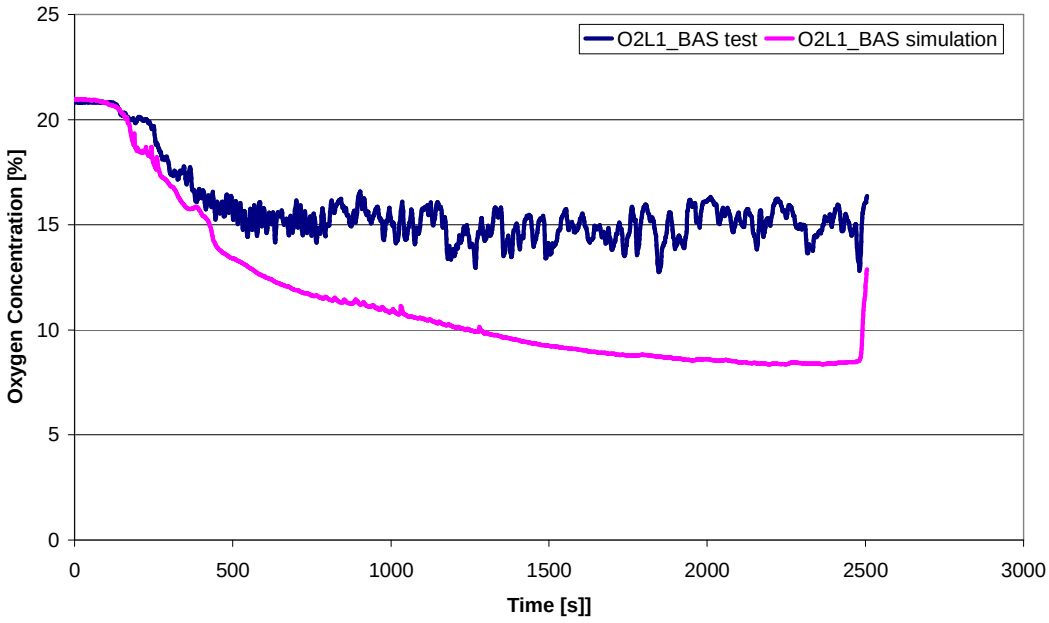

Figure 9: Comparison of the oxygen concentration between the simulation and the experiment in the lower sensor vs. time [s] [8]

The error in the minimum value of the oxygen concentration is shown in the Table 7. The error is less than 2% for the sensor near the ceiling (minus sign means that the simulation peak is smaller than the test one). For the sensor close to the floor, the error is 34%, which is bigger than the experimental uncertainty and is related with the program representation of the values near the floor.

Test	Simulation	Error
8.38867	8.38606	-0.03112
12.7461	8.354231	-34.4566

Table 7: Relative error between the minimal values of OC

5.2.3 Gas temperatures

The comparison between temperatures at five points of the thermocouple tree is depicted in the figure 10. The heights of the points chosen are 0.55m; 1.55m; 2.55m; 3.55m and 3.9m. On the left side, the temperatures of the simulation are illustrated. While in the right side, the temperatures of the test are shown. The values of the simulation are closer to the experiment ones for the curves at middle height and the difference is a little bit bigger for the part near the ceiling. The curves measured and calculated near the floor show a big discrepancy. The oscillations in the curves of the simulation are probably caused by the variations of the MLR used as input.

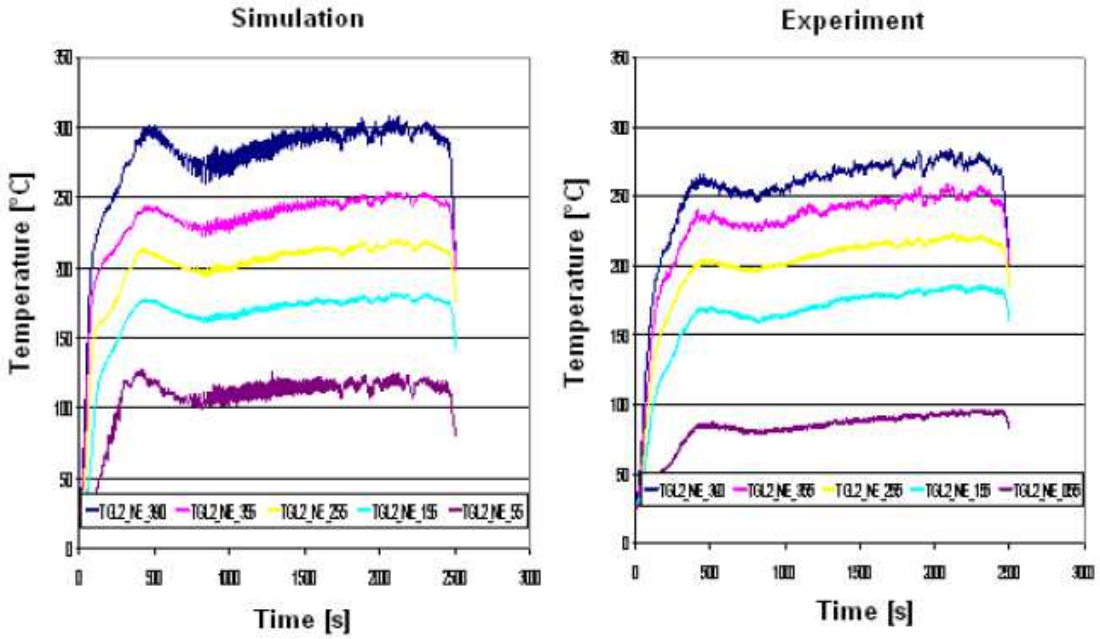

Figure 10: Comparison of the temperatures [°C] in the north-east thermocouple tree at heights 0.55m; 1.55m; 2.55m; 3.55m and 3.9m vs. time [s]

In Figure 11, the relative errors for all temperatures selected are illustrated. At height 0.55m from the floor, the temperature is overestimated with a difference of around 35% for the steady state and 70% for the peak. This can be related with the miscalculation in the values near the floor that agreed with the error in the oxygen concentration in the lower part of the room. All the curves have a peak error and then converge. For all the cases, except the lowest, the error is less than 10% upon convergence.

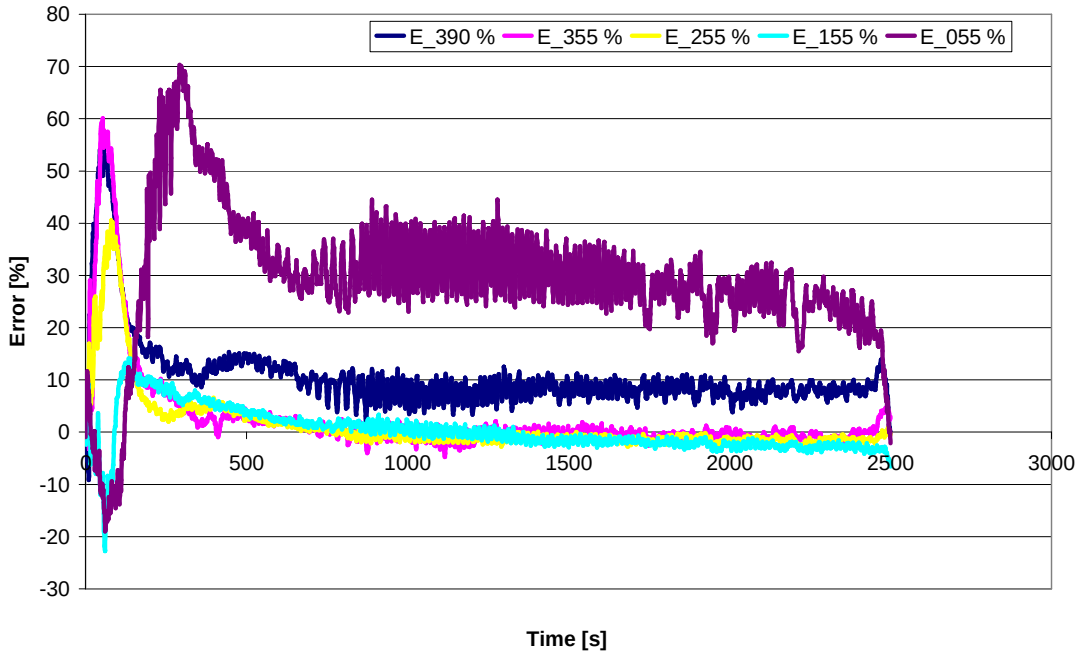

Figure 11: Relative error between the north temperatures in the experiment and in the simulation vs. time [s]

Table 8 describes the error between the maximum values of the temperatures. The differences for the values in the middle are smaller than 5%; the error for the highest is 8.35% and for the lowest is around 32%; in agreement with the previous part of the analysis.

Height[m]	Max_sim	Max_Test	E[%]
390	307.722	283.988	8.357395
355	253.568	258.098	-1.75515
255	219.233	223.307	-1.82439
155	181.175	186.098	-2.64538
55	127.398	96.2547	32.3551

Table 8: Relative error between the peak values of temperature

The temperature has a very good agreement in the middle part of the room when it reaches a semi-stationary state, the shapes of the curves are similar and the peaks are reached in similar time. On the other hand, the rate of growing in the first part is different.

5.2.4 Heat Fluxes

5.2.4.1 Radiant Het Flux (RHF)

The graph showed in the figure 12 is a visualization of radiant heat flux in the North and West walls. The form of the radiation in the walls and ceiling seems reasonable from a qualitative point of view. There is a higher radiation in the centre of the ceiling where the plume reaches the ceiling. The radiation descends as the distance from the fire increase. The fire is place at height 0.4m from the floor that can explain the lower radiation near the floor. In the north wall, the zone with less radiation is due to the fact that the injection duct blocks the radiation of the fire.

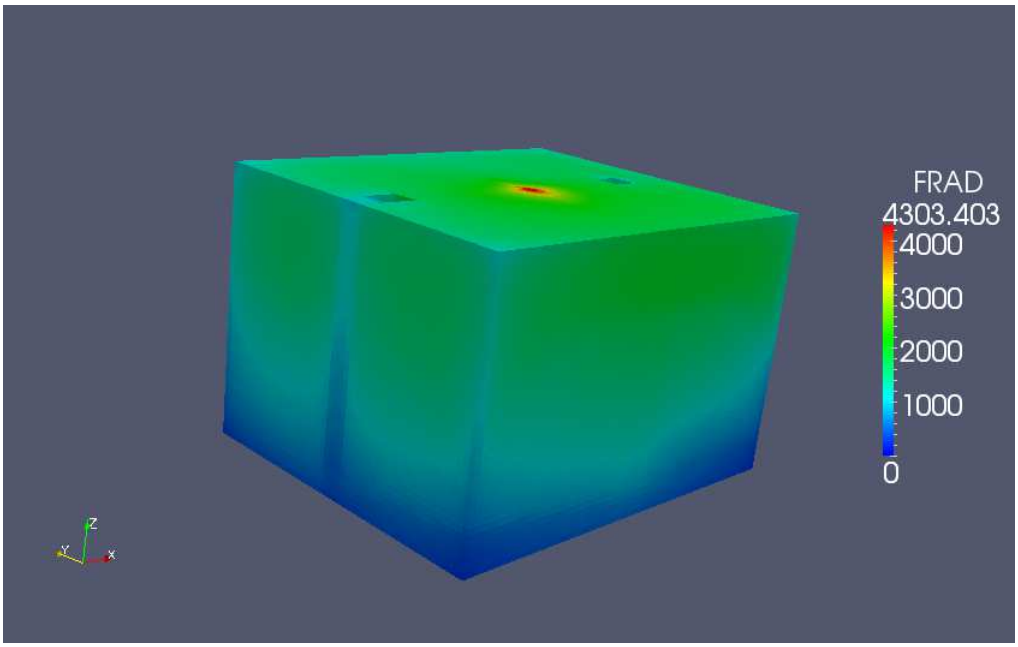

Figure 12: Radiant heat flux [w/m²] visualization

Figure 13 illustrates the radiation in the north wall at diverse heights. The difference between the curves is small for the three highest measurements and is bigger for the lowest one.

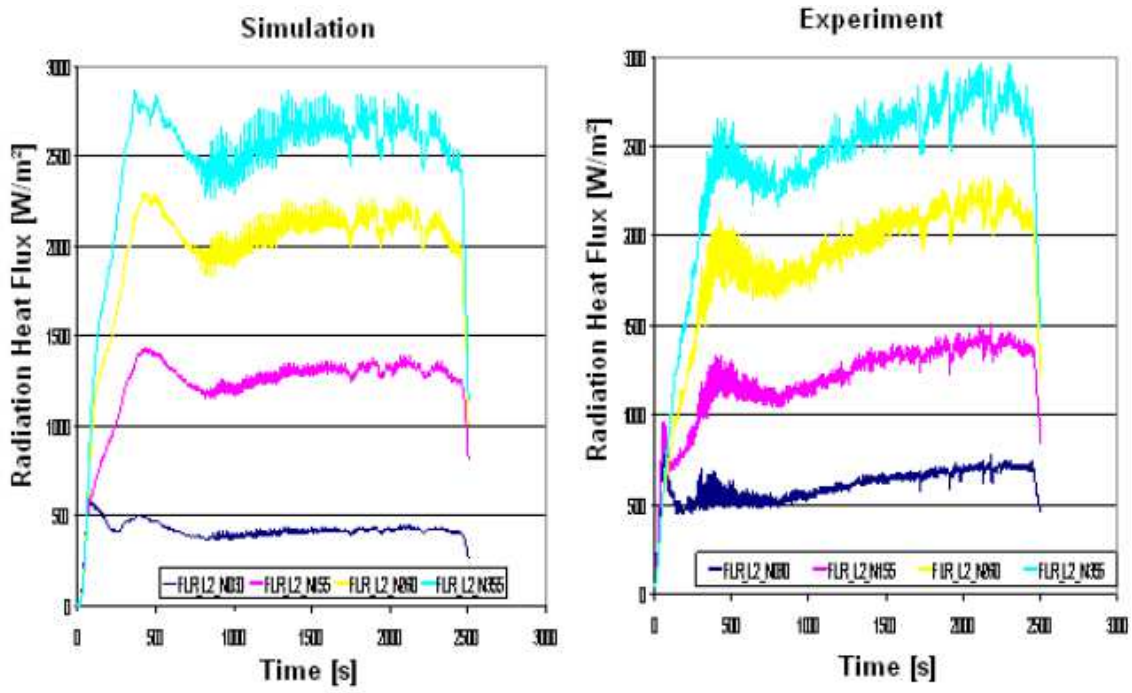

Figure 13: Radiant heat flux [w/m²]in the North wall at heights: 0.3m, 1.55m, 2.6m, 3.55m vs. time [s]

The error between the simulation and the test for the RHF is illustrated in Figure 14. This error converges to a value near 0% for the three highest curves and around -40% for the lowest.

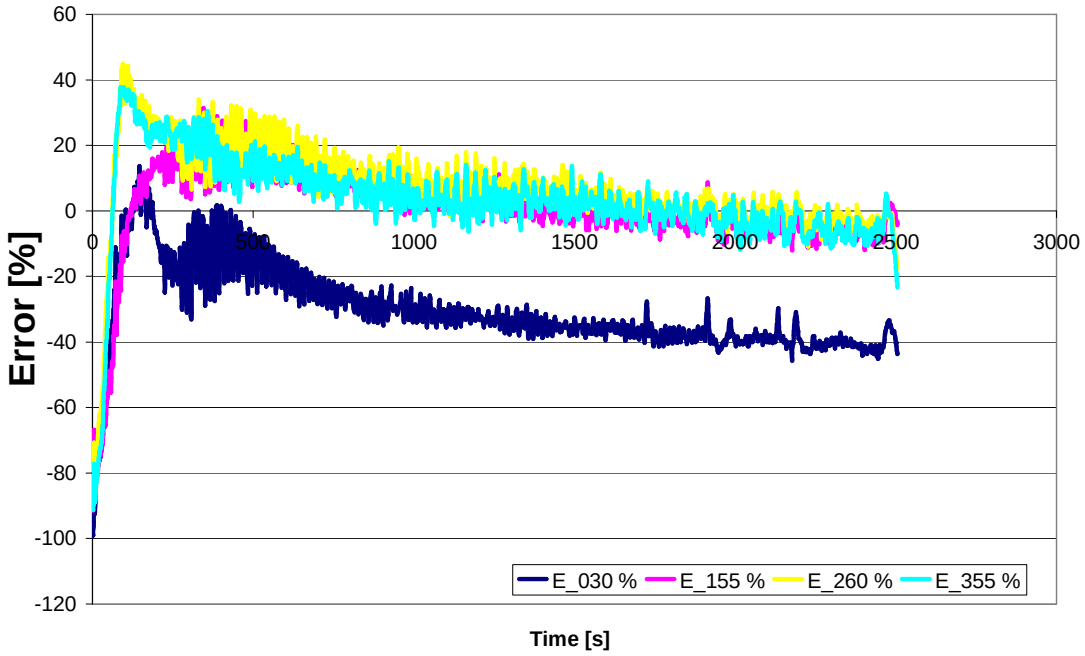

Figure 14: Radiant heat flux [W/m²] in the North wall at heights: 0.3m, 1.55m, 2.6m, 3.55m vs. time [s]

Table 9 shows the discrepancy among the peaks of the RHF in the simulation and in the Test. The calculations underpredict the test values for all the cases. The closest to the real values is the one at height 2.60m.

Height[m]	Simulation	Test	E[%]
0.3	599.286	805.821	-25.6303819
1.55	1433.27	1512.59	-5.24398548
2.6	2298.14	2319.12	-0.90465349
3.55	2870.83	2965.86	-3.20412966

Table 9: Relative error between the maximal values of RHF

The radiant heat flux is underestimated for all the measure points in the north wall. There is a small discrepancy in the radiant heat flux for the highest measurement points but there is a big discrepancy with the values in 0.3m. If the smoke layer is lower than in the experiment, there is more obscuration in the lower part. This can be the reason for the underprediction in the lowest point.

5.2.4.2 Total Het Flux (THF)

The following curves represent the total heat flux in the north wall at four elevations. The curves for the point at 2.6m are very similar while the rest of the curves show a big divergence.

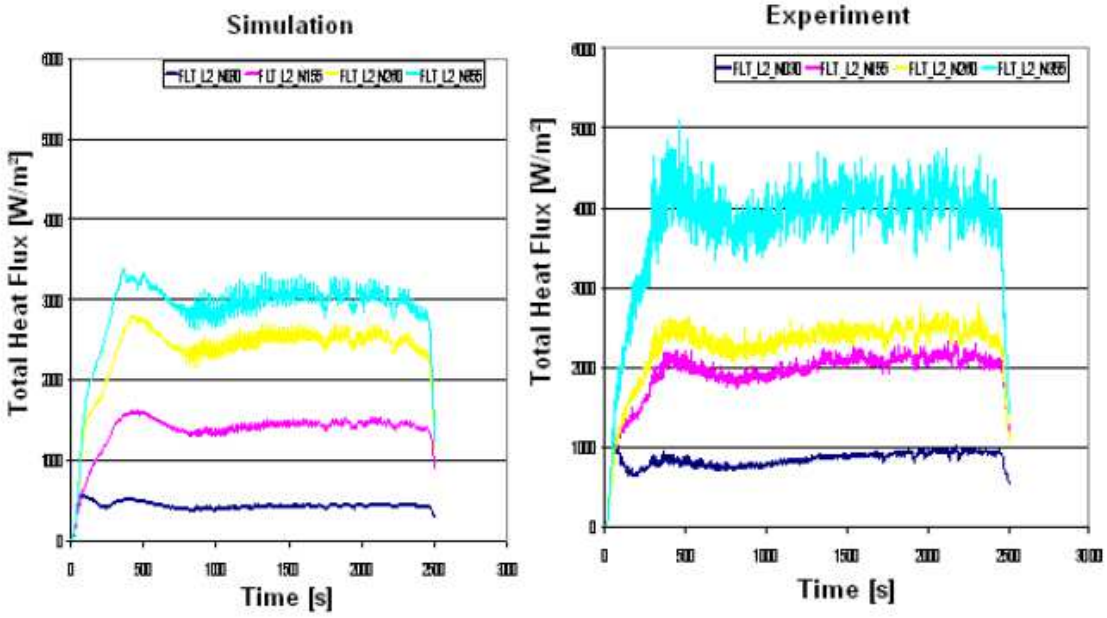

Figure 15: Total heat flux [W] in the North wall at heights of 0.3m, 1.55m, 2.6m, 3.55m vs. time [s]

The relative error for the peak of total heat flux is shown in Table 10. The smallest difference is less than 1% and the biggest is greater than 40%. The difference is too big to consider these results reliable.

Height[m]	Simulation	Test	E[%]
0.3	600.43548	1029.74	-41.6906
1.55	1620.825	2328	-30.3769
2.6	2813.808	2807.78	0.214689
3.55	3394.481	5116.92	-33.6616

Table 10: Relative error between the maximal values of THF

The THF in all the walls at a height of 2.60m is presented in Figure 16. For the simulation, the THF is very similar in all the walls except the north one. In the case of the north wall, the heat

flux is lower because the measurement point is behind the duct for admission of air in the simulation as well as in the test. The THF is underestimated in all the curves. The relative error for the peaks ranges from -16% to -31%.

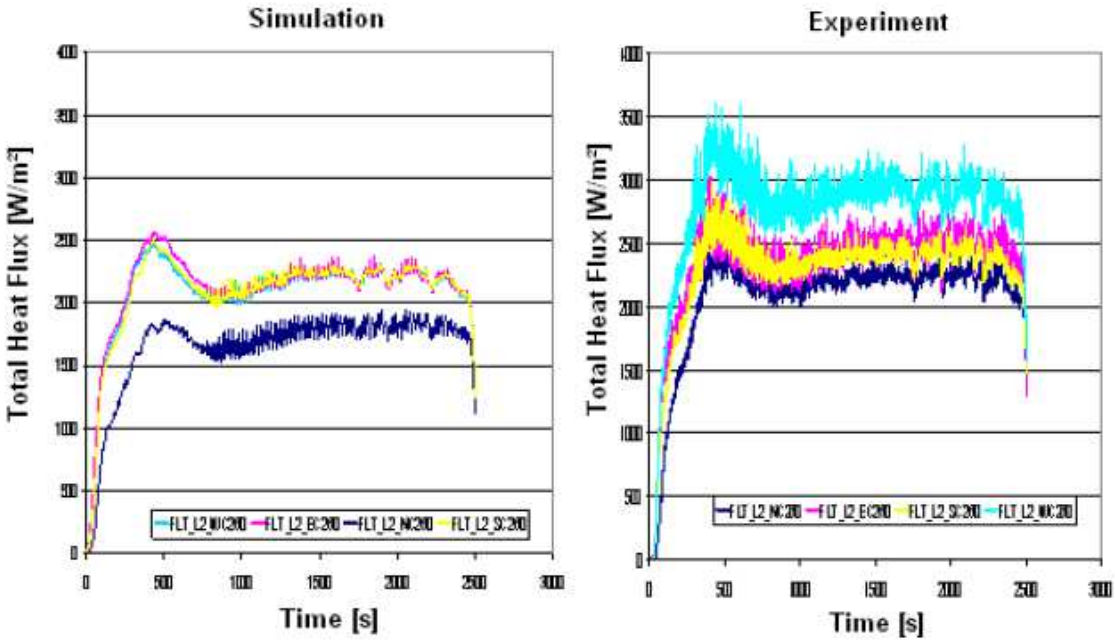

Figure 16: Total heat flux [W/m²] in all the walls at 2.60m vs. time [s]

The temperature in the measurements points of the THF on each edge is illustrated in the figure 17. In this case, the simulation curves have a similar form that the ones measure in the test but the peaks values are smaller for the simulation ones. The difference in the peak values are around 10%.

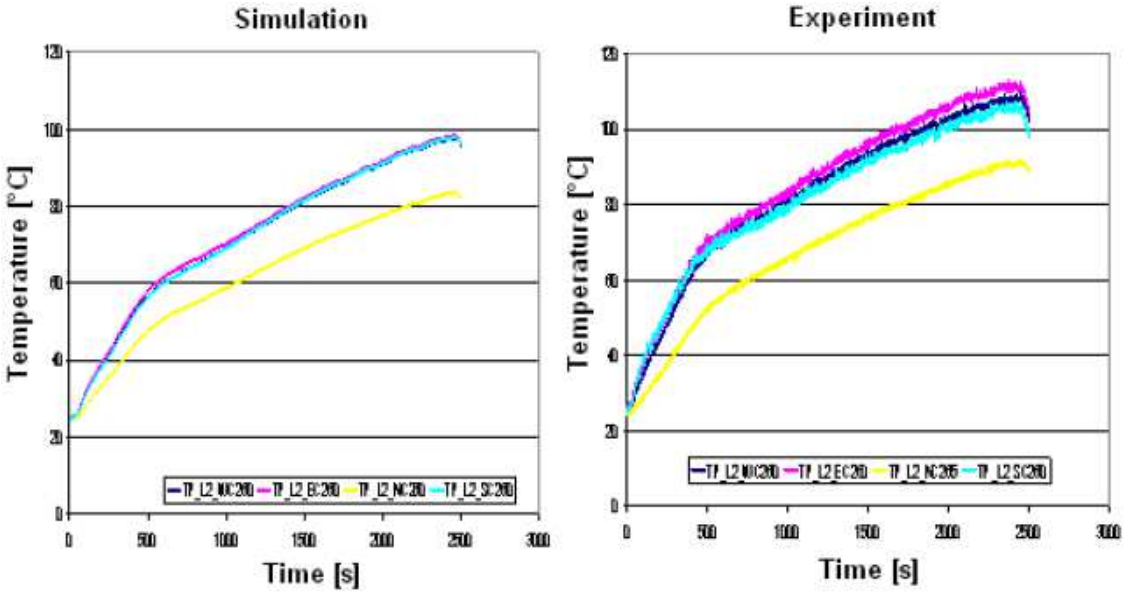

Figure 17: temperature [°C] in all the walls at 2.60m vs. time [s]

It should be noticed that the difference in the THF between the test and the simulation are mostly causes by the convective flux because the error in the RHF is smaller than the one in the THF.

5.3 Discussion

There is very good agreement between the oxygen consumption in the room in the higher part. This is because the Mass Loss Rate is taken as measured in the experiment, leading to a better representation of the fire phenomena. The heat release rate is one of the most important variables in a fire analysis. On the other hand, the agreement between the test and the simulation in the lower part for the OC is not good because of the wrong description of this variable near the floor

The analyses made in the previous section shows that despite of the good agreement in the representation of the fire, by using the measured mass loss rate as input; the values of some variables have a big difference with the experimental ones. This can be observed mostly in the THF, where the error in the peak is bigger than 30% for all the different heights in the north wall except for the measurement point at 2.6m. This error is linked with the convective part of the flux and is related to the wall functions. It was observed in other validation exercises that the program tends to underpredict the THF in the walls, also. The big difference in the Fluxes on the walls makes no trustable the simulations for solve the phenomena below this kind of boundary conditions.

On the other hand, the curves have similar shapes in all the cases. This means that the program can simulate the form of the curve but has an error in the values. This is important because the program represents correctly the physical phenomena.

There is a difference of around 10% in the temperatures in the wall. This can be linked with the underprediction of the THF in the wall. The error for the temperature in the walls could be lower than the error in the THF because radiation is dominant in the THF and its error is smaller than the error in the THF.

In the case of the gas temperatures, the agreement is better with error smaller than 10% except for the lowest measurement point. This reinforces the idea that there is a problem with the transfer of energy to the boundaries. This can be linked with the resolution of the mesh near the wall and with the wall functions.

The biggest difference in almost all the variables is in the lowest part of the room. The height of the smoke layer could be the cause of this difference. If the smoke layer is lower in the simulation than in the experiment, the oxygen concentration and the radiation would be lower but the gas temperature would be higher. It seems to be the reason for the difference between the simulation and the experiment in this region. Another explanation for these results is a bad representation of the program in this region.

6. Blind simulation

6.1 Methodology

The blind simulation was performed on a scenario of the NUREG-1824, Verification and Validation of selected Fire Model for Nuclear Power Plant Applications. The chosen test was the number 3 of the **ICFMP Benchmark Exercise #3 [4] [16]**.

6.1.1 Test characteristics

This test was performed in a room of 21.7m long, 7.04m wide and 3.82m high with a door of 2m x 2m in one of the short walls. The fire was placed in the centre of the room and some cables were located at different places of the room and used as targets. There was mechanical ventilation in the room. The geometric characteristics of this test are shown in the Figure 18:

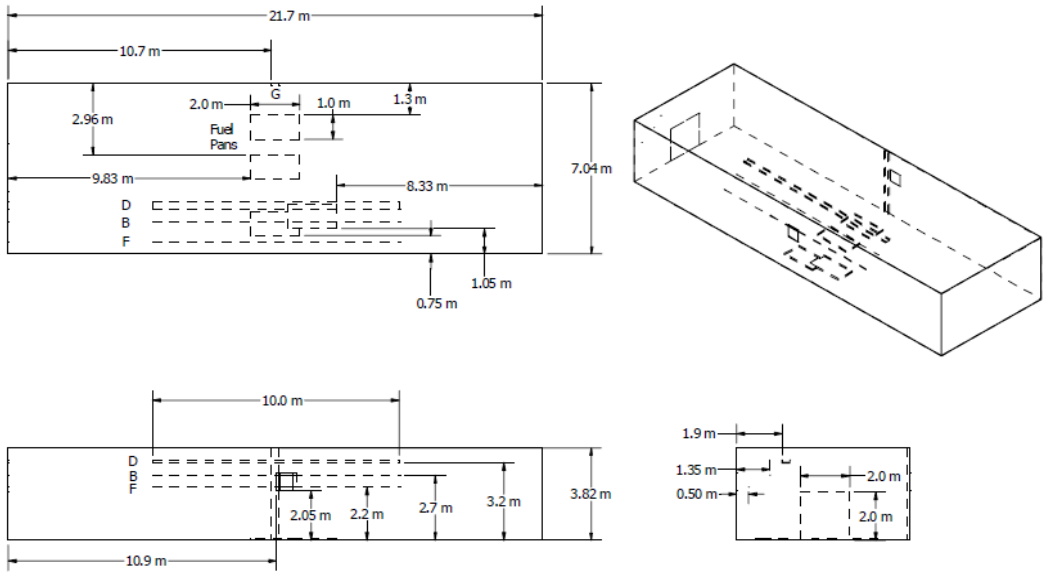

Figure 18: Geometry of the room [4]

Figure 19 shows a view of the room where the cable trays used as targets, the door and the ventilation are present. The thermocouples trees are painted in red. The origin of coordinate system is shown; all positions in the experiment and in the simulation are taken from this origin.

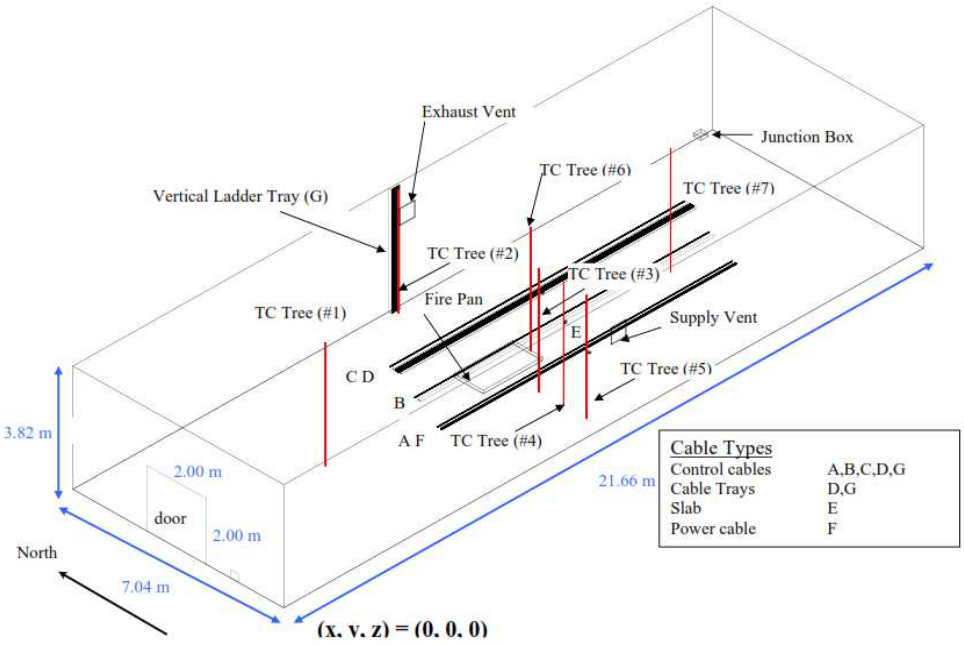

Figure 19: 3D view of the compartment with the different cables trays [16]

For this configuration, the door was open and the ventilation was turned off. The fire consists of a pool fire of 2m long x 1m wide and 0.1m high where a nozzle was installed. A heat release rate as shown on Figure 20 was used. The prescribed curve was employed for the simulation.

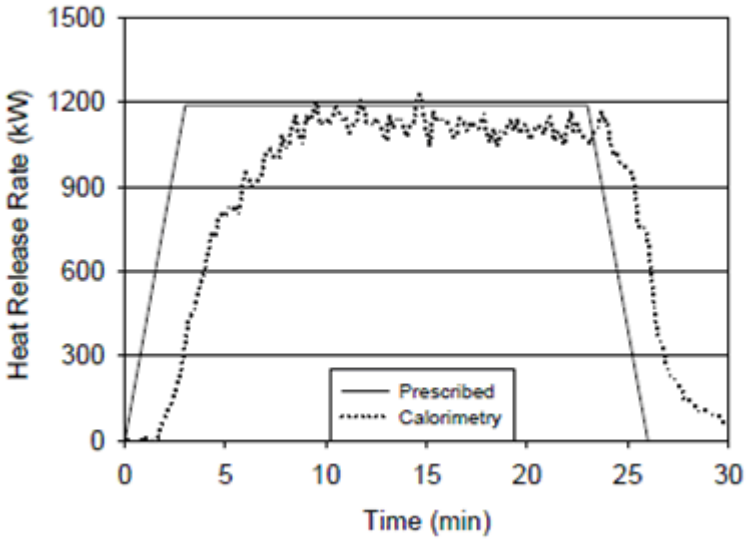

Figure 20: Heat Release Rate of the experiment [4]

The walls of the room were made of gypsum boards of 25mm thickness; the ceiling and the floor were of marinate boards of 25mm thickness. Some characteristics of the room can be seen in Table 11.

Simulation Time = 1800 s							
Compartment							
Size			**Position**				
X (Width) (m)	**Y (Depth) (m)**	**Z (Height) (m)**	**X (Width) (m)**	**Y (Depth) (m)**	**Z (Height) (m)**		
21.7	7.04	3.82	0	0	0		
Compartment Materials (Inside Layer)*							
Ceiling	**Floor**	**Walls**					
Marinite (25 mm)	Gypsum (25 mm)	Marinite (25 mm)					
Ventilation							
Openings							
From	**To**	**Width (m)**	**Height (m)**	**Sill (m)**	**Area (m^2)**	**Position (m)**	**Face**
Fire Room	Outside	2	2	0	4	2.58	Left
Mechanical Vents							
From	**To**	**Area (m^2)**	**Height (m)**				
Outside	Fire Room	0.49	2.4				

Table 11: Compartment characteristics [4]

The measurement of the total heat flux and temperature in the walls, the species concentration and the target temperature were selected as variables for comparison in this experiment. The total heat flux and the wall temperature were measured in all the walls, the ceiling and the floor in several points. The different measurement points of the surface flux and wall temperature are illustrated in Table12.

Targets									
Target	**Position**			**Face**	**Normal Vector**			**Material**	**Target**
	x (m)	**y (m)**	**Z (m)**		**x(m)**	**y(m)**	**z(m)**		
Surface Flux N1	3.91	7.04	1.49	Rear	0	-1	0	Marinite	1
Surface Flux N4	12.15	7.04	1.87	Rear	0	-1	0	Marinite	2
Surface Flux S1	3.91	0	1.49	Front	0	1	0	Marinite	3
Surface Flux S3	9.55	0	1.87	Front	0	1	0	Marinite	4
Surface Flux S4	12.15	0	1.87	Front	0	1	0	Marinite	5
Surface Flux E1	21.7	1.59	1.12	Right	-1	0	0	Marinite	6
Surface Flux E2	21.7	1.59	2.43	Right	-1	0	0	Marinite	7
Surface Flux E3	21.7	5.76	1.12	Right	-1	0	0	Marinite	8
Surface Flux E4	21.7	5.76	2.43	Right	-1	0	0	Marinite	9
Surface Flux C1	3.04	3.59	3.82	Ceiling	0	0	-1	Marinite	10
Surface Flux C2	9.11	5.97	3.82	Ceiling	0	0	-1	Marinite	11
Surface Flux C4	10.85	2.39	3.82	Ceiling	0	0	-1	Marinite	12
Surface Flux C5	10.85	5.17	3.82	Ceiling	0	0	-1	Marinite	13
Surface Flux C7	13.02	5.97	3.82	Ceiling	0	0	-1	Marinite	14
Surface Flux F1	3.04	3.59	0	Floor	0	0	1	Gypsum	15
Surface Flux F2	9.11	2.00	0	Floor	0	0	1	Gypsum	16
Surface Flux F4	10.85	2.39	0	Floor	0	0	1	Gypsum	17

Table 12: Heat flux measurements points [4]

The oxygen, the carbon dioxide and the carbon monoxide concentrations were measured at a high point in the room. The oxygen concentration was also determined in the lower part of the room. In Table13, the position of the species measurement devices is shown:

data	X[m]	Y[m]	Z[m]
O2-1	6.85	3.52	3.2
O2-2	6.85	3.52	0.5
CO	6.85	3.52	3.2
CO2-4	6.85	3.52	3.2

Table 13: Species measurements points [4]

Two of the cables were selected to make a comparison with the simulation results, namely cables B and F. Table 14 shows the position of the thermocouples in the cables (superficial thermocouples) and in the gas(thermocouples trees) 10cm away from the cables.

Data	X[m]	Y[m]	Z[m]
Cable B, tree 4-8	10.85	1.35	2.8
Cable B superficial thermocouple 14	10.83	1.4	2.7
Cable F superficial thermocouple 20	10.83	0.5	2.175
Cable F, tree 5-6	10.85	0.55	2.1

Table 14: Target temperature measurements points [4]

6.1.2 Simulation parameters

Table 15 shows the different models of ISIS and the selected parameters for these models:

Model	Parameter	Value
Time management	Initial time	0
	Final Time	1800
	Time step	Automatic_time_step: velocity prediction
	Time order	Order1
Meshing	Geometry	Cartesian_3D
	Type	Structured_mesh
	Space discretization	Finite_volumes
	Type	Gambit_meshing
Physical modelling	Navier-Stokes	Low_mach
	Energy_balance	Enabled
	Turbulence_model	K_ ε
	Combustion model	EBU
	Radiation model	FVM
	Soot_model	Khan_model
Boundary conditions Walls	Type	Wall
	Velocity	Wall_law
	Temperature	Wall_conduction
Boundary conditions door	Type	Inlet_oulet
	Velocity	Inlet_outlet_velocity
Boundary condition fire source	Type	Inflow: fixed_mass_flow_rate (from file)
	Velocity	Peatross_Beyler
Turbulence	Wall_law type	Log_law

Table 15: Simulation models

The Khan model was chosen because there was not enough information for using the Moss model. The constants used by the model (nucleation, surface growth, coagulation) were not available for this combustible. The Peatross and Beyler model was used in order to simulate the oxygen consumption in the room; this model was not used in the previous case because the MLR as measured in the test was known. The domain for this modelled was chosen around the fire, one meter away from the sides and from the floor to the base of the fire.

Table 16 depicts the combustible and air characteristics. It also describes the initial values in the compartment of the fire.

Properties	Variable	Value
Air properties	Laminar Viscosity	1.7x 10^{-5}kg/m.s
	Specific Heat Capacity	1020J/kg.K
	Reference Temperature	300K
	Turbulent Prandtl	0.7
	Turbulent Schimidt	0.7
	Absorption coefficient	0.1m^{-1}
	Reference Density	1.2kg/m^3
Fuel	Heat of combustion	4.5x10^7J/kg
	Boiling point	371 K
	Formula	C_7H_{16}
	Soot Coefficient	S= 0.308, y_s= 0.037 from [2]
Initial Conditions	Velocity	0.0 0.0 0.0 m/s
	Initial Temperature	300 K
	Pressure	101325.0Pa
	Turbulence Kinetic Energy	1 x 10^{-6} m^2/s^2
	Dissipation Rate of Turbulent Kinetic Energy	1 x 10^{-9} m^2/s^3
	Mixture Fraction	0.0
	Fuel Fraction	0.0

Table 16: fire, air and room properties and initial values

6.2 Results

6.2.1 Computational times

The mesh used for this simulation is a structure mesh with cells of 10cm in each side and it is composed by:

- Number of vertices: 959805
- Number of cells: 923538

The total time for running this case in 20 processors was: 93:15:53.3 h:m:s with an automatic mean time step of 0.4989s.

6.2.2 Heat release rate

In Figure 21, the heat release rate of the experiment and the heat release of the simulation are presented. The curve in magenta represents the input HRR in the simulation whereas the blue one represents the output HRR applying the Peatross and Beyler model [17]. In this model, when the oxygen concentration (OC) is less than 21% the mass loss rate will decrease with the equation:

$$Q = Q_0\left(0.1\times 100\times X_{0_2} - 1.1\right) + Q_{ext}$$

Where Q_0 is the mass loss rate defined by the user, X_{0_2} is the OC and Q_{ext} is an external mass flow rate that can be added. Figure 21 reveals that, there is a significant difference between the curve measured in the experiment (dot curve) and the curve determined by the implementation of the Peatross and Beyler model in ISIS. This difference can be observed in two aspects: the shape of the curve and the values. Both curves are similar in the raising part, but the curve of the simulation shows a peak and subsequently decreases until it arrives at the steady state. The experimental curve reaches the maximum and stays around that value until it descends. The disparity between the functions is larger in the region of the plateau; this value is around 1184kW in the curve of the test and around 900kW in the computed curve.

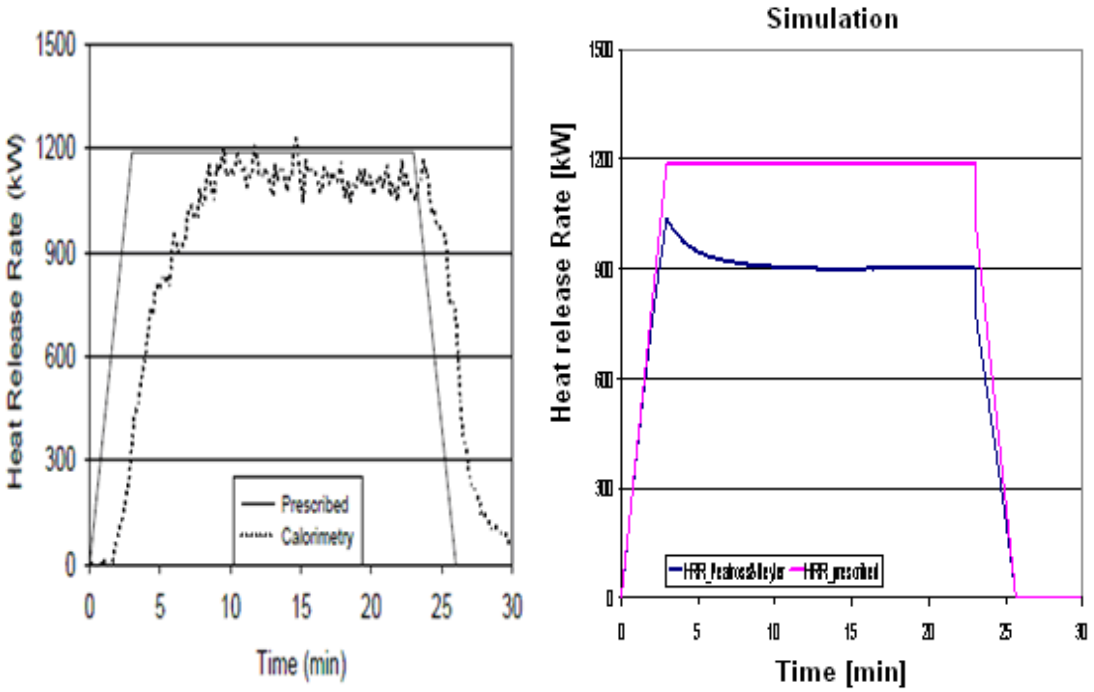

Figure 21: Heat Release Rate [kW] of the experiment and the one of the simulation vs. time [min] [4]

Figure 22 shows the relative difference between the input curve and the one used in the simulation. The error in the steady period is almost 25%. Taking into account that the HRR is one of the most influential parameters, it is reasonable to think that results such as temperatures and heat fluxes will be under predicted.

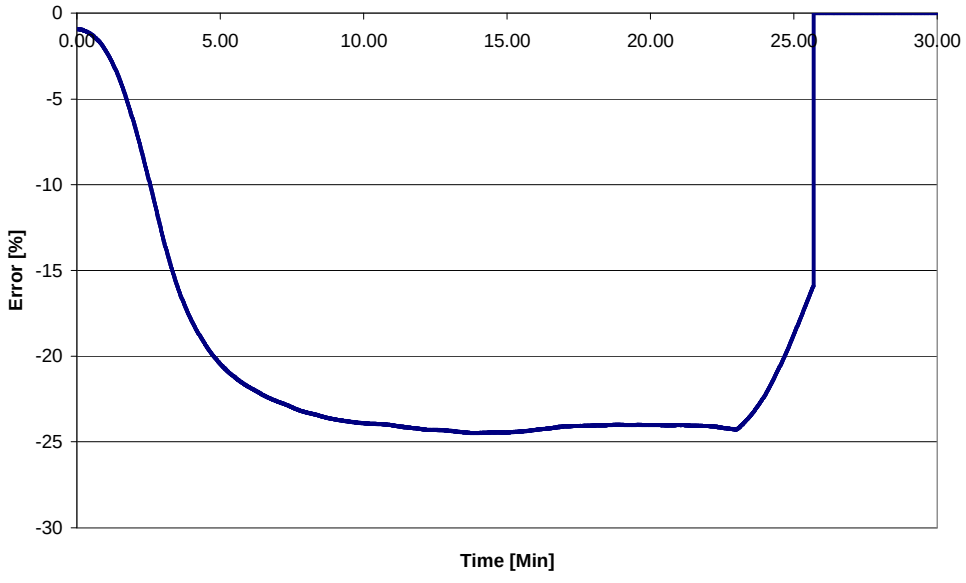

Figure 22: Relative error between the heat Release Rate of the experiment and the one of the simulation vs. time [min]

Table 17 illustrates the peaks of the HRR, in the test and in the simulation, and the relative difference between them. The error is about half of the error of the steady state. This suggests that taking the error in one point can be insufficient for quantification of the quality of a simulation.

	Peak_sim	Experiment	E[%]
HRR	1037.21	1190	-12.83954

Table 17: Relative error between the peak of the HRR in the test and in the simulation

6.2.3 Species concentration (SC)

In Table 18, the relative error of the species concentration is shown. In all the cases the delta is under-predicted.

	Peak_sim	Delta_sim	Experiment	E[%]
O2-1	0.176047	0.032953	0.052	-36.62962
O2-2	0.206163	0.00285	0.006	-52.5
CO2-4	0.01748	0.01748	0.032	-45.37594

Table 18: Relative error between the delta of the SC in the test and in the simulation

In this case, the difference is bigger than the one of the HRR. Because the HRR is lower than the one in the experiment the consumption of oxygen is lower too. In the upper layer, the discrepancy is smaller than in the lower layer. This was also observed in the previous simulations. Also a mistake in the chemical formula used as input in the simulation was discovered, this error makes the oxygen consumption smaller than it should be (9 molecules of oxygen were consumed per molecule of fuel instead of 11).

It can be confirmed by observing Figure 23, where the species concentration of the test is shown in the left part of the chart and the one of the simulation in the right part. It is important to mention that the shape of all the curves is similar in the simulation and in the test because it shows that the model is capable of represent qualitatively what is happening in the test, although it has a quantitative error.

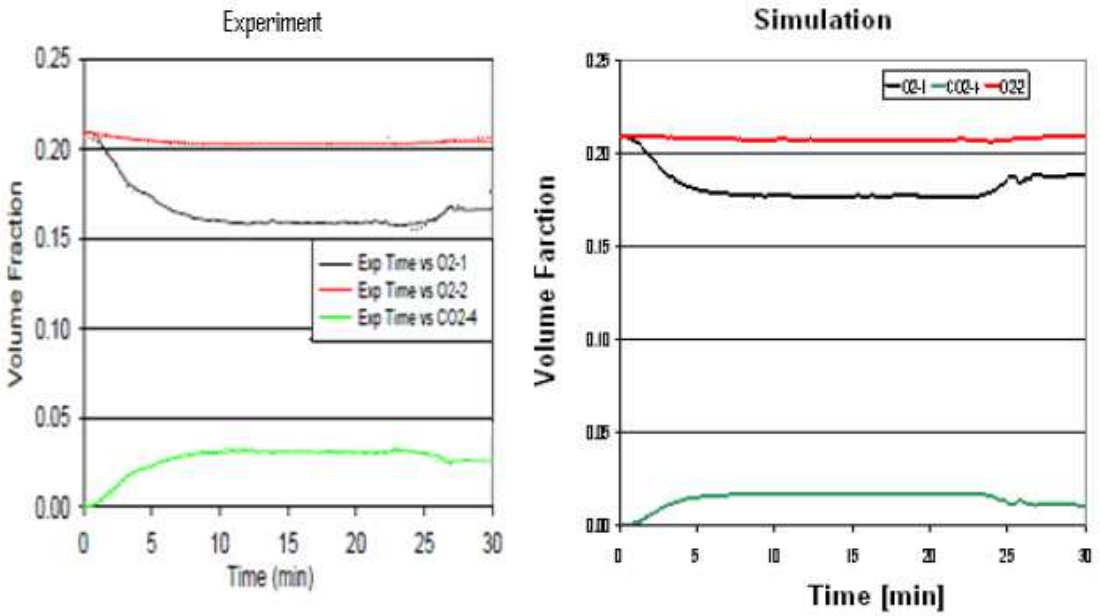

Figure 23: Species concentration vs. time [min] [4]

6.2.4 Target temperature

The distribution of temperatures in the plane X=10.85 at steady state can be observed in Figure 24. In this plane, the measurement point of the cable B and the cable F are presented. At 1000s, the temperature is in steady state, the hot layer and cold layer can be detected.

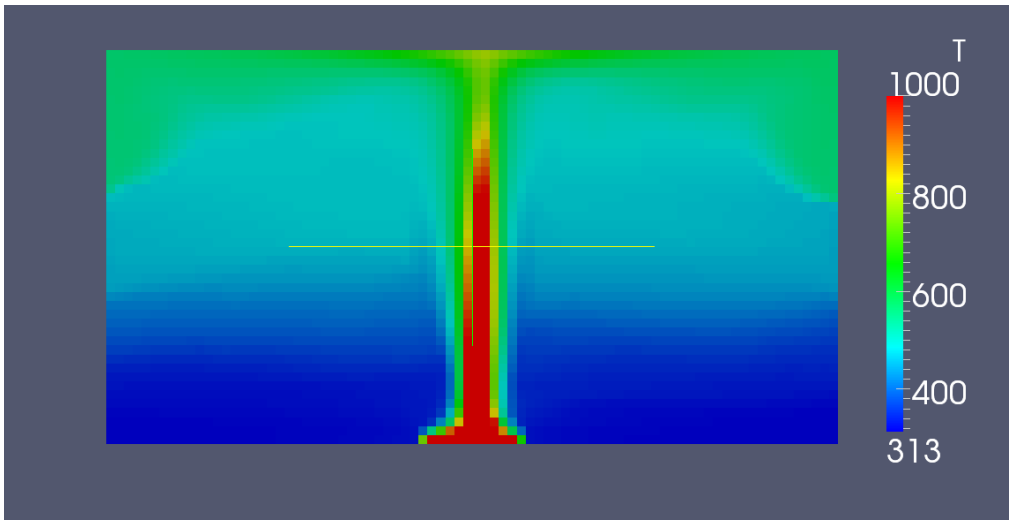

Figure 24: temperature [K] distribution in the plane X=10.85m at t=1000s

6.2.4.1 Cable B temperature

The temperature in the gas near the cable B is depicted in Figure 25 for the experiment (left) and for the simulation (right). They are similar in the growth phase but the simulation curve reaches a steady state while the temperature in the test continues to rise until it arrives at a peak and starts to decrease. This dissimilarity in the curves is caused by the different shape of the HRR curves (Figure 19), while the measured one remains constant the computed one descend to a plateau that is lower than the measurements. The latter explains the underpredicted temperature in the simulation.

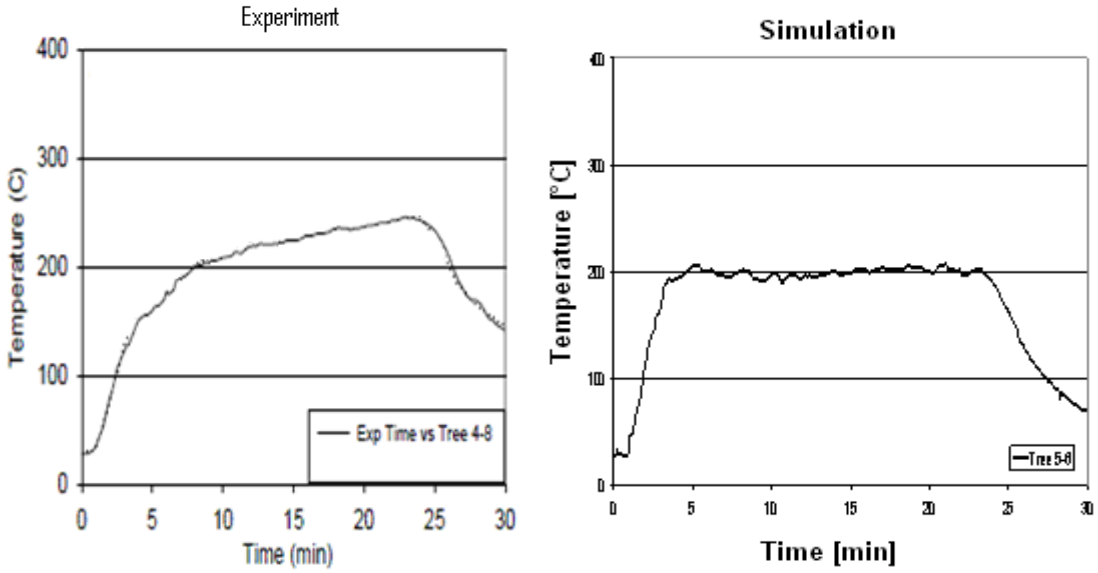

Figure 25: Temperature[k] in the cable B vs. time [min] [4]

Table 19 shows the relative difference between the variations of the temperature in the gas near the cable B. This difference can be correlated with the HRR using the formula used in NUREG-1934[3] table 4-3:

$$\frac{\Delta T}{T} = \frac{2}{3}\frac{\Delta Q}{Q}$$

Which is derived from $T - T_0 = cQ^{2/3}$. The $\frac{\Delta Q}{Q} = 100\left(\frac{1184kW - 900kW}{1184kW}\right)$ is around 24% and the $\frac{\Delta T}{T}$ is 16.83% as it can be observed in Table 19, dividing these values it is obtained:

$$\frac{\Delta T / T}{\Delta Q / Q} = \frac{16.83\%}{24\%} = 0.70$$

This value is close to 2/3 of the equation, suggesting that the relationship is correct.

	Peak_sim	Delta_sim	Experiment	E[%]
Cable B, tree 4-8	207.473	180.473	217	-16.83272

Table 19: Relative error between the deltas of the cable temperatures

6.2.4.2 Cable F temperature

The temperatures near the cable F are illustrated in Figure 26. The results are similar to the ones for cable B. The temperatures are lower than the previous ones since the measurement point is further away from the fire than the target B.

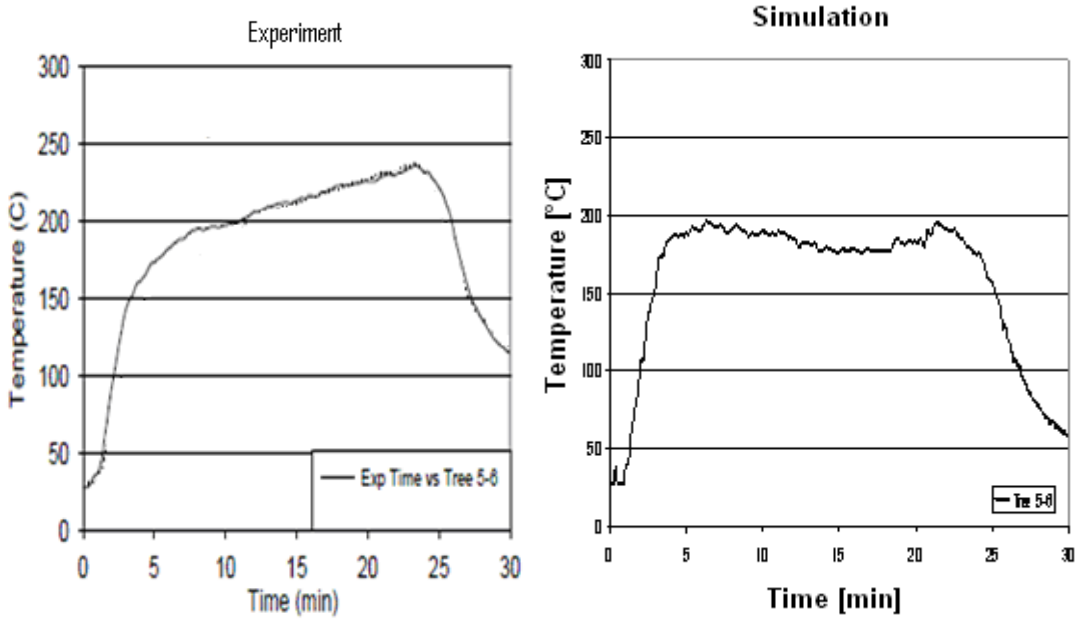

Figure 26: Temperature [k] in the cable F vs. time [min] [4]

The relative error between the variations of the temperature is shown in Table 20. For this case, the relationship between the HRR and the temperature is:

$$\frac{\Delta T / T}{\Delta Q / Q} = \frac{17.98\%}{24\%} = 0.749$$

This is again close to the 2/3 of the formula, confirming the validity of the equation.

	Peak_sim	Delta_sim	Experiment	E[%]
Cable F, tree 5-6	195.957	168.957	206	-17.98204

Table 20: Relative error between the deltas of the cable temperatures

6.2.5 Wall heat flux

The Total Heat Flux (THF) on the east wall at two different points is shown in Figure 27. Although the divergence in the shape of the curves and in the values is large, the growth phase of the graphs is similar. The difference in the shape is the result of the difference in the shape of the HRR curves, while the difference in the values can be attributed to two main reasons: the difference between the HRR steady state and the tendency to under predict the heat flux of the simulations, especially in convective heat flux.

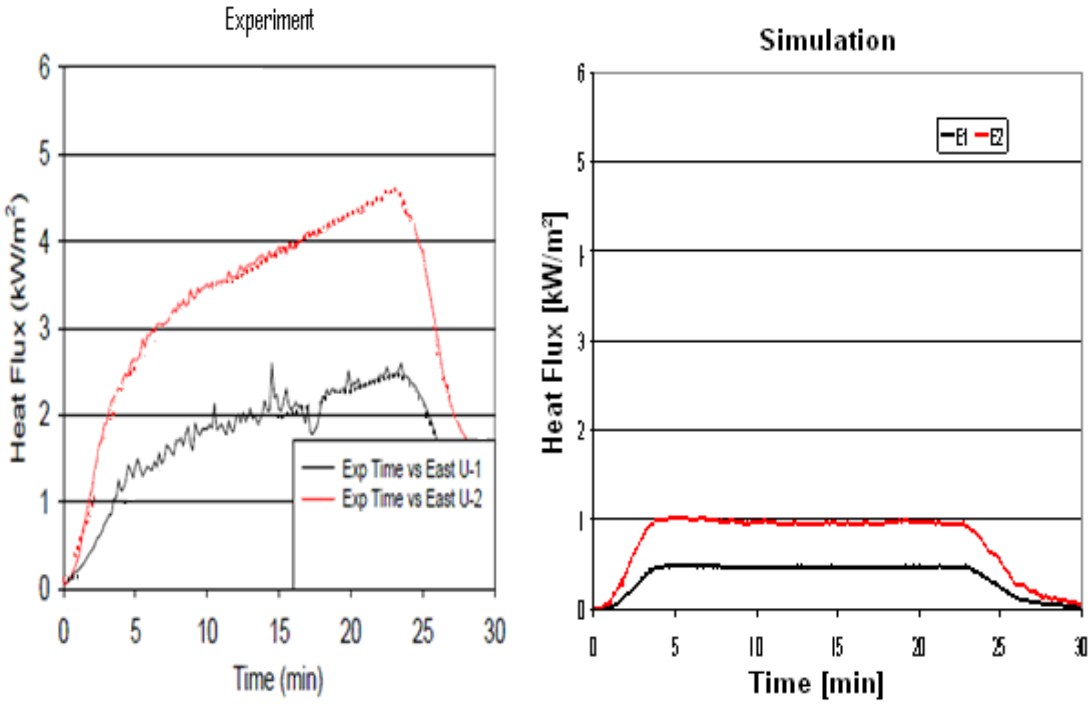

Figure 27: Total Heat Flux [Kw/m²] in the East wall vs. time [min] [4]

The Curves of the THF for the north wall are presented in Figure 28. The same differences appear as mentioned for the previous curve.

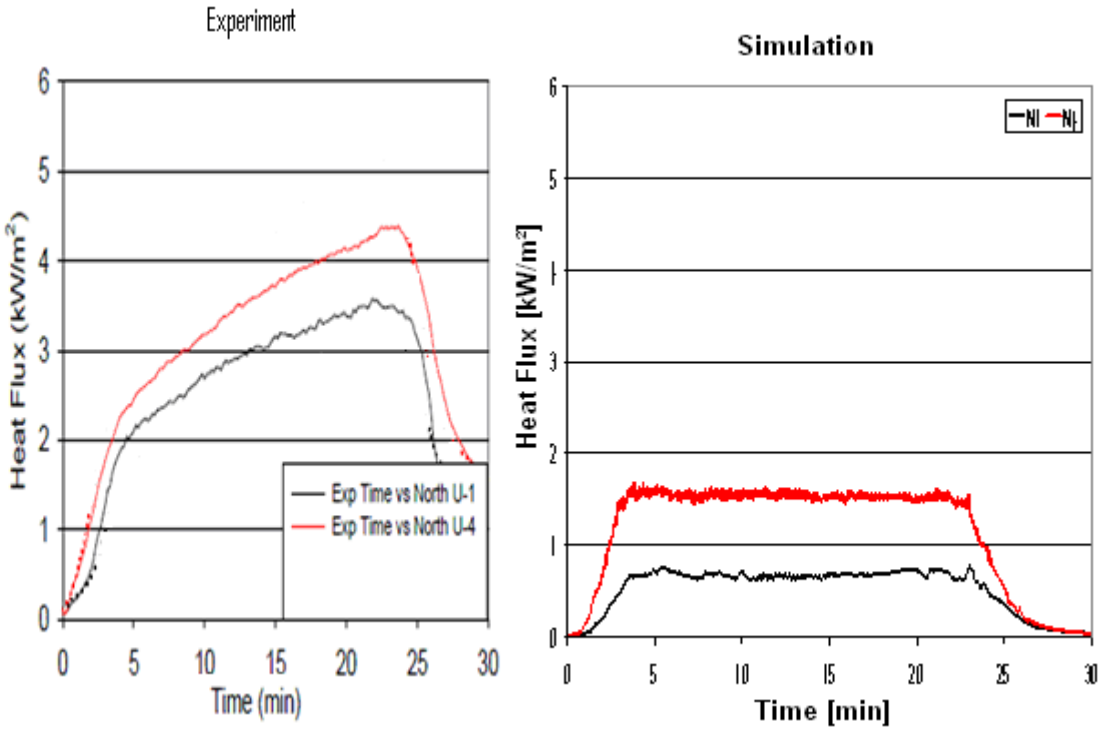

Figure 28: Total Heat Flux [kW/m²] in the north wall vs. time [min] [4]

The diagram of the THF on the ceiling is presented in Figure 29 with similar results.

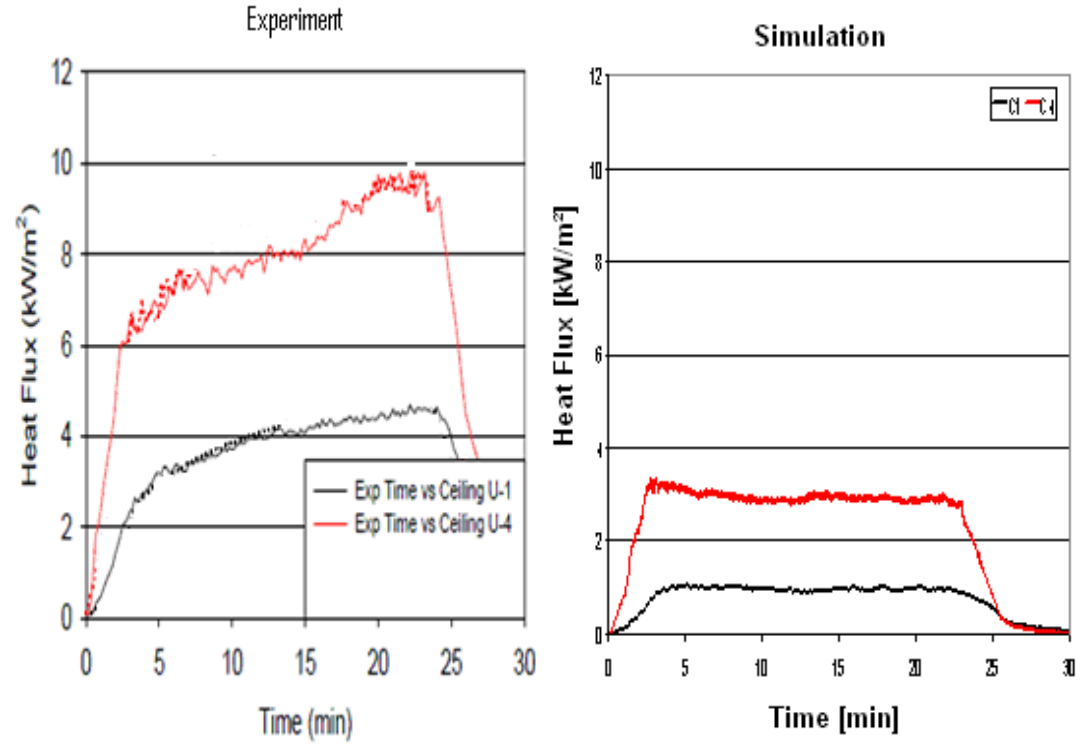

Figure 29: Total Heat Flux [kW/m²] in the ceiling vs. time [min] [4]

The same graph for measurement at floor level is displayed in Figure 30; the outcomes are comparable to the previous ones.

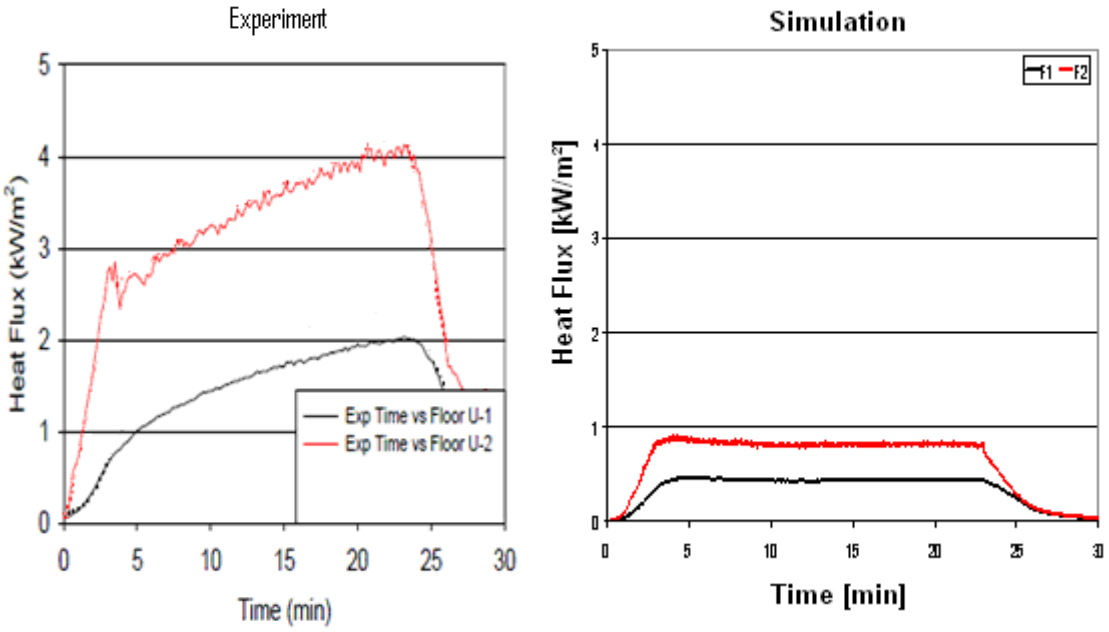

Figure 30: Total Heat Flux [kw/m²] in the floor vs. time [min] [4]

The difference between the measured peak values and the computed ones are summarised in Table 21. In these cases, the values are among -66% and 79%, expressing a big divergence between the experiment and the simulation. Taking the values that relates the HRR with the total heat flux form the NUREG 1934 [3], the HRR is related to the THF by the formula:

$$\frac{\Delta THF}{THF} = \frac{4}{3}\frac{\Delta Q}{Q}$$

With that equation the expected difference would be around 32%. This suggests that there is an under-prediction of the heat fluxes due to a bad representation of the physical phenomenon.

	Peak_sim	Delta_sim	Experiment	E[%]
E1_THF	0.493381	0.493381	2.36	-79.094
E2_THF	1.025077	1.025077	4.5	-77.2205
N1_THF	0.767642	0.767642	3.15	-75.6304
N4_THF	1.686959	1.686959	5.09	-66.8574
C1_THF	1.050666	1.050666	4.62	-77.2583
C4_THF	3.34471	3.34471	9.88	-66.1467
F1_THF	0.462883	0.462883	1.97	-76.5034
F2_THF	0.908376	0.908376	4.07	-77.6812

Table 21: Relative error between the peaks of the THF

6.2.6 Wall temperatures

The distribution of temperatures in the north wall and ceiling can be observed in Figure 32. The highest temperature is in the centre of the ceiling where the plume impinges. The temperature decreases as the distance from this point increases. The hot layer stays more or

less constant, except for the corners where it goes down. The reason for this is that the smoke arrives at the wall and continues to move downward also the loss of buoyancy affect this height. The shape of the distribution of the temperatures seems reasonable, at least in a qualitative way.

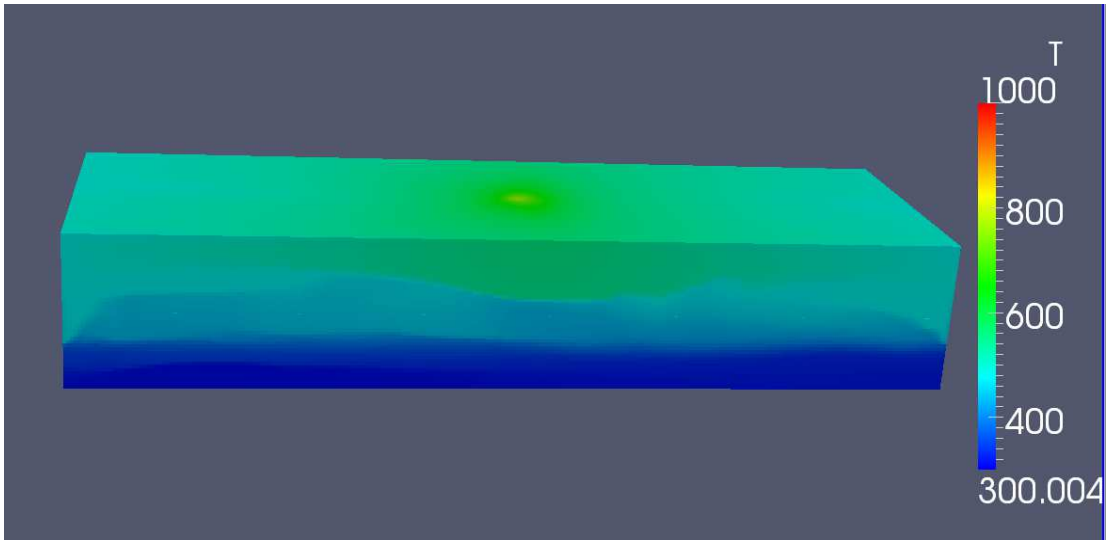

Figure 31: Distribution of temperature [k] in the north wall and ceiling

The temperature measured in the north wall is displayed in Figure 32. The difference between the experimental values and the computed are related with the difference in the HRR. The experimental curve increases until the heat release rate reaches the maximum value (Figure 18) and then starts to descend, while the computed curve grows until it reaches the lower steady state value. The discrepancy between the values is very big. Whereas the curve in the point N4 reaches 200°C for the test, it does not even reach 100°C for the simulation.

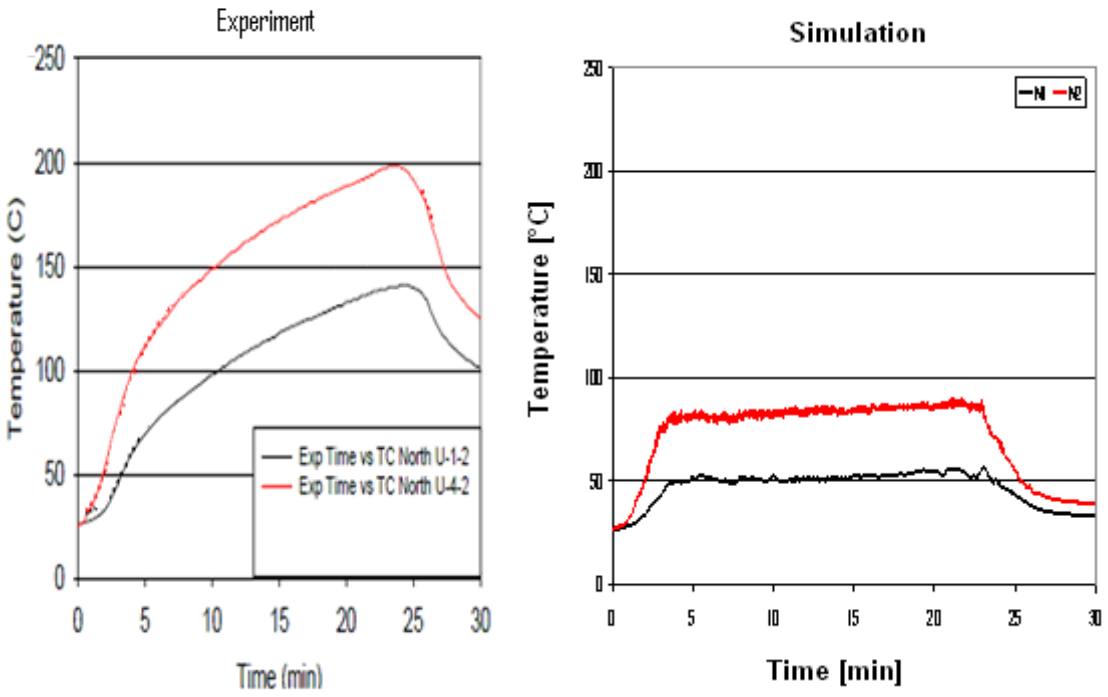

Figure 32: Temperatures [k] on the north wall vs. time [min] [4]

Similar results can be observed for the temperature in the east wall. This is also for the values obtained at the floor and ceiling.

In Table 22, the error in predicting the experimental values can be observed. The error is among 58% and 77% that is in the order of the error in the total heat flux. This makes sense for the reason that the temperature in these places is related with energy that arrived at these points.

	Peak_sim	Delta_sim	Experiment	E[%]
E1_temp	46.511	19.511	87	-77.57356
E2_temp	65.67	38.67	146	-73.5137
N1_temp	57.066	30.066	114	-73.62632
N4_temp	90.236	63.236	172	-63.23488
C1_temp	66.668	39.668	155	-74.40774
C4_temp	146.122	119.122	287	-58.49408
F1_temp	44.614	17.614	54	-67.38148
F2_temp	60.339	33.339	119	-71.98403

Table 22: Relative error between the variations of the temperature

6.2.7 Sensitivity analysis

A sensitivity analysis was carried out in order to know the variation of the outputs with the variation of the HRR. The HRR was increased and decreased by 10% and the variation of the outputs is the one described in Figure 33. The deviation is bigger in the heat flux that can be related with the factor of variation shown in the NUREG-1934 [3].

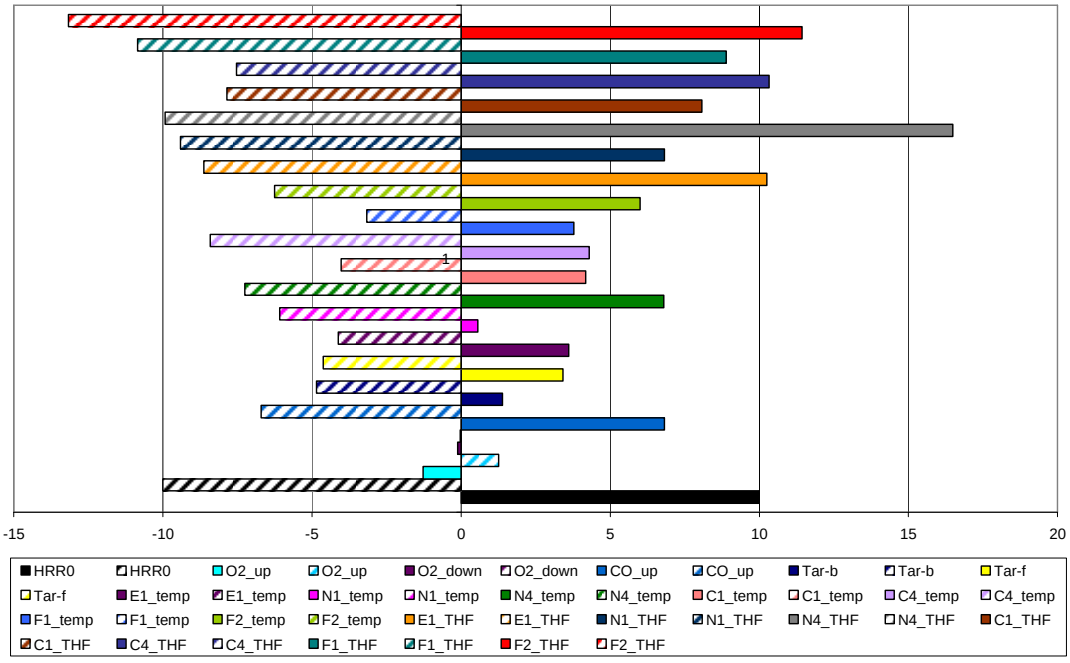

Figure 33: variation in the peak values for a change of ±10% in HRR

In Table 23, the power dependence of the outputs related with the most important inputs is presented. For this case the expected change in the heat flux with a change of 10% in the HRR is 13.33% which are no far from the obtained values. For the temperature, this law is also

applicable; the anticipated value for the temperature is 6.66% and the values attained are in this order. The non dimensional number applied to the change of the HRR in the program seems to be correct for the heat flux and the temperature in the gas and walls in most of the case. On the other hand, it does not seem to be followed for the species concentration, for OC the variation is 1% in the higher part and smaller in the lower part.

Output Quantity	Important Input Parameters	Power Dependence
HGL Temperature	HRR Surface Area Wall Conductivity Ventilation Rate Door Height	2/3 -1/3 -1/3 -1/3 -1/6
HGL Depth	Door Height	1
Gas Concentration	HRR Production Rate	1/2 1
Smoke Concentration	HRR Soot Yield	1 1
Pressure	HRR Leakage Rate Ventilation Rate	2 2 2
Heat Flux	HRR	4/3
Surface/Target Temperature	HRR	2/3

Table 23: Sensitivity of model outputs [3]

6.2.8 Simulation without the Peatross and Beyler model

A simulation without the Peatross and Beyler model and with a grid refinement in the boundaries (walls) was run in order to achieve better results. The same variables, as in the previous sections, were computed. Without the use of the model and the changes in the grid at walls, the HRR curve will follow the curve proposed by the NUREG-1824 and the result should be closer to the experimental ones.

The difference between the experimental values and the calculated ones is smaller than the previous. In the case of the oxygen concentration in the upper layer, the difference is 5.5% that shows a good agreement between the simulation and the experiment. This difference is less that 10% with is a reasonable range for error. The difference in the CO2 is -24.95%, which is 12.5% less than in the previous. These values show that the simulation is more appropriate for this scenario but the creation of carbon dioxide is not totally correct. Although the values for the low oxygen concentration are closer, the error is still big; this was observed in the previous section too.

	Peak	Delta	Exp	E[%]
O2-1	0.154112	0.054888	0.052	5.55332
O2-2	0.205213	0.003787	0.006	-36.8796
CO2-4	0.024015	0.024015	0.032	-24.95344

Table 24: Relative error between the delta of the species in the test and in the simulation

Table 25 shows the difference between temperature at the target for the simulation and the test. The discrepancy for these cases is around 16%. This can be considered a good agreement between the result of the test and the computed results taking into account the uncertainty in the measurements (5% for temperature) and the uncertainty in the HRR (17% of uncertainty). Although the values of the peaks are different, the shape of the curve is similar (as it can be observed in the figure 34).

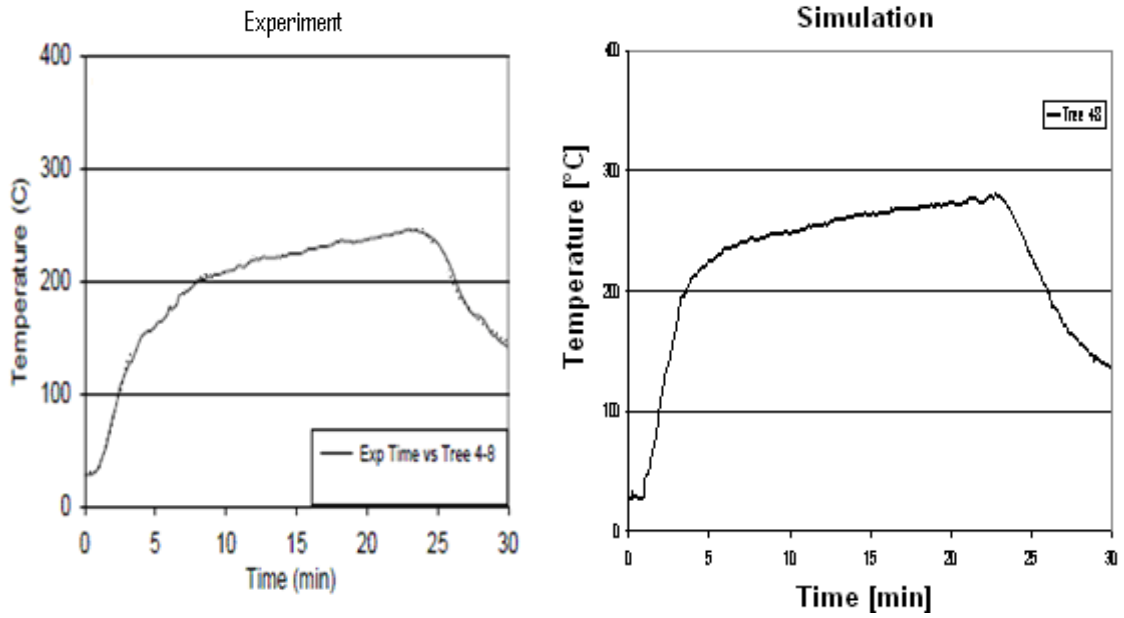

Figure 34: Temperature [°C] in the cable B vs. time [min] [4]

The difference in the curves is mostly in the first part, where the simulation temperature grows faster and arrives at a higher value before changing the slope. Then, both curves have a similar slope and reach a peak almost at the same time. The decreasing part of the curves is comparable too.

	Peak	Delta	Exp	E[%]
Tar-b	280.20	253.201	217	16.6825
Tar-f	267.00	239.998	206	16.5039

Table 25: Relative error between the deltas of the cables temperature

Table 26 shows the divergence between the experimental values of the total heat flux and the simulated results. In spite of the decrease in the discrepancy, the error is still bigger than 50%. This shows a problem in the simulation to calculate the heat flux in the walls.

	Peak	Delta	Exp	E[%]
E1_THF	0.946215	0.946215	2.36	-59.90615
E2_THF	1.28239	1.28239	4.5	-71.50244
N1_THF	1.08968	1.08968	3.15	-65.40698
N4_THF	2.394412	2.394412	5.09	-52.95851
C1_THF	1.234753	1.234753	4.62	-73.27374
C4_THF	2.363694	2.363694	9.88	-76.07597
F1_THF	0.638536	0.638536	1.97	-67.587
F2_THF	1.305198	1.305198	4.07	-67.93125

Table 26: Relative error between the peaks of the THF

Table 27 illustrated the difference between the calculated and measured temperatures; the error is smaller than the ones of the previous simulation. The error is between -20% and 30%. For the negative values of the error, the measurement points where situated in the upper part of the room. This means that there is an underestimation of the temperature values in the higher region. While, there is an overestimation of the values that are in the lower region. This was observed in the previous chapter.

	Peak	Delta	Exp	E[%]
E1_temp	129.818	102.818	87	18.18161
E2_temp	166.651	139.651	146	-4.34863
N1_temp	147.421	120.421	114	5.632456
N4_temp	247.882	220.882	172	28.41977
C1_temp	156.284	129.284	155	-16.591
C4_temp	257.811	230.811	287	-19.578
F1_temp	95.205	68.205	54	26.30556
F2_temp	159.492	132.492	119	11.33782

Table 27: Relative error between the variations of the temperature

The temperature in the east wall is shown in Figure 35. The curves have a similar shape and reach the peak in similar time. Although the temperature is underpredicted for the thermocouple in the higher part, the values are really close. For the thermocouple in the lower part, the temperature is over predicted and the difference in the peak values is bigger.

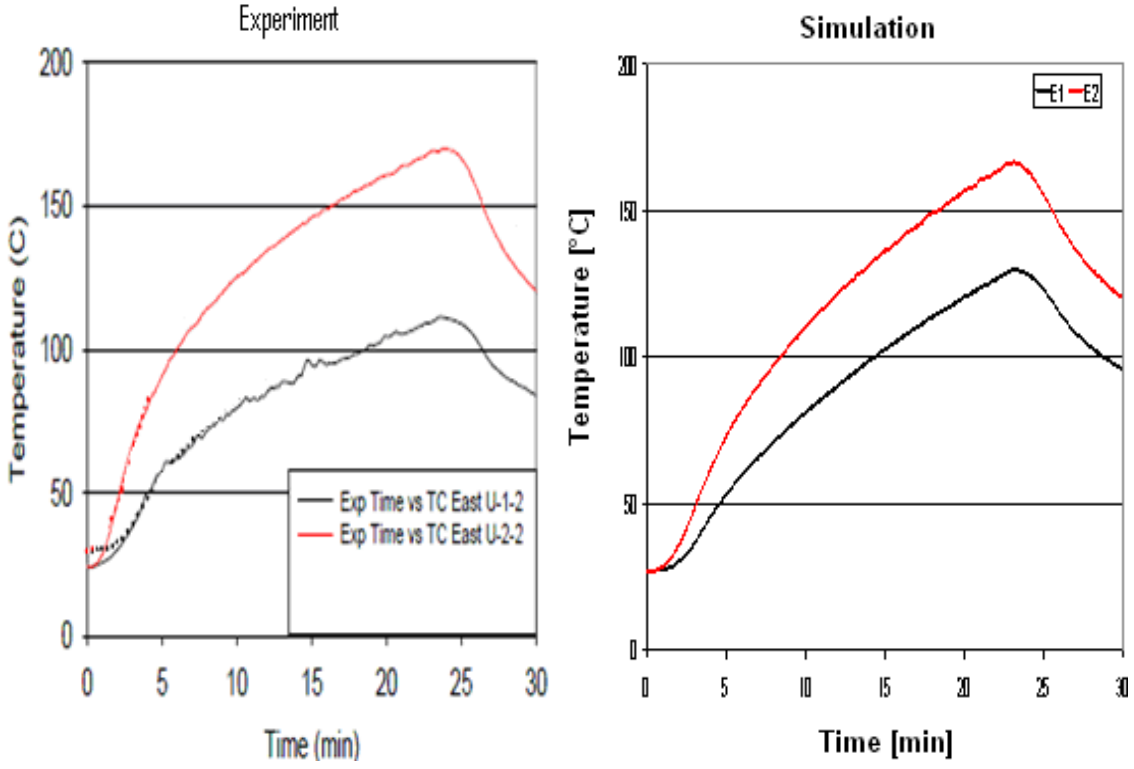

Figure 35: Temperatures [°C] on the East wall vs. time [min] [4]

6.3 Discussion

A good agreement in the shape of the species concentration curves was noticed but the quantitative results differ between the test and the simulation for the blind simulation. An error in the formulation of the chemical reaction in the simulation was discovered. This error and the disparity in the HRR can explain the difference in the oxygen concentration in the higher part but the difference in lower part is bigger. The mistake in the chemical reaction was detected in the blind simulation but it was corrected for the last case without the Peatross and Beyler model. After the correction of HRR, the wall definition and the oxygen consumption, the values for the oxygen in the upper layer were close to the experimental ones. The result for the lowest part was better but it was still far from the experimental one. This was also observed in the case of chapter 5.

For the blind simulation, the difference in the values of the temperature in the air is because of the discrepancy between the HRR curves. There is also a difference in the shape of the curve. This difference is a consequence of difference in the shape of the HRR curves and the energy balance in the room. Because of the coarse grid in the walls boundaries, there is more loses in the simulation than in the experiment. This causes a lower conduction of energy through the wall.

For the corrected case, there is a good agreement in the values of the temperature in the air and in the shape of the curves. There is an over estimation of the peaks values. This was observed in the case of chapter 5 too.

There is a very big disparity in shape of the curves and the values for the total heat flux between the simulation and the test for the case of the blind simulation and for the case without the Peatross and Beyler model. This big divergence makes the calculated values of the total heat fluxes not trustable. The difference in the temperature at the walls are between --20% and 30% of error for the corrected case, this is smaller difference than the one for THF. This confirms that the representation of the temperature in the boundaries is better than the representation of the THF.

The sensitivity analysis shows that the relation presented in NUREG 1934[3] for the inputs and outputs (table 23) seems to be correct for the THF and the temperatures but not for the species concentration where the variation are smaller than the expected ones.

7. Real case I

7.1 Methodology

For analyzing this scenario the modelling process described in the NUREG-1934 [3] is chosen, this model has six steps:

- Define fire modelling goals and objectives
- Characterize the fire scenarios
- Select fire models
- Calculate fire generated conditions
- Conduct Sensitivity and uncertainty analysis
- Document the analysis

The scenario is a fire compartment with three electrical pumps inside each pump contains 120l of oil and is feed with a 6kV cable. The room has two ventilation systems with different rates of air movement. Due to the fact that these pumps are considered safety equipment, at least one should continue working in the case of a fire.

The geometry of the room with three pumps is shown in Figure 36. The size of the room is 25m long, 8m wide and there are two different ceiling heights, one of 3.3m and the other of 5.5m. A double door is the only opening in the room. The three pumps are separated by walls of 4.4m long, 2.4m high and 0.15m wide. The origin of coordinates can be found in the Figure 36 in the right upper corner. The value Z=0m corresponds to the floor level.

The ventilation system is composed of two sub-systems, one for normal operation with an inflow and two extractions of a total of 7000m³/h and an emergency system integrated by two inflows of 14000m³/h and an extraction of 28000m³/h. The Emergency system starts to act when the temperature is higher than 40°C. In a fire situation, the person in charge chooses to maintain the ventilation or turning it off. There are fire dampers in the system and they are activated in the same way, manually from the control room. The ducts are represented by the red rectangles in Figure 36 and the grids are shown in light blue. The outlets for the normal operation system are grid 4 and grid 5. The inlet is made through the grid 1. For the emergency system, extraction is made through grid 3 and inflow through grid 2.

The room is a fire compartment itself, the door is 1 hour fire resistant and the walls, ceiling and floor are of concrete of at least one hour fire resistance. A deluge system was installed over each pump. There are smoke detection and cameras in the room that are connected to a main control room. In case of alarm, site personnel will check if the fire is real and will start the deluge if is necessary. Personnel will also give advice to the intervention team.

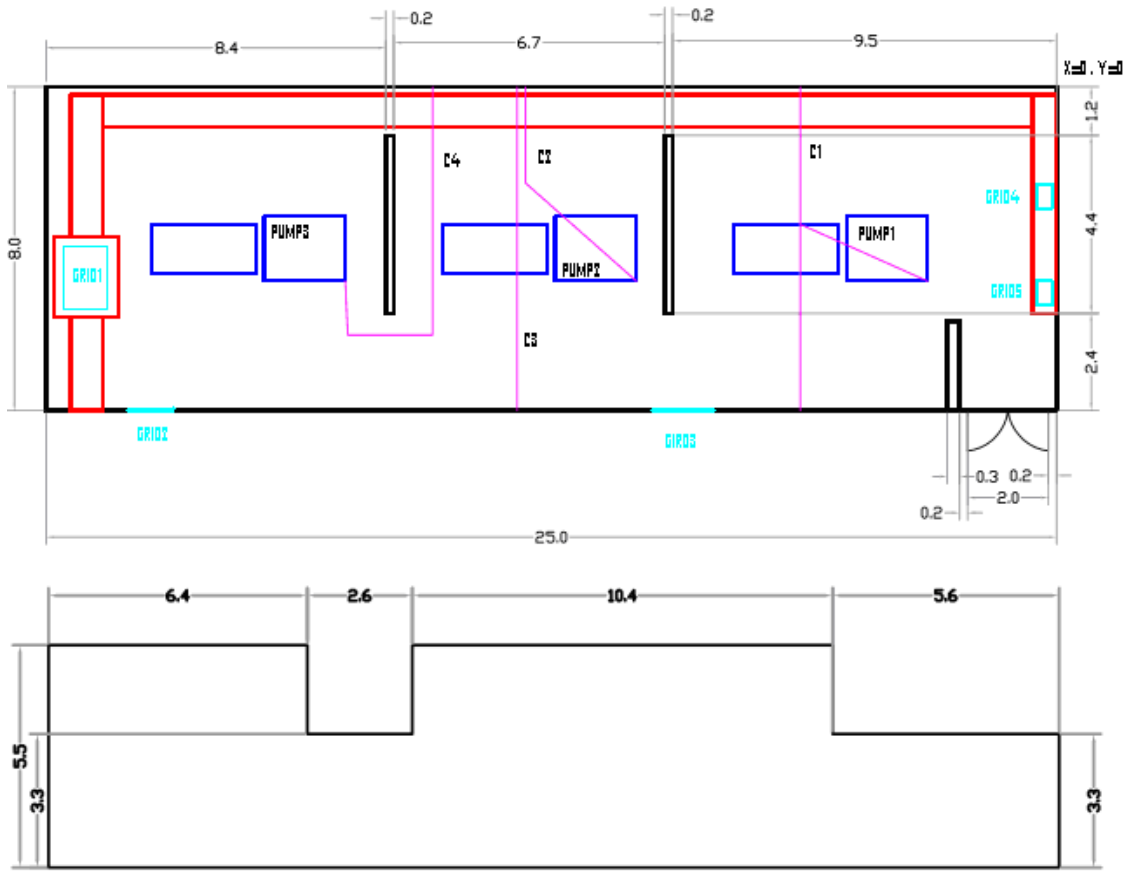

Figure 36: plan of the "pumps room"

Each pump contains 120l of oil and is feed by 6kV cables. Underneath the pumps, there is a container for oil spill of 1.1m x1.1m surface. There are no other combustible materials in the compartment in a relevant amount. For this reason, no secondary sources are considered. The fire chosen for this evaluation is a spill of oil of the. The characteristics of similar oils as the one used in the pumps are displayed in Table 30.

Parameter	Value	Source
Effective Fuel Formula	C_nH_{2n+2}	Assumption ($C_{14}H_{30}$)
Mass burning rate	0.039 kg/s.m^2	NUREG-1805 Table 3-4
Density	760 kg/m^3	NUREG-1805 Table 3-4
Heat of Combustion	46,000 kJ/kg	NUREG-1805 Table 3-4
Heat of Combustion per unit mass of oxygen consumed	13,100 kJ/kg	Hugget 1980, Average value
CO_2 Yield	2.64 kg/kg	*SFPE Handbook*, 4th ed., Table 3-4.16*
Soot Yield	0.059 kg/kg	*SFPE Handbook*, 4th ed., Table 3-4.16*
CO Yield	0.019 kg/kg	*SFPE Handbook*, 4th ed., Table 3-4.16*
Radiative Fraction	0.34	*SFPE Handbook*, 4th ed., Table 3-4.16*
Mass Extinction Coefficient	8700 m^2/kg	Mulholland and Croarkin (2000)

*Material identified as "Hydrocarbon" in SFPE Handbook used to derive properties.

Table 28: Fuel properties [3]

The targets are the cables of the pumps and the pumps themselves. The cables are of the kind 'thermoset' and their failure threshold is taken as 330°C [15]. The failure threshold of the pump is also selected as 330°c, because it is expected that the cables connected to the pump will fail faster than the pump itself since the electrical part of the pump are covered with the motor casing.

7.1.1 Define Fire Modelling Goals and Objectives

The main goal of this analysis is related to the continuity of the operation of the equipment in the compartment and can be stated as:

- To evaluate whether at least one of the three pumps in the room will continue working in the case of a fire.

The performance criteria used for this evaluation are:

- The maximum acceptable exposure temperature for the cables and the pumps is shown in Table 28. The criteria is composed by two part the exposure temperature and the time to failure at that temperature. While temperature grows the time descends.

Exposure Temperature		Time to Failure (min.)
°C	°F	
330 ≤ T < 335	625 ≤ T < 634	28
335 ≤ T < 340	634 ≤ T < 642	24
340 ≤ T < 345	642 ≤ T < 651	20
345 ≤ T < 350	651 ≤ T < 660	16
350 ≤ T < 360	660 ≤ T < 680	13
360 ≤ T < 370	680 ≤ T < 700	10
370 ≤ T < 380	700 ≤ T < 716	9
380 ≤ T < 390	716 ≤ T < 735	8
390 ≤ T < 400	735 ≤ T < 752	7
400 ≤ T < 410	752 ≤ T < 770	6
410 ≤ T < 430	770 ≤ T < 805	5
430 ≤ T < 450	805 ≤ T < 840	4
450 ≤ T < 470	840 ≤ T < 880	3
470 ≤ T < 490	880 ≤ T < 915	2
T ≤ 490	T ≥ 915	1

Table 29: Failure time-temperature for thermoset cables [15]

- The highest suitable radiation for the cables and the pumps are displayed in Table 29. This criterion acts in a similar way than the temperature one.

Exposure Heat Flux		Time to Damage (minutes)
BTU/ft^{2}s	kW/m^2	
<1.0	<11	No Damage
1.0	11	19
1.2	14	12
1.4	16	6
1.6	18	1
1.75 or greater	20 or greater	1

Table 30: Failure time-radiation heat flux for thermoset cables [15]

- The structure stability will be reviewed in order to ensure that the pump will continue working.

There are no people working in the room in a permanent way, so life safety objectives do not apply.

7.1.2 Characterize Fire Scenarios

Different scenarios were chosen in order to have a complete understanding of the diverse variables present in this situation. As it was stated, the main source of fuel is the oil of the pump therefore other small sources are not considered. The different scenarios are:

Ventilation	Fire source	Deluge System	Scenario
The ventilation is not working	Pump 1	On	1.1.1
		Off	1.1.2
	Pump 2	On	1.2.1
		Off	1.2.2
	Pump 3	On	1.3.1
		Off	1.3.2
The ventilation is working at 7000m³/h	Pump 1	On	2.1.1
		Off	2.1.2
	Pump 2	On	2.2.1
		Off	2.2.2
	Pump 3	On	2.3.1
		Off	2.3.2
The ventilation is working at the highest rate (28000m³/h +7000m³/h)	Pump 1	On	3.1.1
		Off	3.1.2
	Pump 2	On	3.2.1
		Off	3.2.2
	Pump 3	On	3.3.1
		Off	3.3.2

Table 31: Scenarios

The scenarios with the fire source in the pump 1 and the pump 3 are covered by the scenarios with the fire source in the pump 2 since fire in this pump will rapidly affect cables from pump 2 and pump 3 because they are closed to the fire plume. In this case, the failure of the pump 1 will lead to a failure if the system.

The scenarios without ventilation lead to higher temperatures in the compartment and to a more threatening scenario because of this, the activation of the deluge system is simulate only for this case. The cases with the ventilation are covered by this scenario.

The following scenarios are analysed: scenario 1.2.1, scenario 1.2.2, scenario 2.2.2 and scenario 3.2.2.

7.1.3 Select Fire Models

The selected fire model is ISIS 3.0.1 as explained previously a CFD model developed for simulations in NPP. The complexity of the room and the position of the targets require a CFD analysis.

The method described in the NUREG 1934 [3] proposes a number of dimensionless parameters to check if the scenarios are inside the range of validation that was performed for different approaches (manual calculations, CFAST, MAGIC and FDS). The method states that if the simulation is between the validation ranges, no further validation is needed. The validation ranges shown in Table 32 were obtained for FDS through comparison of experimental data and simulations. These comparisons were made for several configurations and in different conditions. Then, a statistical analysis was made. The agreement between the simulations and the tests were considered correct if the error was between the measurement uncertainties. NUREG 1934[3] propose that for scenarios that are between the validation range for FDS, the simulation are considered validated and the uncertainty and the error can be found in table 4-1 of this document. The different dimensionless numbers used for this approach are shown in Table 32. The knowledge of the uncertainties and error for each variable gives a degree of reliability to the results.

Quantity	Normalized Parameter	Result		Validation Range FDS
Fire Froude Number	$Q^* = \frac{\dot{Q}}{\rho_\infty T_\infty D^2 \sqrt{gD}}$	2.21		0.4-2.4
Flame Length Ratio	$\frac{H_f + L_f}{H_f}$ $\frac{L_f}{D} = 3.7\dot{Q}^{\frac{2}{5}} - 1.02$	0.73		0.2-1.0
Equivalence Ratio	$\varphi = \frac{\dot{Q}}{\Delta \dot{H}_{O_2} \dot{m}_{O_2}}$ $\dot{m}_{O_2} = 0.23 \times \frac{1}{2} A_0 \sqrt{H_0}$ $\dot{m}_{O_2} = 0.23 \rho_\infty \dot{V}$	No ventilation, open door.	0.105	0.04-0.6
		Ventilation 7000m³, closed door	0.1096	
		Ventilation 28000m³, closed door	0.027	
Compartment Aspect Ratio	$\frac{L}{H}$	4.54		0.6-5.7
	$\frac{W}{H}$	1.45		
Distance Ratio	$\frac{r}{D}$	11.68		2.2-5.7

Table 32: Non-dimensional number

It is important to remark that these statistical analyses are not able for ISIS. It would be interesting to create a data base in order to obtain the uncertainties and error related with each variable in ISIS.

The different models selected for running these simulations are depicted in Table 33. Fixed_soot_fraction was chosen as Soot_model because there were not available the data for using the Moss model neither the Khan model. Even this implies a simplification the expected variation, taking into account previous validations of the software, is in the order of the expected error for radiation. The Peatross and Beyler model was applied because a lack of oxygen was expected, mostly for the case without ventilation.

Model	Parameter	Value
Time management	Initial time	0
	Final Time	5500
	Time step	Automatic_time_step: velocity prediction
	Time order	Order1
Meshing	Geometry	Cartesian_3D
	Type	Structured_mesh
	Space discretization	Finite_volumes
	Type	Gambit_meshing
Physical modelling	Navier-Stokes	Low_mach
	Energy_balance	Enabled
	Turbulence_model	k_ ε
	Combustion model	EBU
	Radiation model	FVM
	Soot_model	Fixed_Soot _fraction
Boundary conditions Walls	Type	Wall
	Velocity	Wall_law
	Temperature	Wall_conduction
Boundary conditions Ventilation	Type	Inflow
	Velocity	fixed_mass_flow_rate
Boundary condition fire source	type	Inflow
	Velocity	Fixed_mass_flow_rate
Turbulence	Wall_law type	Log_law

Table 33: Simulation models

.

The values of the most important variables are depicted in Table 34. The ambient temperature is the higher one before the ventilation start. The soot coefficient was calculated from the soot yields of the Table 28.

Properties	Variable	Value
Air properties	Laminar Viscosity	$1.7x\ 10^{-5}$kg/m.s
	Specific Heat Capacity	1020J/kg.K
	Reference Temperature	313K
	Turbulent Prandtl	0.7
	Turbulent Schimidt	0.7
	Absorption coefficient	$0.1m^{-1}$
	Reference Density	$1.13kg/m^3$
Fuel	Heat of combustion	$4.6x10^7$J/kg
	Boiling point	494.1 K
	Formula	$C_{14}H_{30}$
	Soot Coefficient	s= 0.9735
Initial Conditions	Velocity	0.0 0.0 0.0 m/s
	Initial Temperature	313 K
	Pressure	101325.0Pa
	Turbulence Kinetic Energy	$1 \times 10^{-6}\ m^2/s^2$
	Dissipation Rate of Turbulent Kinetic Energy	$1 \times 10^{-9}\ m^2/s^3$
	Mixture Fraction	0.0
	Fuel Fraction	0.0

Table 34: Simulation values

The geometry used for the simulation is shown in Figure 37; the geometry of the room is really complex. Thus, it was simplified in order to achieve a compartment that could be reproduced. The simplification made where related with the impossibility of represent curved objects in gambit for the structured meshes. For example, the cables and pumps were taken as hexahedrons instead of cylinders. The mesh is a structured mesh with cells of 20cm x 20 cm x20cm, thus the details that are smaller than 20cm cannot be represented. The objects, that were considered not relevant for the movement of the mass and heat, were not represented.

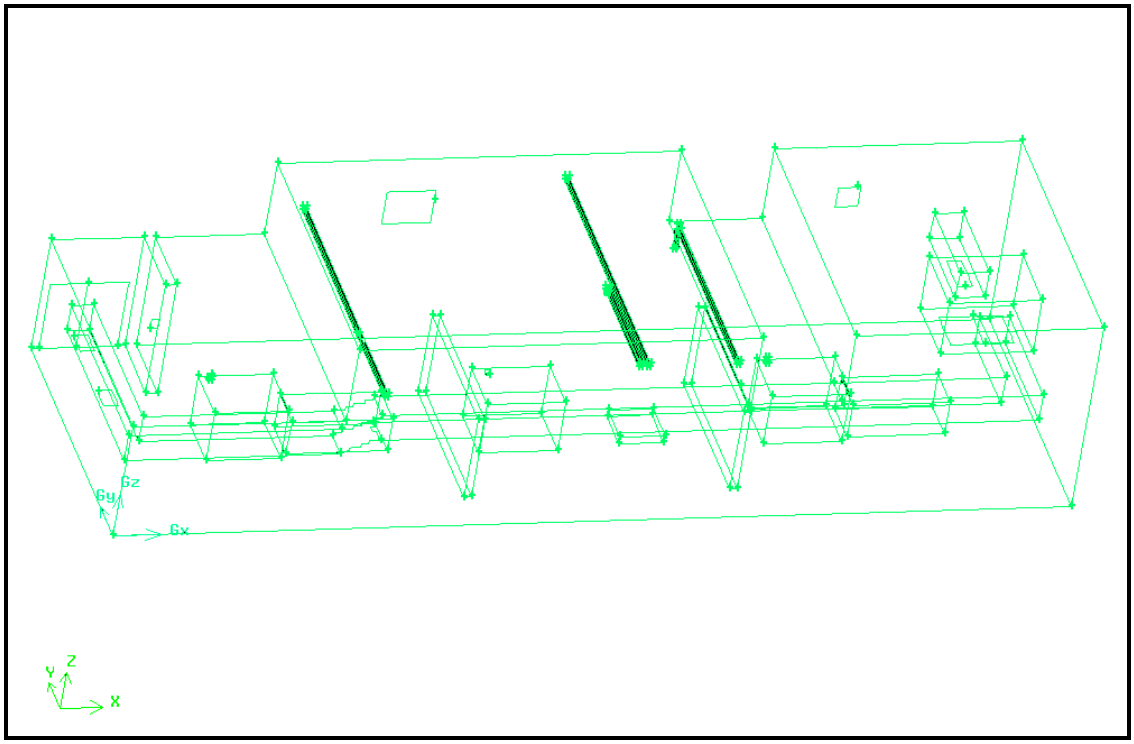

Figure 37: 3D view of the "pumps room"

7.1.4 Calculate Fire-Generated Conditions

The outputs picked for this study were the gas temperature near the cables and the radiant heat flux on these targets. Because the targets are in the higher part of the room, they will probably be in the smoke layer. In the validation of NUREG 1824[4], and there is almost not difference between the temperature in the gases and in the surface of the cable. The criteria of Table 29 will be taken in the gas temperature near the cables. Another essential variable is the duration of the fire.

7.1.5 Sensitivity Analysis

A sensitivity analysis is carried out on the most important variable for the scenario 1.2.2, namely the Heat Release Rate, the value of which can change the results significantly. The study was carried with a HRR 10% higher and a HRR 10% lower than the used in the scenario.

A grid sensitivity study has been performed in order to check the results independence of the grid. The cell size was divided by two in every direction. This generated an increase in the computational time of at least 16 times (2 times in each direction and 2times in the steps) more than the one of the coarser grid. For this reason the simulation was carried out for a smaller duration in time.

7.2 Results

7.2.1 Scenario 1.2.2

The mesh used for this scenario is a structured mesh made with gambit 2.4.6 with cells of 20cm x 20cm x20cm. It is composed by:

- Number of vertices: 130263
- Number of cells: 117473

The total time for running this case in 20 processors was: 33:13:06.9 h:m:s with an automatic mean time step of 0.3734s

The HRR used in scenario 1.2.2 for the ISIS is presented in the Figure 38, the input curve is the magenta one and the curve after applying the Peatross and Beyler model is the blue one. This curve starts with a fast t-square imposed by the user to simulate the growing stage and subsequently, it continues with the Babrauskas pool fire model [2], for the steady state ($k\beta$=0.7 and m_{∞}=0.039). The duration of the fire is almost 1 hour and it extinguishes because all the fuel is consumed. The peak Heat Release Rate is 1485kW and then it starts to decrease until it reaches 1093kW at 57min and after that it descends to 0kW.

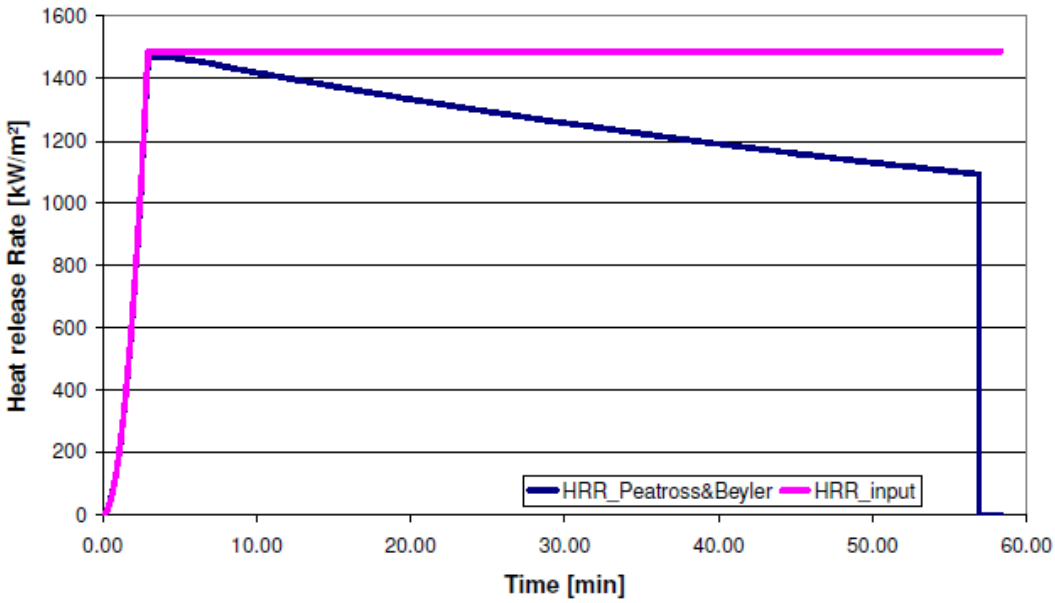

Figure 38: Heat Release Rate [kW] in scenario 1.2.2 vs. time [min]

The different measurement points of the cable are shown in Table 34.

Cable1	6.10	4.00	4.00
Cable2	13.00	1.00	4.70
Cable3	13.50	4.00	4.70
Cable4	15.80	4.00	4.80

Table 35: Target temperature in gas near the cables

Figure 39 depicts the temperature in the cables in the measurement points of Table 34. All the cables are beyond the failure temperature for more time than what is needed for the failure. This means that all the pumps will fail within 18 minutes, creating an unsafe situation.

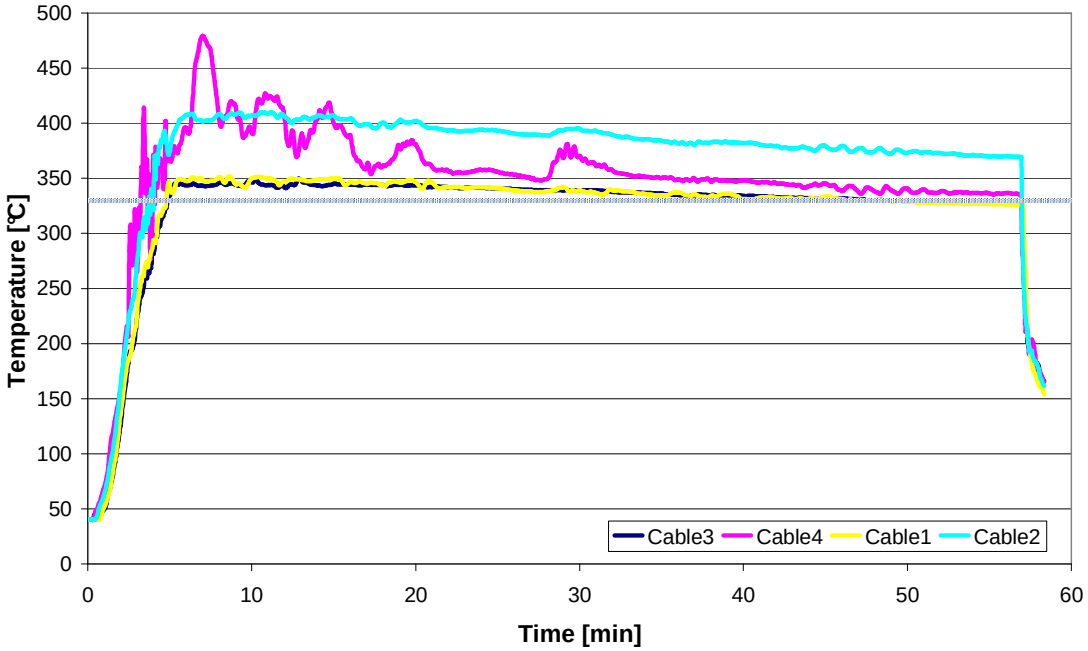

Figure 39: Temperature [°C] in the gases near cables in scenario 1.2.2 vs. time [min]

The temperature distribution in the plane Y=4m and X=6.46m is shown in the figure 40 at 3 and 43 minutes; this pictures confirm the fact that the cable are exposed to a higher temperature than what they can stand. The temperature around the gas near cable 1 in figure 40 (C) and (D) are 330°C or more all around the cable.

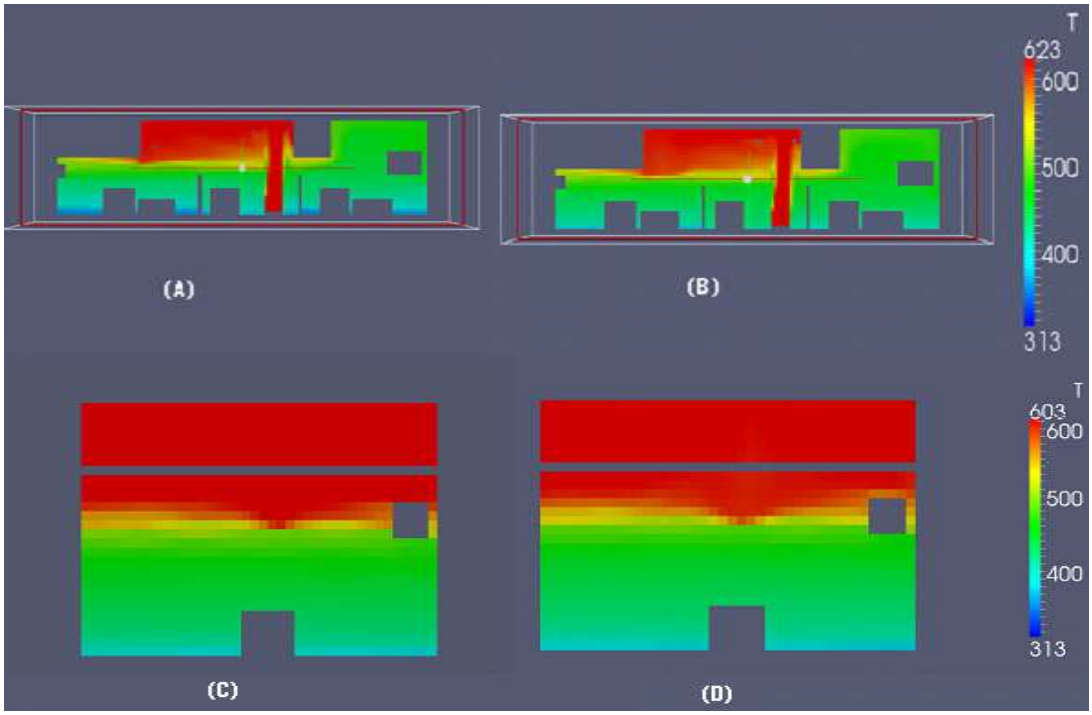

Figure 40: Temperature [K] distribution at planes Y=4m at 3min (A) and 43 min (B) and X=6.46m at 3min (C) and 43 min (C).

The radiation in cable 1 and Cable 4 for 3 different points is depicted in Figure 41. The temperature is below the criteria which is 11kW/m².

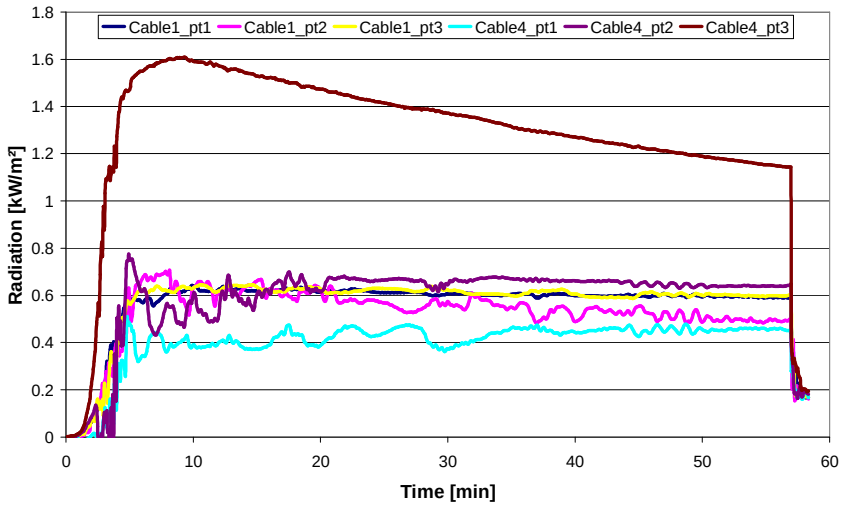

Figure 41: Radiation in Cable 1 and Cable 4

The distribution of the smoke with temperature larger than 200°C is depicted in Figure 44. The smoke almost reaches the door and is spread throughout the room, hampering the intervention of the fire fighters.

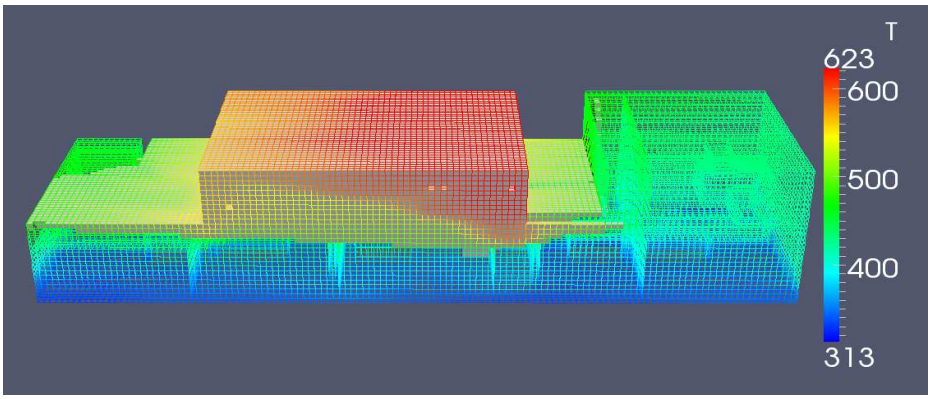

Figure 42: Temperature [K] distribution for the scenario 1.2.2 at 4min

The study of this scenario leads to a negative outcome, this means that the performance criteria selected was overcome generating an unsafe situation. This can be observed in Table 36 where the outputs are compared against the failure criteria. Action should be taken to avoid this scenario or to improve the fire resistance of the cables and the pumps.

Target	Criteria		Peak temperature	Time over Temperature criteria	outcome
	time	Temp			
Cable 1	28 min	330°C	350°C	45 min	Fail
Cable 4	28 min	330°C	475°C	53 min	Fail
Target	Criteria		Peak RHF	Time over Temperature criteria	outcome
	time	RHF			
Cable 1	19 min	11kW/m²	0.7	0 min	No Fail
Cable 4	19 min	11kW/m²	1.6	0 min	No Fail

Table 36: Comparison of simulation values with failure criteria

7.2.1.2 Sensitivity analysis

As it was stated, a sensitivity analysis was performed in order to have knowledge of variation in the temperature of the cables with the change of the HRR. Figure 43 shows the change in the temperature in each cable with a variation of the 10% in the HRR of scenario 1.2.2 by excess and by shortage. The change in the peak of temperature is less than expected following the approach of Table 23 (the variation in temperature should be 2/3 of the variation in HRR) with the exception of the cable 4. This bigger difference can be because this measurement point is in the plume.

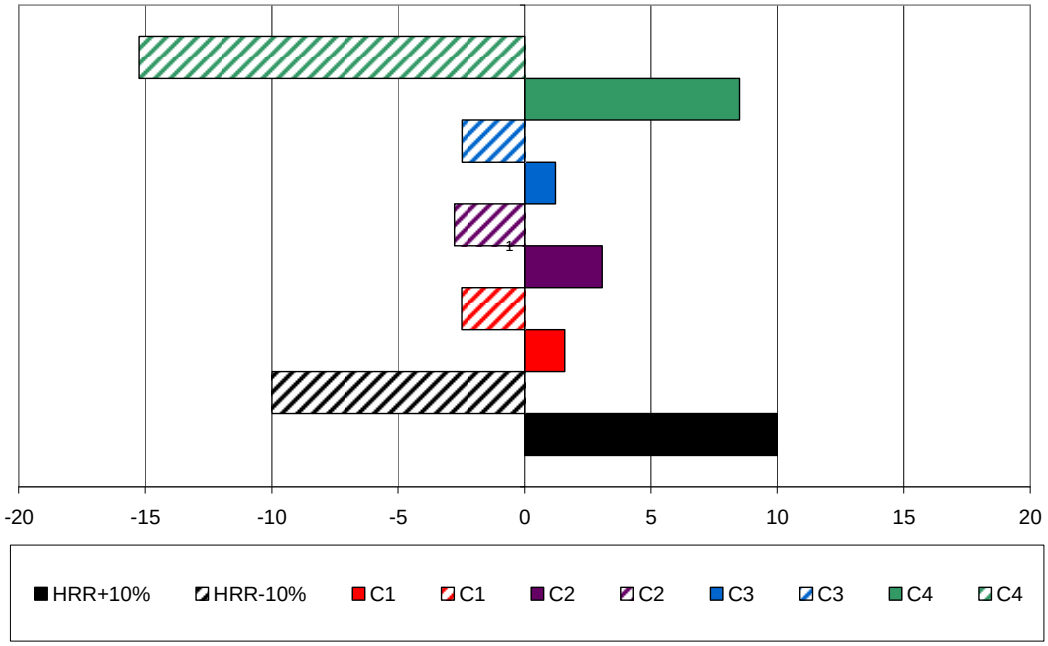

Figure 43: Variation of the cable temperature with a change in the HRR

The temperature in the cable 1 for all the different Heat Release Rates is depicted in Figure 44. It can be observed that the curve is over the failure criteria for the three. For the case of the 10% of HRR, the failure criteria is reached at 5 minutes and it cross the criteria for last time at 36 minutes. It is 31 minutes over the criteria. In Table 37, the comparison of the temperatures for the different HRR and the failure criteria is shown.

Target	Criteria		Peak temperature	Time over Temperature criteria	outcome
	time	Temp			
Cable 1	28 min	330°C	330°C	1 min	Fail
Cable 1 HRR+10	28 min	330°C	355°C	52 min	Fail
Cable 1 HRR-10	28 min	330°C	341°C	31 min	Fail
Target	Criteria		Peak RHF	Time over Temperature criteria	outcome
	time	RHF			
Cable 1	19 min	11kW/m²	0.7	0 min	No Fail
Cable 1 HRR+10	19 min	11kW/m²	0.7	0 min	No Fail
Cable 1 HRR-10	19 min	11kW/m²	0.6	0 min	No Fail

Table 37: Comparison of simulation values with failure criteria

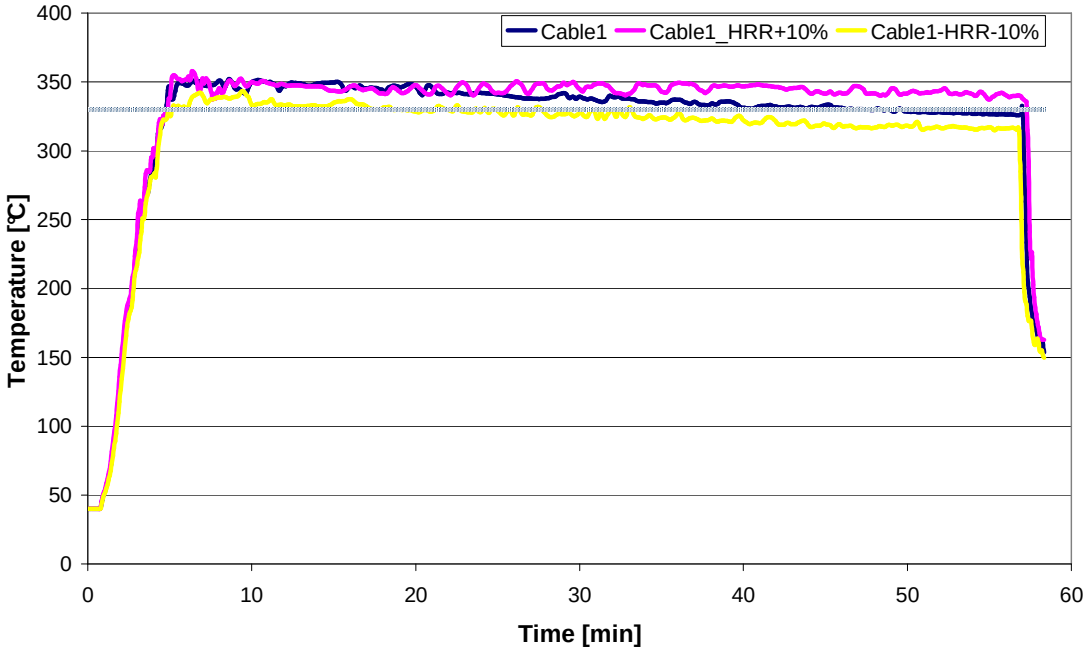

Figure 44: Temperature [°C] in the gases near cable 1 with the change of the HRR vs. time [min]

7.2.1.3 Grid independence analysis

The mesh used for this scenario is a structured mesh made with gambit 2.4.6 with cells of 10cm x 10cm x10cm. It is composed by:

- Number of vertices: 1019002
- Number of cells: 967085

The curves for the measurement point near cable 1 for the two different grids are shown in Figure 45. The curve for the finer grid is lower than the one for the coarser. The difference in this period does not allow making a comparison of the quality of the simulation. The coarser mesh complies with some quality measure, the fire is represented for more than 5 cells in each direction and there are more than 10 cells between the floor and the ceiling.

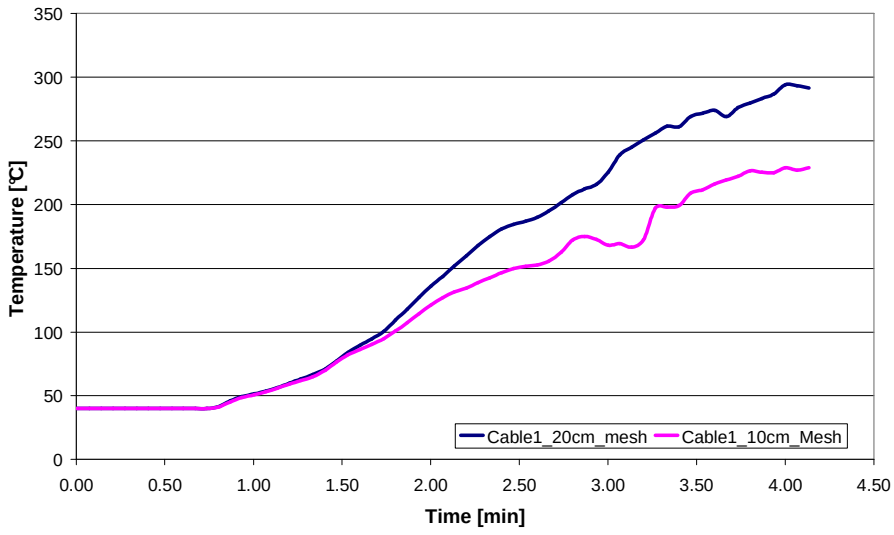

Figure 45: Temperature in the gases near Cable 1 for 10cm and 20cm grid vs. time [min]

7.2.1.1 Scenario 1.2.1 with activation of Deluge System

The scenario 1.2.2 was run with the activation of the deluge system. For this case, a calculation of the maximum HRR that can be accepted, taking into account the maximum temperature that the cables can resist was performed using the power dependence for these parameters. The relationship of the HRR and the target temperature is:

$$\frac{\Delta T}{T} = \frac{2}{3}\frac{\Delta Q}{Q}$$

For this scenario, the peak HRR is 1473kW and the target temperature in the cable C1 is 350°C, the maximum allowable temperature is 330°C and taking a margin of 10%, it becomes in 297°C. The variation of the temperature is:

$$\Delta T = 297°C - 350°C = -53°C$$

Then:

$$\Delta Q = \frac{3}{2}\frac{\Delta T}{T}Q = -334.58kW$$

And the HRR in the Peak is:

$$Q_n = Q + \Delta Q = 1138kW$$

The HRR should be 23% lower in order to have a positive outcome in this scenario. This means that the cable of the pump 1 will not reach the failure temperature. The deluge system is considered to control the fire, as stated in the NFPA 13 standard [21]. Consequently, the fire will be considered to stop growing at the point that the system is activated, making the HRR to stay constant. To achieve this desire effect, the deluge system has to be activated within 160s after the fire has started (for a peak HRR of 1138kW). This rapid respond can be achieved by automatic activation of the deluge system. Manual activation could lead to a similar outcome than the scenario 1.2.2.

The curves of the HRR for the scenario 1.2.1 and 1.2.2, with and without the activation of the deluge system, are displayed in Figure 46.

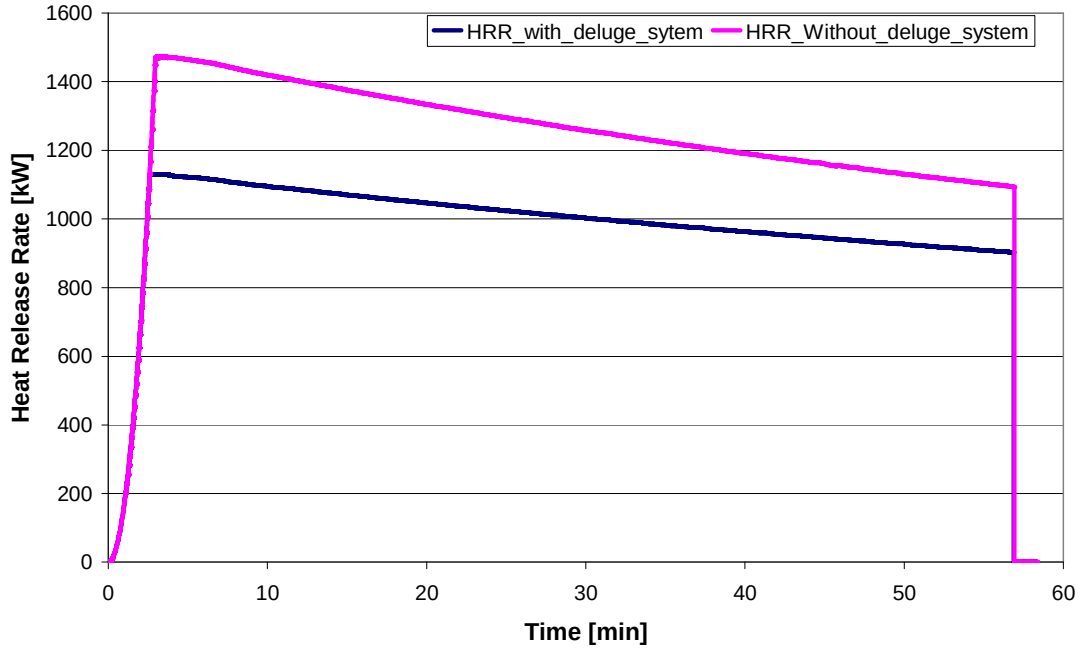

Figure 46: Comparison of the HRR [kW] in scenario 1.2.1 and 1.2.2 vs. time [min]

The temperature near the cables is shown in Figure 47. The temperature in the cable 1 reaches the failure criteria for a time smaller than the time for failure. This means that for this scenario the pump 1 would withstand the fire.

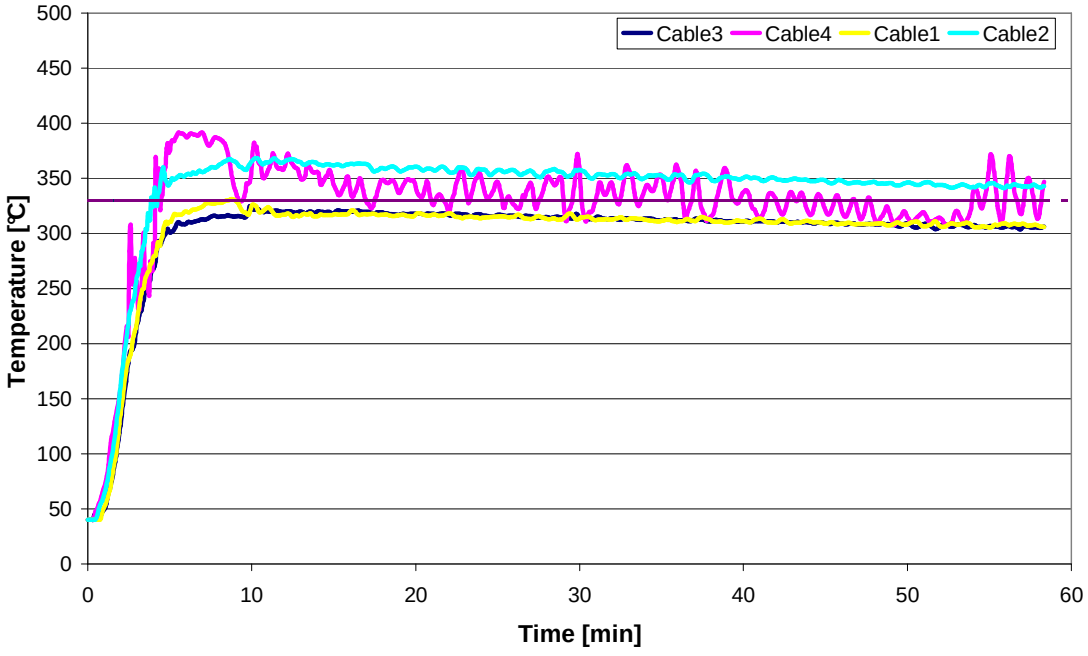

Figure 47: Temperature [°C] in scenario 1.2.1 vs. time [min]

The comparison between the temperature in the cables and the failure criteria are shown in Table 38. The temperature for Cable 4 is over the criteria for 44 minutes, leading to a failure of the pump. On the other hand, the temperature Cable 1 is over the criteria for one minute, leading to a positive outcome.

Target	Criteria		Peak temperature	Time over Temperature criteria	outcome
	time	Temp			
Cable 1	28 min	330°C	330°C	1 min	No Fail
Cable 4	28 min	330°C	390°C	44 min	Fail
Target	Criteria		Peak RHF	Time over Temperature criteria	outcome
	time	RHF			
Cable 1	19 min	11kW/m²	0.5	0 min	No Fail
Cable 4	19 min	11kW/m²	0.9	0 min	No Fail

Table 38: Comparison of simulation values with failure criteria

The temperature distribution in this scenario at 50min is present in Figure 48. The temperature in the cable 1 is below the failure temperature during all the simulation. But the temperature in the rest of the cables reaches the failure criteria.

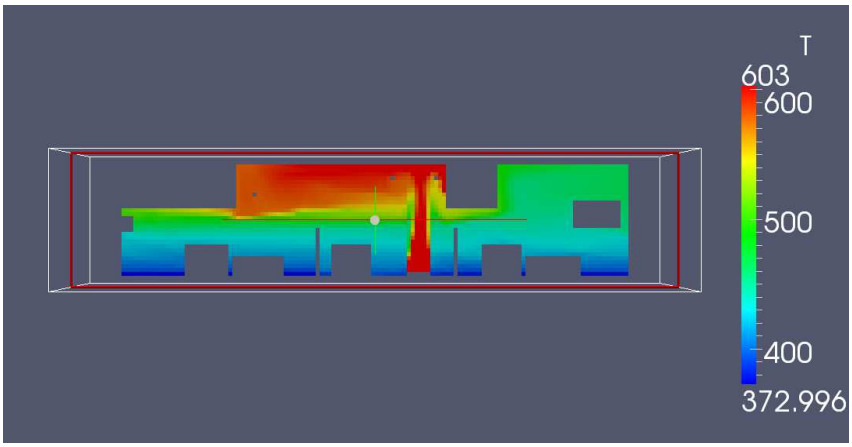

Figure 48: Temperature [K] distribution for the scenario 1.2.1 at 50min

Figure 49 shows the distribution of the smoke with temperature larger than 200°C, this smoke has arrived at the door zone, making the access to the fire more difficult for fire fighter. Even in the situation where the deluge system is working and the HRR is almost a 23% less than the previous one, the action of the fire brigade is hampered by the temperature of the gases inside the compartment.

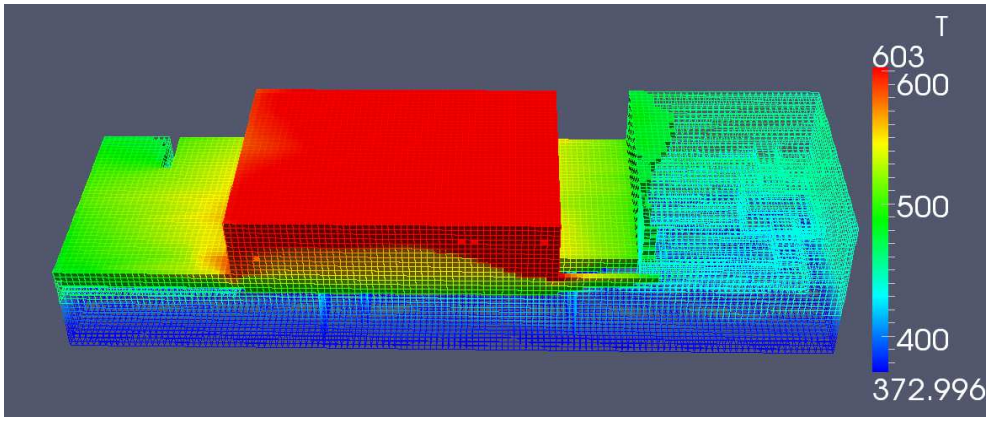

Figure 49: Temperature [K] distribution for the scenario 1.2.1 at 5min

7.2.2 Scenario 2.2.2

The HRR for scenario 2.2.2 is shown in Figure 50. The duration of the fire is shorter than the previous one but it has a higher steady HRR. This is due to the higher amount of oxygen available in the room as a consequence of the ventilation system.

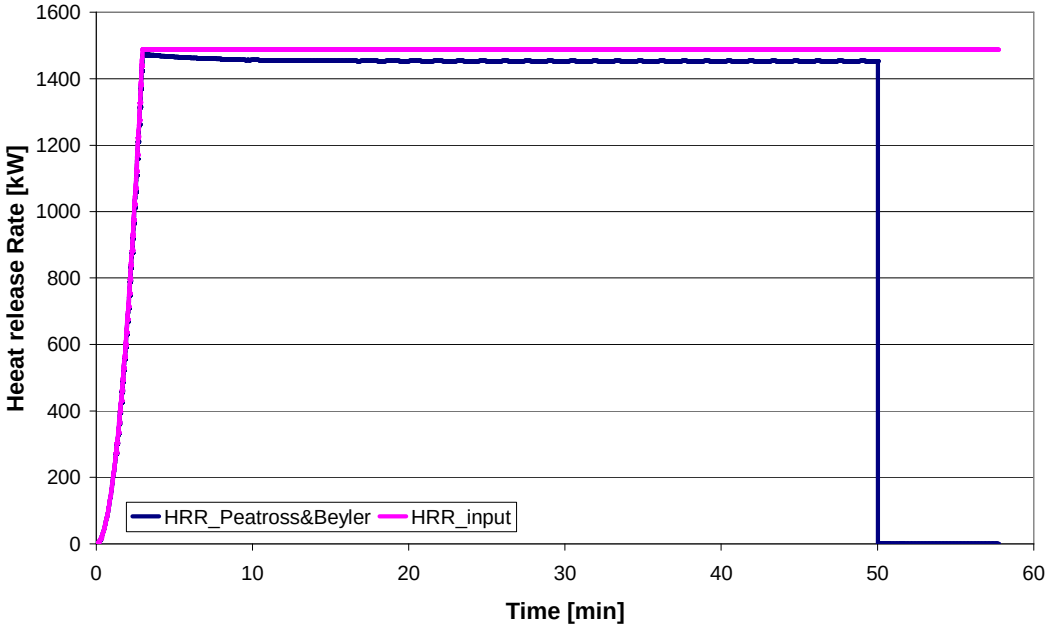

Figure 50: HRR for scenario 2.2.2 vs. time [min]

The temperature in the cables can be examined in the figure 50. Two of the cables are below the failure criteria. Although this indicates that only pump 1 can still work in this condition (Cable 4 is over the failure criteria for more than 28minutes and pump 2 is on fire), the ventilation system cannot be guaranteed to function with temperature higher than 200°C since the system is not fire resistant and the electric motors, the filters, and the seals will probably fail. The ventilation system works as a closed system, meaning that the smoke will return to the room after being cooled. Under these conditions, the system will stop, leading to scenario 1.2.2 as soon as the ventilation system stops working.

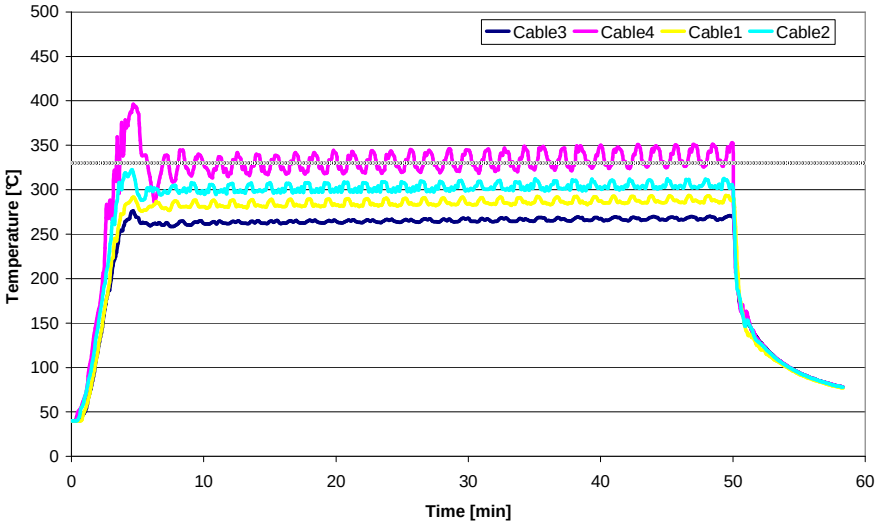

Figure 51: Temperature [°C] in the gases near the cables in scenario 2.2.2 vs. time [min]

The comparison between the failure criteria versus the temperature and the radiant heat flux is shown in Table 39. Cable 1 does not reach the criteria, so the final outcome is positive but the ventilation is threatened, leading to a scenario similar to 1.2.2.

Target	Criteria		Peak temperature	Time over Temperature criteria	outcome
	time	Temp			
Cable 1	28 min	330°C	330°C	0 min	No Fail
Cable 4	28 min	330°C	400°C	46 min	Fail
Target	Criteria		Peak RHF	Time over Temperature criteria	outcome
	time	RHF			
Cable 1	19 min	11kW/m²	0.4	0 min	No Fail
Cable 4	19 min	11kW/m²	0.6	0 min	No Fail

Table 39: Comparison of simulation values with failure criteria

In Figure 52, the distribution of the temperature after 3 minutes can be observed. In this case, the temperature is at least 200°C in the extraction point in the rear wall. This point is the only one that is extracting smoke. This probably leads to the failure of the ventilation system, creating conditions similar to the scenario 1.2.2 after a few minutes.

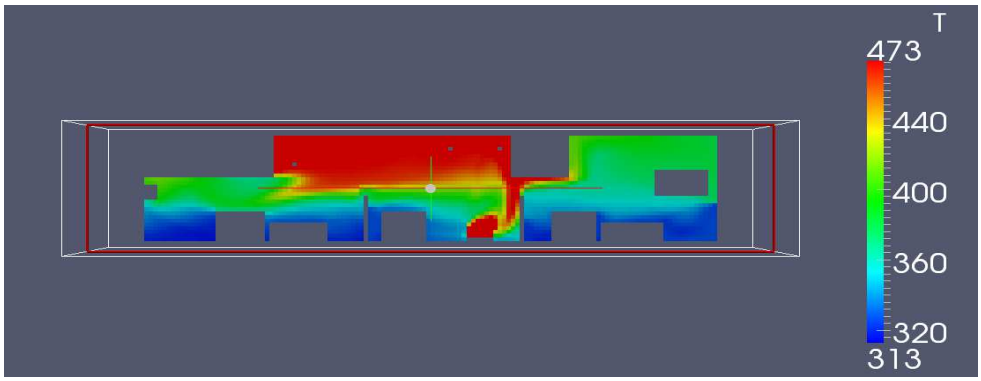

Figure 52: Temperature [K] distribution for the scenario 2.2.2 at plane Y=4m at 3 minutes

Figure 53 shows the smoke at temperature above 200°C in this scenario. The smoke has reached the door at an early stage of the fire, making the intervention of the fire brigade difficult.

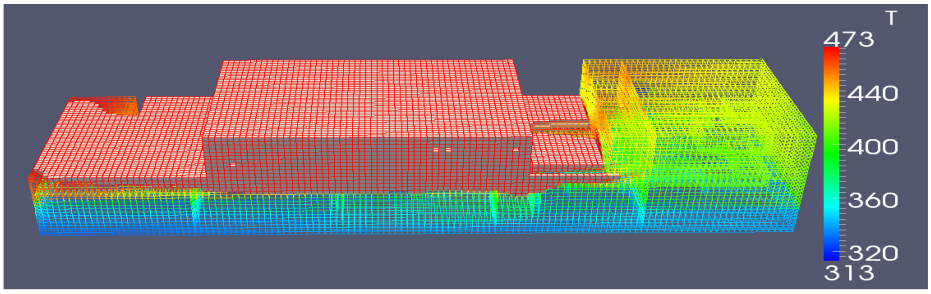

Figure 53: Temperature [K] distribution for the scenario 2.2.2 at 4min

Even though this scenario does not exceed the performance criteria, the ventilation system cannot be trusted to continue working after high temperatures (higher than 200°C) because it is not a fire resistant system and without the ventilation system similar conditions to scenario 1.2.2 can be expected.

7.2.3 Scenario 3.2.2

Scenario 3.2.2 is very similar to Scenario 2.2.2, but with a higher rate of air changes. In spite of the higher rate of air change, the temperature of the smoke reaches the value of 200°C, causing the ventilation system to fail, again leading to a comparable environment to scenario 1.2.2. Figure 54 reveals that the temperature distribution arrives at 200°C within 5 minutes, leading to the probable failure of the ventilation system in an early stage of the fire.

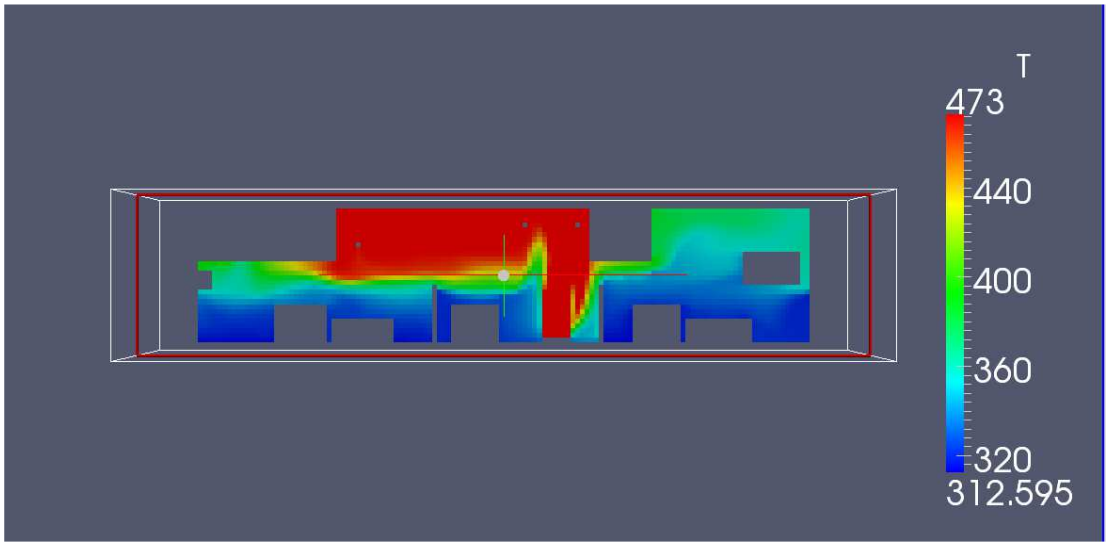

Figure 54: Temperature [K] distribution for the scenario 3.2.2 at plane Y=4m at 5 minute

7.2.4 Summary table

In Table 40, the summary of the different scenarios is shown. The possible outcomes are “Fail” or “No Fail”, meaning that all pumps are out of work due to the fire or that at least one of the pumps will survive, respectively. The activation of the deluge system should be automatic in order to achieve the positive outcomes. In all scenarios with mechanical ventilation, the temperature is over 200°C, leading to a scenario similar to the one without ventilation. Taking into account the different outcomes, the fire safety of this scenario should be improved in order to have an acceptable level.

Ventilation	Fire source	Automatic deluge system (Activation time <160s)	HRR peak [kW]	Pump situation			Ventilation	Outcome (At least one pump do not fail)
				P1	P2	P3		
The ventilation is not working	Pump 1	On	1138.4	Fail	No Fail	No Fail	Off	No Fail
		Off	1485	Fail	Fail	Fail	Off	Fail
	Pump 2	On	1138.4	No Fail	Fail	Fail	Off	No Fail
		Off	1485	Fail	Fail	Fail	Off	Fail
	Pump 3	On	1138.4	No Fail	Fail	Fail	Off	No Fail
		Off	1485	Fail	Fail	Fail	Off	Fail
The ventilation is working at 7000m³/h	Pump 1	On	1138	Fail	No Fail	No Fail	Fail	No Fail
		Off	1478	Fail	Fail	Fail	Fail	Fail
	Pump 2	On	1138	No Fail	Fail	Fail	Fail	No Fail
		Off	1478	Fail	Fail	Fail	Fail	Fail
	Pump 3	On	1138	No Fail	Fail	Fail	Fail	No Fail
		Off	1478	Fail	Fail	Fail	Fail	Fail
The ventilation is working at the highest rate (28000m³/h +7000m³/h)	Pump 1	On	1138	Fail	No Fail	No Fail	Fail	No Fail
		Off	1487	Fail	Fail	Fail	Fail	Fail
	Pump 2	On	1138	No Fail	Fail	Fail	Fail	No Fail
		Off	1487	Fail	Fail	Fail	Fail	Fail
	Pump 3	On	1138	No Fail	Fail	Fail	Fail	No Fail
		Off	1487	Fail	Fail	Fail	Fail	Fail

** For this scenarios the deluge system is considered manually operated or not operated at all. It is assumed that the deluge system manually operated is not fast enough to change the HRR curve.*

Table 40: summary of the outcomes of the scenarios

7.2.5 Recommendations

Different approaches can be taken to improve the situation in the compartment ranging from passive fire safety measures to active ones. In the compartment, there is automatic fire detection and a deluge system installed. As it was stated, the deluge system works manually. It generates a big intervention time, making a positive outcome less probable. The use of an automatic deluge system could lead at safer situation; under the condition that it is activated fast enough to avoid the total heat release rate is reached. More research for the interaction of the deluge system and the HRR is needed to have a better understanding of this situation.

Two systems were proposed to the author to improve the fire safety:

- Thermal Isolation of cables

- Install water curtains between the pumps

These two proposals are analysed in order to have a complete picture of the possible situation.

7.2.5.1 Thermal Isolation of cables

The isolation of the cables can be done in different ways. First, the isolation through intumescent paint will be analysed. This paint reacts to the heat creating a carbonaceous layer of low thermal conductivity that isolates the material to be protected from the external heat. The thickness of the layer can increase until 50 times.

This paint is used mostly in steel structures but the Institute for Construction Materials, Massive Construction and Fire Protection of the Technical University of Braunschweig has perform test showing the applicability of this kind of paints to cables[22]. The test consists of cables exposed to the smoke of three pools fire of oil and to the flame of a gas burner. The cables are placed in a room of 3.6m length, 3.6 wide and 5.4m height. The cables were exposed to an environment of more than 330°C (failure criteria) for 45 minutes and the temperature in cables did not reach this critical temperature. More information of the test can be found in [22]. Although this test shows some evidence of the applicability of this coating to cable, more research is needed in order to asses this particular scenario.

Another option of passive fire protection is covered the cables with a material of low thermal conductivity. For this purpose, there are Electric Raceway Fire Barrier Systems (ERFBS) that have been tested and have different classification (one or three hour fire resistance). For more information about this barrier, the reader should refer to NUREG 1924[]

7.2.5.2 Water curtain system

Drencher Systems are installed to substitute fire resistive barrier, as doors or walls. The systems should stop the heat and smoke of crossing to the protected area. In [23], the authors have arrived to the conclusions that the radiation can be attenuate with water curtains but the convective heat and smoke can still spread through them. Smoke and heat can spread through the air voids of the water screen, these voids are related with the pattern of the water. This pattern is very dependent on the system characteristic. The bigger the droplets, the more smoke and heat is spread. Taking into account that the failure criteria is reached due to the spread of smoke and not to radiation, the use of this kind of water curtains is not recommended. In [23], water mist curtain are not studied. This could be an option but more research is needed in order to have a better answer on the effectiveness these systems for this situation.

7.3 Discussion

The case I was separated in several scenarios in order to analyzed it. The scenarios were divided in scenarios with mechanical ventilation at different rates or mechanical without ventilation. The position of the fire was other variable used for dividing the scenarios and also the activation of the deluge system. A sensitivity analysis was performed on the scenario 1.2.2 where the fire was in pump 2, the mechanical ventilation was turn off and the deluge system was not activated.

The scenarios without ventilation and without deluge system lead to a failure when it is compared with the temperature criteria. It was checked in the sensitivity analysis that the temperature for the failure was in the limit for a 10% less of HRR. A positive outcome was obtained for the cases with ventilation on but the temperature in the gases will probably cause the failure of the ventilation system leading to a scenario similar to the one without ventilation.

A positive outcome was found for the scenarios with the deluge system activated. For this case, the deluge system was assumed as controlling the fire and the peak of the HRR was set as the maximum when the system was activated. This result depends of the activation time in a strong way. An early operation of the system is needed to obtain this outcome. Then, it is necessary to activate the deluge system automatically.

None of the scenarios fails because of the radiation heat flux criteria.

Two possible ways of improving the safety were discussed: isolating the cables with intumescent coating or with a material of low thermal conductivity and the use of water curtain to separated the pumps. For the both proposals, more research is needed in order to obtain more reliable information for this particular scenario.

One of the advantages of the intumescent coat is that it has been tested in several cases as protection of still columns and the performance tends to be good (when it is correctly applied). On the other hand, the cables should be maintained with some periodicity.

The water curtain system can help to reduce the radiation to the cables but it is not probed that it can stop the spread of smoke and heat. The smoke can spread through the void in the curtain. The result will be very dependent of the characteristic of the system, as pressure, size of the droplets, etc.

8. Real case II

8.1Methodology

This scenario has also been analyzed with the modelling process described in the NUREG-1934 [3], the steps followed are:

- Define fire modelling goals and objectives
- Characterize the fire scenarios
- Select fire models
- Calculate fire generated conditions
- Conduct Sensitivity and uncertainty analysis
- Document the analysis

The scenario is a fire compartment with two electrical pumps inside, each of these pumps is feed with a 6kV cable; as it is shown in Figure 55. The origin is taken in the upper corner of the left at floor level. The values of X are measured in the largest wall and the ones of Y in the shortest.

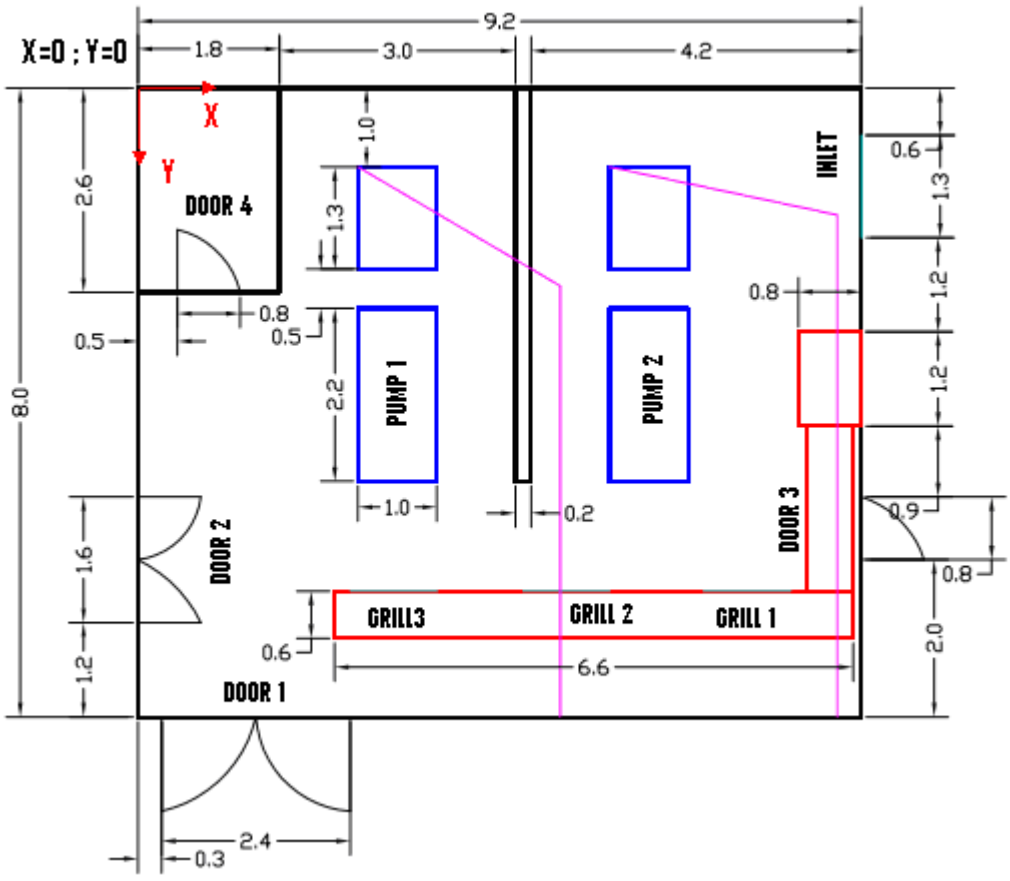

Figure 55: Plant of the real case II

The configuration of this scenario is shown in Figure 55. It consists of two electrical pumps that are feed through 6kV cables. The pumps are separated by a wall with a height of 2m height. All the doors in the room are 1 hour fire resistant except for the one on the wall at X=9.2m. This door is the only one towards the exterior.

There is a ventilation system. This system consists of two extraction motors that are redundant, each having an extraction capacity of 13.000m³/h. The exhaust of the air is made through the ventilation grills (shown in gray) within the duct, shown in red in Figure 55. The air inlet is an opening with a filter in the right wall. The system is turned on when the temperature in the room is higher than 37.4°C.

The only combustible materials in the room are cables and the pumps. For this analysis, the pumps will be considered the fire source. The HRR of the fire was obtained from the NUREG-6850 [15], where a cabinet fire is proposed. The fire curve is displayed in the Figure 56, the HRR increases with a t-square shape until it reaches the steady state at 369kW. Then, it decreases in a linear way to reach 0 kW at 39 minutes.

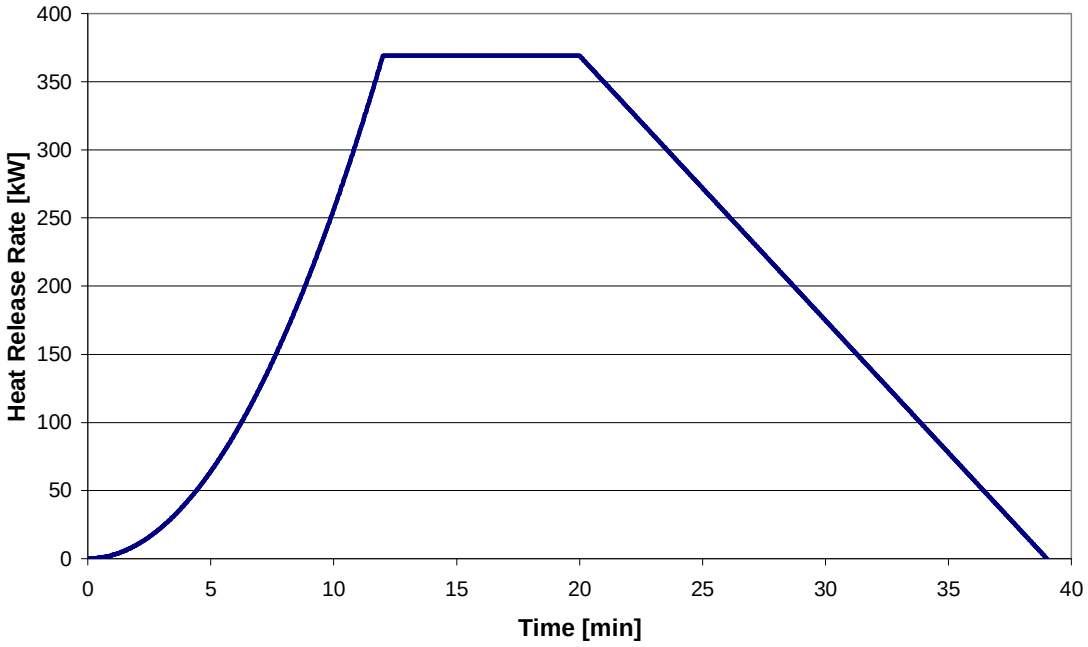

Figure 56: HRR [kW] of an electrical pump vs. time [min]

Some of the steps for the analysis of this case are identical or very similar to the previous case due to their similarity.

8.1.1 Define fire modelling goals and objectives

The objectives and goals are the same as for the case I: one of the two pumps has to survive a fire in the compartment. The criteria are identical, because the cables that feed the pumps are identical (Tables 29 and 30).

8.1.2 Characterize the fire scenarios

The scenarios that are considered for this case are shown in Table 41.

Ventilation	Fire source	Scenario
The ventilation is off	Pump 1	1.1
	Pump 2	1.2
The ventilation is on	Pump 1	2.1
	Pump 2	2.2

Table 41: Scenarios of Real case II

The scenarios, that are analyzed, are the ones with the pump 2 as fire source. The orders scenarios are covered by these ones because the cable of the pump 1 is close to pump two. For this reason, scenarios 1.2 and 2.2 are considered more threatening for fire safety.

8.1.3 Select fire models

The fire model chosen for this case is ISIS 3.0.1. In appendix B a simulation with CFAST is also presented for completeness. All the models are set as in the previous case (Table 33), the only difference is the end time of the simulation, which is 2340s.

Figure 56 depicts the compartment of the fire in a 3D view. The cables are placed over the duct for the ventilation system. Several measurements points were placed in the cables and near the cables.

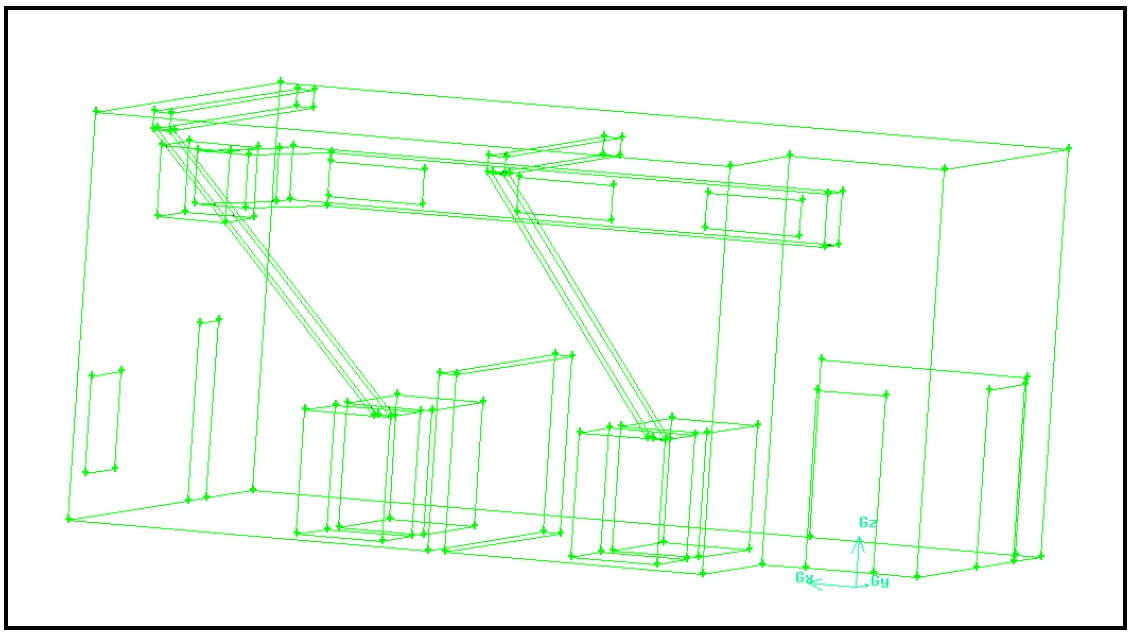

Figure 57: 3D view of the case II

Table 42 shows the values set for the simulation in ISIS. The variables that have change are the related to the combustible material of the pump. The values of the Fuel were obtained from the NUREG-1934 [3].

Properties	Variable	Value
Air properties	Laminar Viscosity	1.7x 10^{-5}kg/m.s
	Specific Heat Capacity	1020J/kg.K
	Reference Temperature	310K
	Turbulent Prandtl	0.7
	Turbulent Schimidt	0.7
	Absorption coefficient	0.1m^{-1}
	Reference Density	1.13kg/m^3
Fuel	Heat of combustion	1.03x10^7J/kg
	Boiling point	-
	Formula	C6H9
	Soot Yield	0.17
Initial Conditions	Velocity	0.0 0.0 0.0 m/s
	Initial Temperature	313 K
	Pressure	101325.0Pa
	Turbulence Kinetic Energy	1 x 10^{-6} m^2/s^2
	Dissipation Rate of Turbulent Kinetic Energy	1 x 10^{-9} m^2/s^3
	Mixture Fraction	0.0
	Fuel Fraction	0.0

Table 42: Simulation values

8.1.4 Calculate Fire-Generated Conditions

The outputs picked for this study were also the gas temperature near the cables and the radiant heat flux. As it was explain in the previous section, the temperature is measure in the gas near the cable because small difference was found between the temperature in the cables and in the gas surrounding it. Another essential variable is the duration of the fire.

8.1.5 Sensitivity Analysis

As in the previous case, a sensitivity analysis is carried out on the most important variable of the scenario 1.2, namely the Heat Release Rate. This was studied by changing the HRR in 10% in excess and in shortage.

A grid sensitivity study has been performed in order to check the results independence of the grid. The cell size was divided by two in every direction. This generates an increase in the computational time of 16 times the one of the coarser grid. For this reason, the simulation was carried out for a smaller duration in time.

8.2 Results

8.2.1 Scenario 1

Figure 58 depicts the HRR for the case II, scenario 1.2. The HRR with and without the application of the Peatross and Beyler model is almost the same. This indicates that there is little oxygen consumption in the surrounding of the fire.

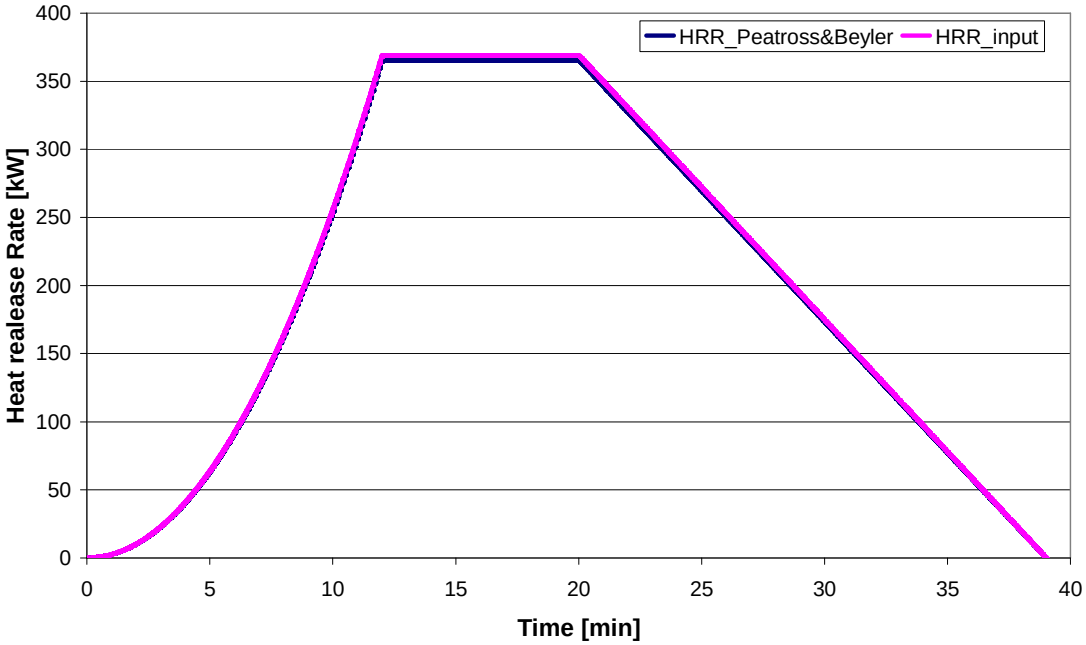

Figure 58: HRR [kW] of case II, scenario 1.2 vs. time [min]

In Table 43, the points of measurement in the gas near the cable 1 are shown. These positions are taken from the origin of coordinates of the upper corner on the left of Figure 55.

	X[m]	Y[m]	Z[m]
pt0	4.8	1	3
pt1	5.3	1	4.4
pt2	5.3	3	4.4
pt3	5.3	5	4.4
pt4	5.3	7	4.4

Table 43: Position of the measurement points near cable1

The temperatures in those points are displayed in Figure 59. The temperature near cable 1 reaches the 120°C in the hottest spot which is below the failure criteria. For this scenario, the continuity of operation of the pump 1 seems to be guaranteed.

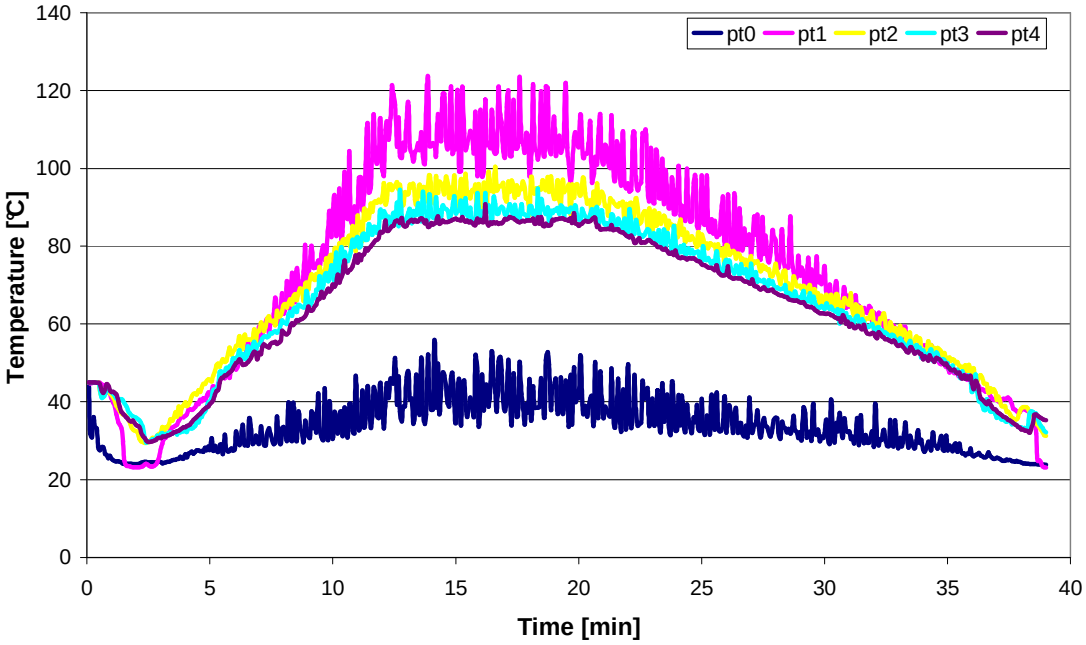

Figure 59: Temperature [°C] in the gases near the cable 1 vs. time [min]

The temperature distribution at steady state of the HRR curve is shown in Figure 60. In this case the temperature is around 100°C. Under these conditions, the ventilation system should continue working and fire intervention would be possible.

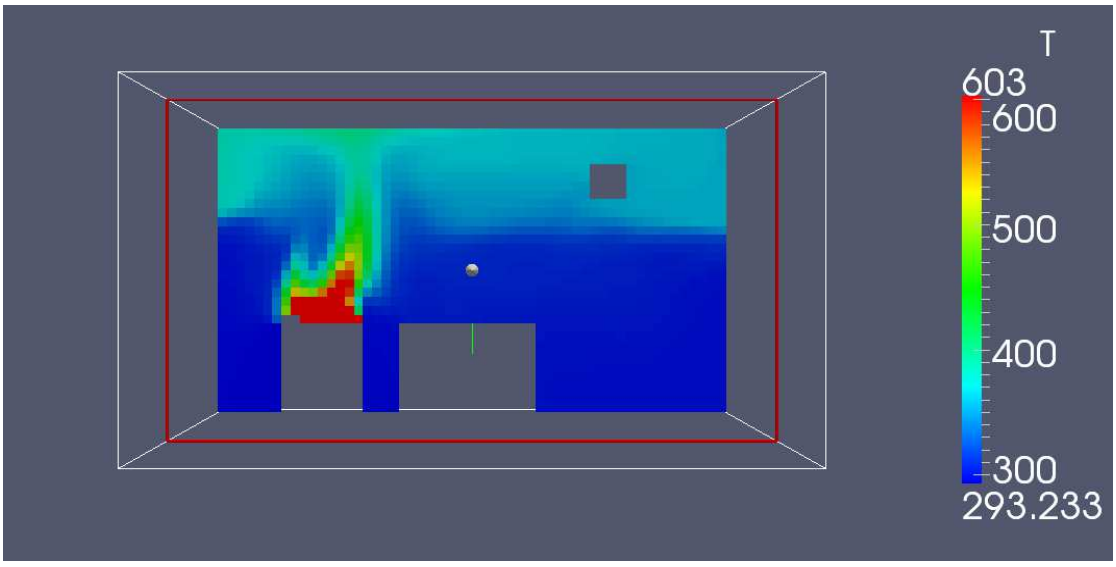

Figure 60: View of the compartment temperature [K] at steady state (t=15min) plan X=6m

Table 44 shows the position of the measurement points in the cable 1. These points are used to measure the radiant heat flux and the total heat flux. The positions are closed to the points where the temperature of the air near cable 1 was measure.

	X[m]	Y[m]	Z[m]
PT1	5.25	1.05	4.60
PT2	5.25	3.07	4.60
PT3	5.25	4.93	4.60
PT4	5.25	6.95	4.60

Table 44: Position of the measurement points in cable1

The radiant heat flux is shown in Figure 61. In PT1, the radiant heat flux is the highest, it reaches 350W/m². Although this value could be underestimated by the program, it is far from the value of the criteria (11kW/m²).

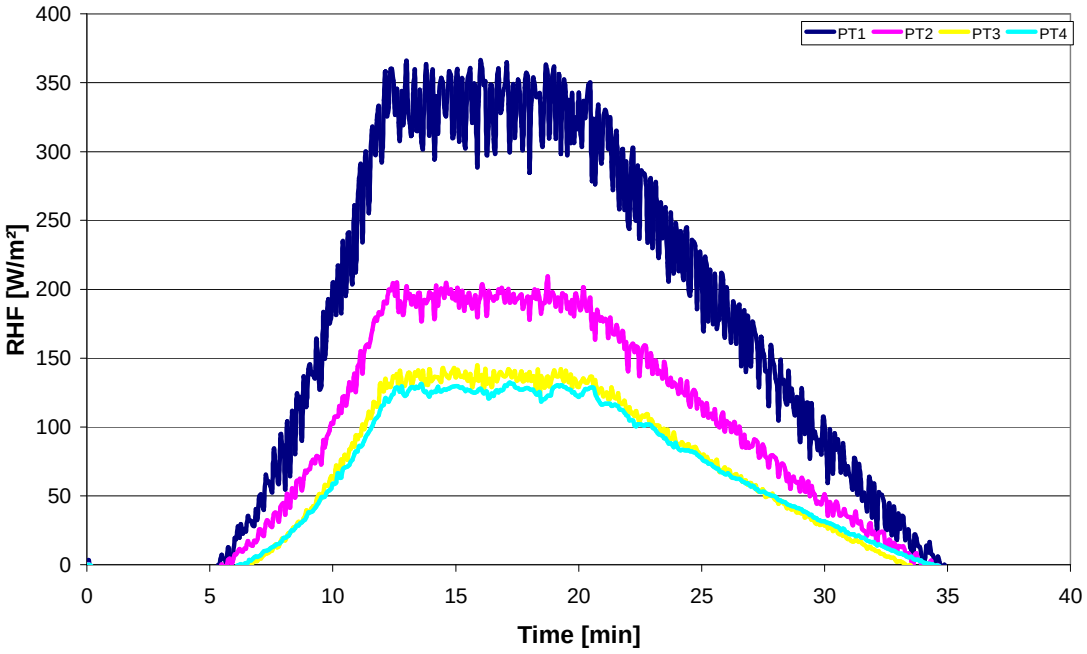

Figure 61: Radiant Heat flux [w/m²] in cable 1 vs. time [min]

The measurements points of the air temperature near cable 2 are shown in Table 45.

	X[m]	Y[m]	Z[m]
pt0	7.8	1	3
pt1	8.9	1	4.3
pt2	8.9	3	4.3
pt3	8.9	5	4.3
pt4	8.9	7	4.3

Table 45: Position of the measurement points near cable 2

Figure 62 depicts the temperature curves for the air near the cable 2. The maximum values are around 100°C that is below the failure criteria. Even though this cable can fail because it is considered that the pump 2 is on fire, it is interesting to observe that with this fire curve this cable is not damaged.

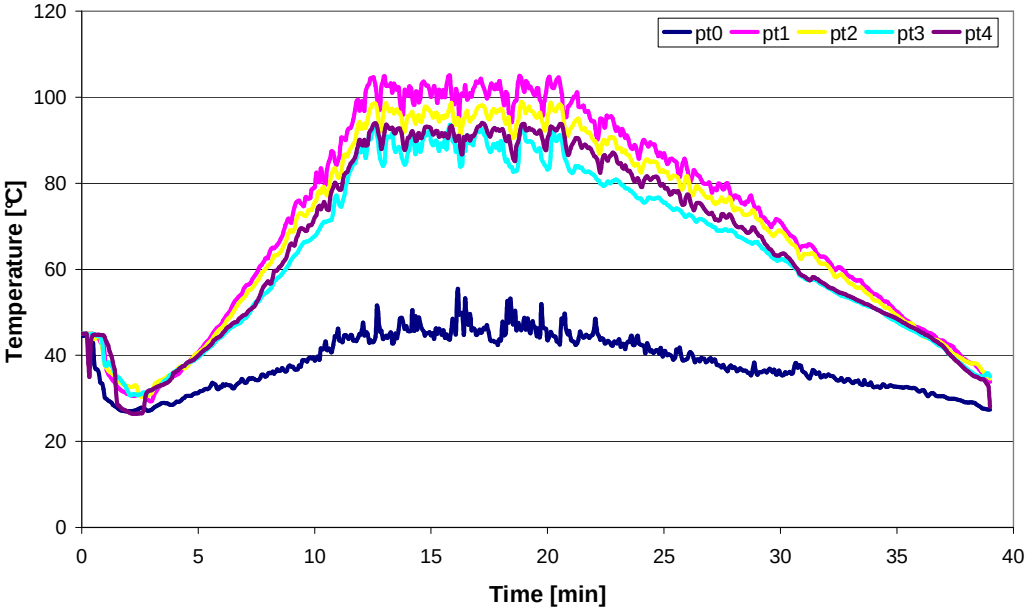

Figure 62: Temperature [°C] in the gases near the cable 2 vs. time [min]

Table 46 shows the comparison between the temperature and radiation criteria with the values obtain in the simulation. There is big margin to assume that under these objectives, the room can be considered safe from a fire safety point of view.

Target	Criteria		Peak temperature	Time over Temperature criteria	outcome
	time	Temp			
Cable 1	28 min	330°C	124°C	0 min	No Fail
Target	Criteria		Peak RHF	Time over Temperature criteria	outcome
	time	RHF			
Cable 1	19 min	11kW/m²	0.35	0 min	No Fail

Table 46: Outcome of scenario 1.2

8.2.1.1 Sensitivity analysis

The HRR for the scenario 1.2 of the case II and the variation for the sensitivity analysis are shown in figure 63. The curve for HRR plus 10% is not complete because all the fuel is consumed just after 30 minutes.

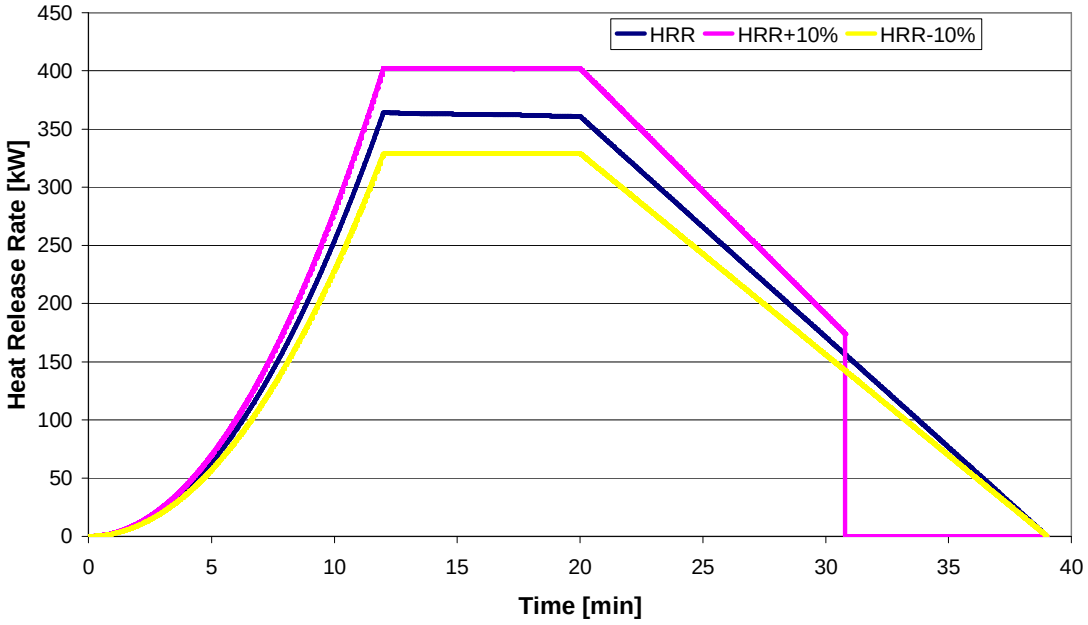

Figure 63: Heat release rate [kW] for the sensitivity analysis vs. time [min]

The temperature in the gas near the cable 1 is shown in the figure 64. For all the cases, the temperature is far from the failure criterion that is displayed in this figure. The difference for the hottest point is around 200°C.

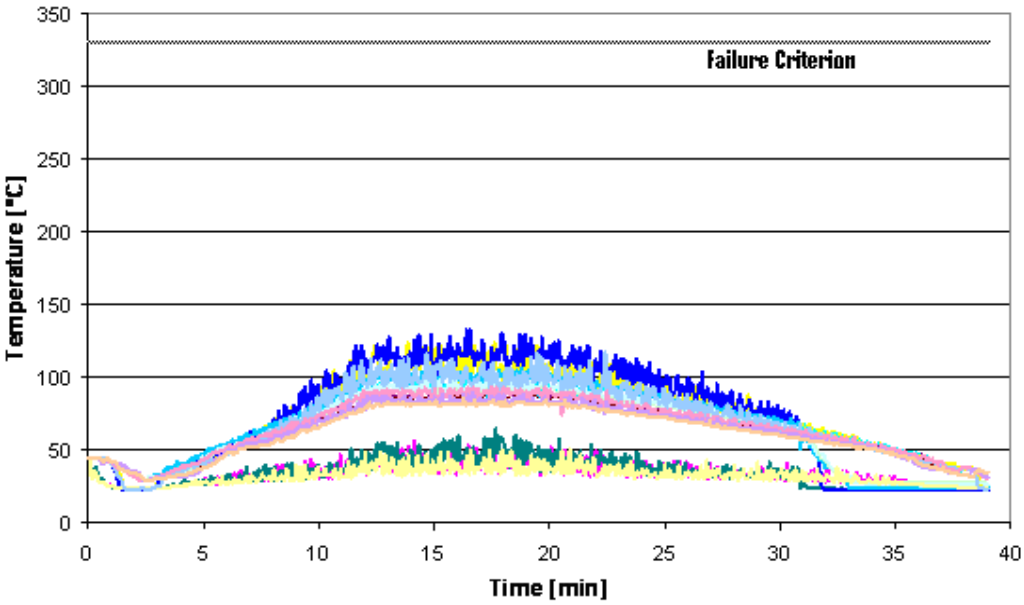

Figure 64: temperature [°C] near Cable 1 for the different HRRs vs. time [min]

A tornado graph with the variation of the temperature near the cable 1 and cable 2 due to the variation of the HHR is described in Figure 65. All the temperatures are near the 6.66% of

variation expected except the temperature in PT0 of both cables. These points are the closets to the floor. The reason for this divergence can be a bad representation of the temperature in the cold layer. For the case of cable 2, this point is close to the inlet of air too.

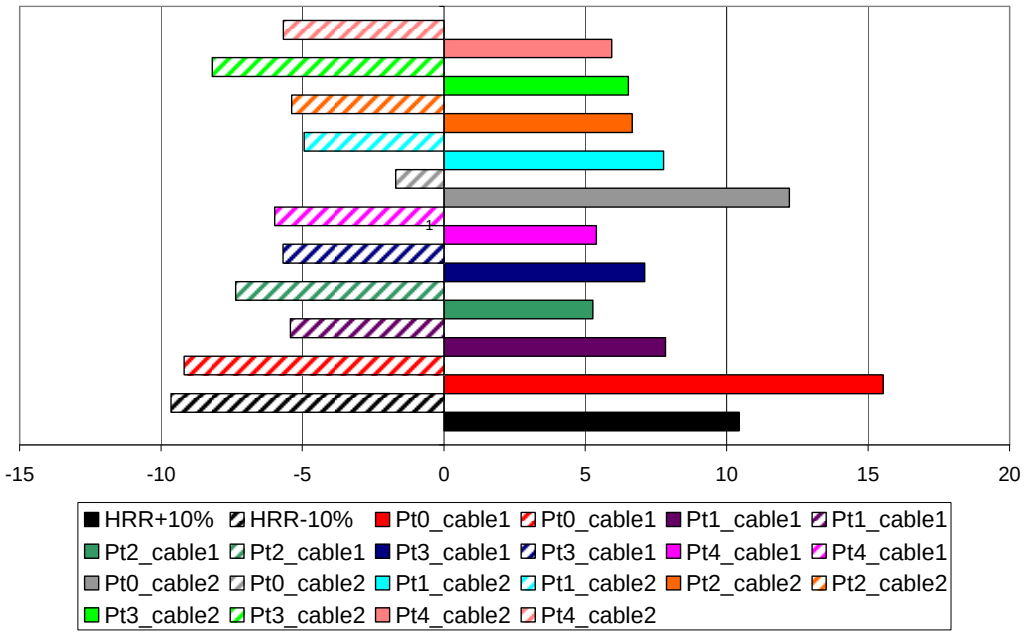

Figure 65: Variation of the temperature near the cables with HRR

8.2.1.2 Grid independence analysis

The temperature in cable 1 at point 2 and 3 are depicted in figure 66. The temperatures are similar for both cases. A comparison in of a bigger period of time is desirable but because of big amount of cell used for the finer grid this could not be obtained. The quality of the coarser grid can be considered good because it complies with the quality criteria of having more than 5 cells in each direction on the fire and having more than 10 cells between the floor and the ceiling.

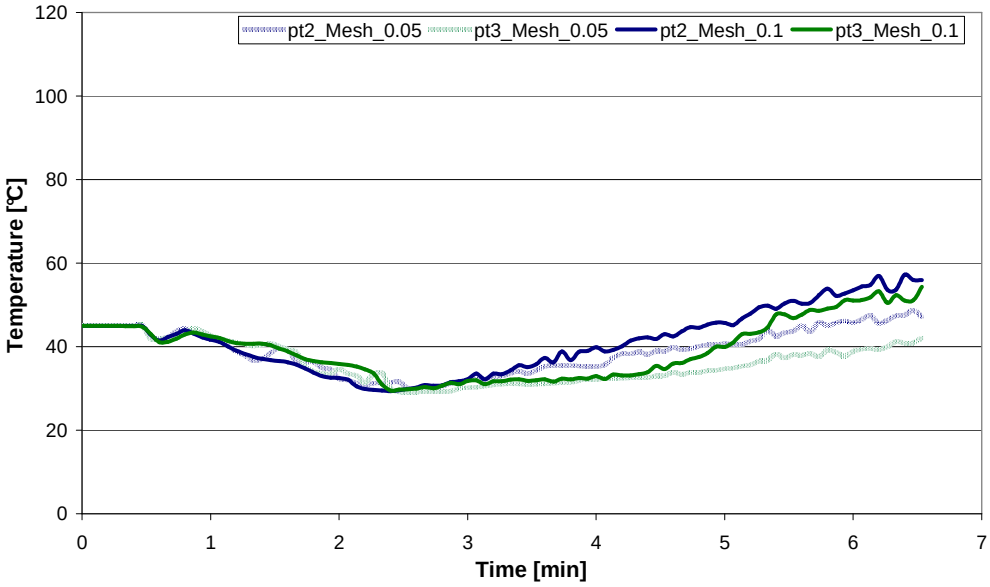

Figure 66: Temperature [°C] in cable 1 point 2 and 3 for the different grids vs. time [min]

8.2.2 Scenario 2.2

Figure 67 shows the HRR before and after the application of the Peatross a Beyler model. There is availability of oxygen for the fire to almost follow the original curve. This could be because there is an opening to the outside.

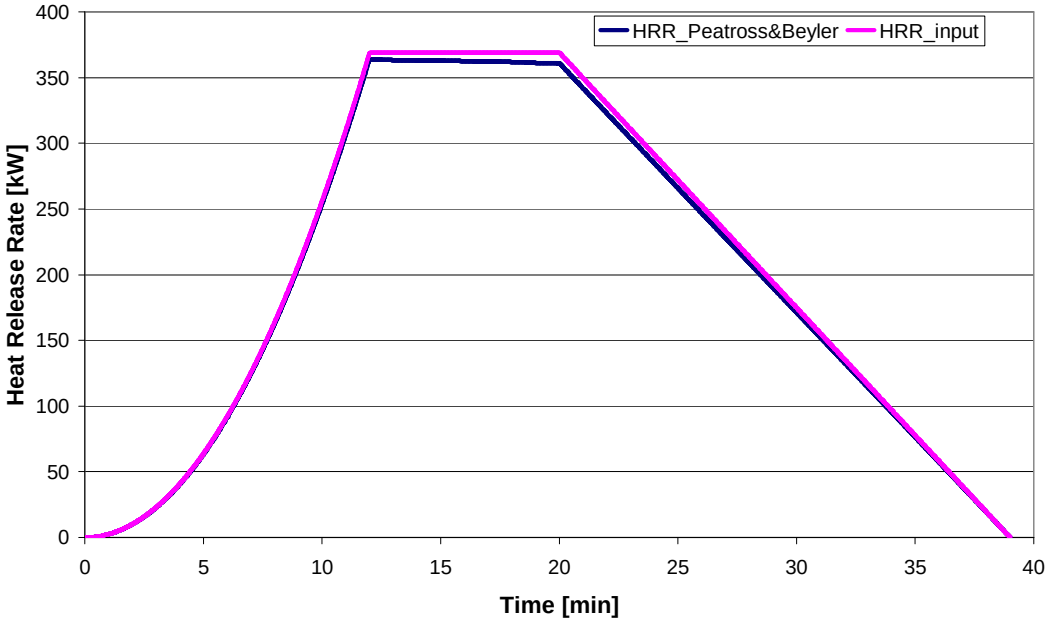

Figure 67: HRR [kW] for case II, scenario 2.2 vs. time [min]

The temperatures in the points near (Table 43 displays the coordinates of these points) cable 1 are shown in Figure 68. Although the temperatures are higher than in scenario 1.2, they are far below from the failure criteria (330°C).

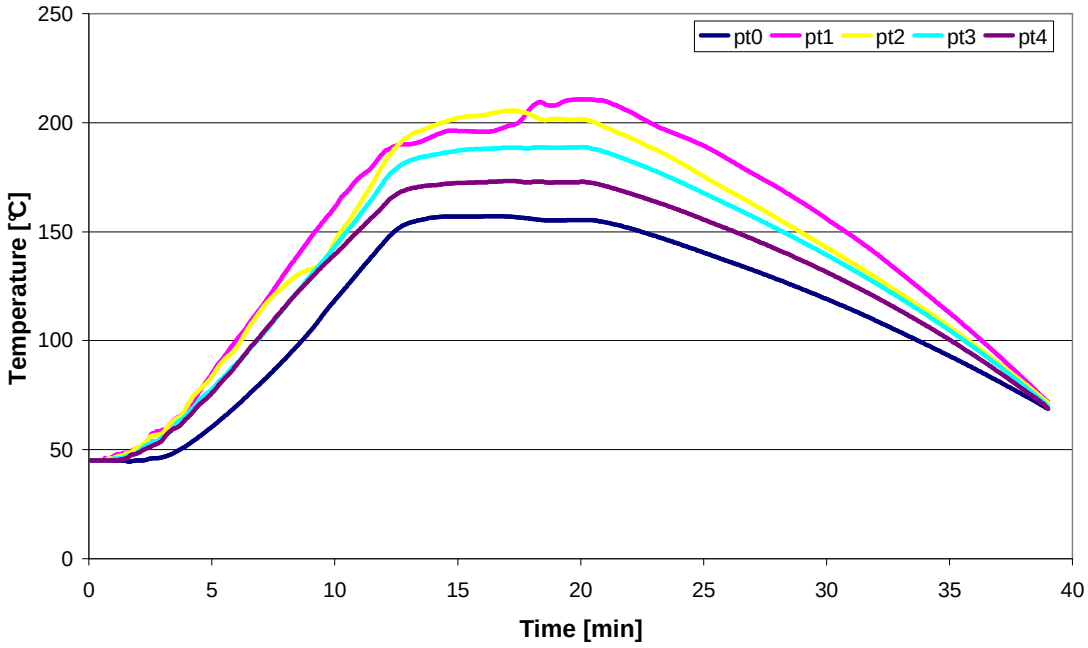

Figure 68: Temperature [°C] in the gases near the cable 1 vs. time [min]

The temperatures in the proximity of the cable 2 are shown in Figure 69; all the temperatures are well below the failure criteria.

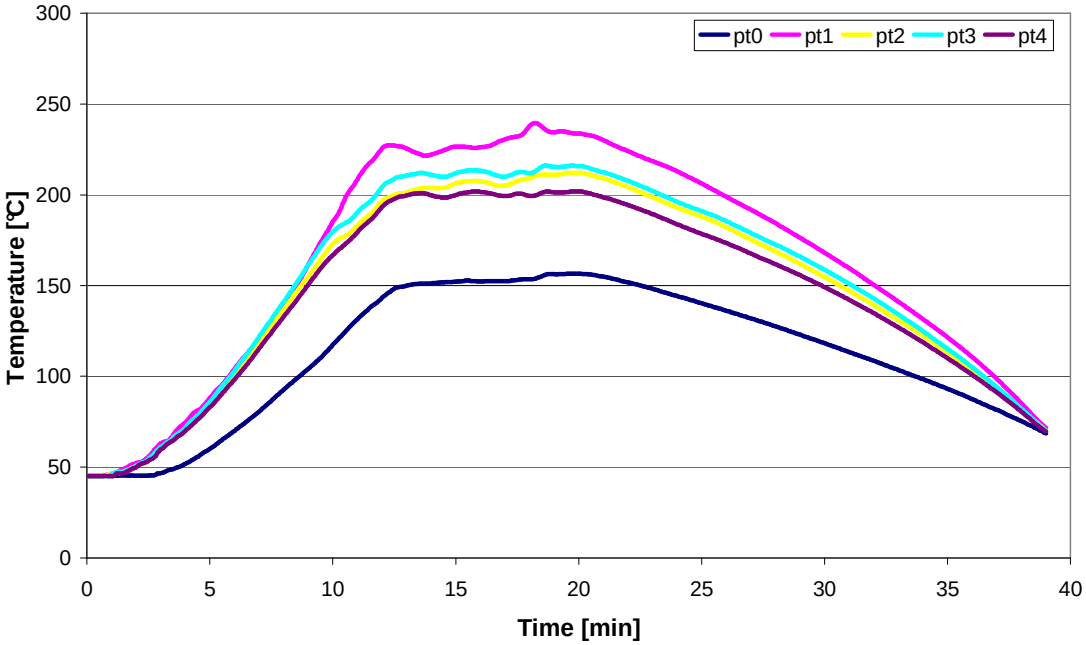

Figure 69: Temperature [°C] in the gases near the cable 2 vs. time [min]

Table 47 depicts the comparison between the criteria of temperature and radiation heat flux with the temperature and radiation heat flux obtained from the simulation. The margin is smaller than for the previous scenario but it is still large enough to consider the room safe from a fire safety point of view.

Target	Criteria		Peak temperature	Time over Temperature criteria	outcome
	time	Temp			
Cable 1	28 min	330°C	208°C	0 min	No Fail
Target	Criteria		Peak RHF	Time over Temperature criteria	outcome
	time	RHF			
Cable 1	19 min	11kW/m²	1.8kW/m²	0 min	No Fail

Table 47: Outcome of scenario 2.2

8.2.3 Summary table

Table 48 shows the summary of the scenarios of case II. The outcome is positive for all the cases and the margin is large enough to consider the objectives reached.

Ventilation	Fire source	HRR peak [kW]	Pump situation		Ventilation	Outcome
			P1	P2		
The ventilation is off	Pump 1	369	No Fail	Fail	Off	No Fail
	Pump 2	369	No Fail	Fail	off	No Fail
The ventilation is on	Pump 1	369	No fail	Fail	off	No Fail
	Pump 2	369	No Fail	Fail	off	No fail

Table 48: Summary of the outcomes of the scenarios

8.3 Discussion

The case II presents a room with two electrical pumps. The biggest fire load is represented by these pumps. This fire load is low, leading to a successful outcome for all the scenarios. The cables are below the failure criterion with a margin of 200°C for the scenario with ventilation and around 130°C for the scenario without ventilation. Most of the assumptions made for this case where conservative, like the selection of 369kW for the HRR; that leads to a bigger margin of safety.

The fire doors are not threatened by the fire; even the not fire resistant door could survive a fire of this characteristic.

If there is no change in the fire load, the room can be considered safe from a fire engineering point of view and no extra safety measure should be taken.

9. Conclusions

The comparison of the simulation in ISIS and the experiments has shown a good agreement between the temperatures measures in the gases. This is confirmed for some exercises of validation [10] and previous works [13]. This makes this simulation reliable for this specific variable. There were some problems in the representation of this variable near the floor, where the values were over predicted. The representation of the oxygen concentration is also good for the higher part of the compartment but the error is bigger for the points near the floor. The radiation has a similar behavior than the previous variables. On the other hand, it was not possible to achieved trustable results for the total heat flux because the error were bigger than 30% for almost all the calculated points. The major error for this variable is related with the convective heat flux that is underestimated by the program. This can be related to the size of the cells near the wall and the representation of this zone by the wall functions. The validation scenarios with refinement of the mesh near the wall can be run in order to achieve more knowledge for this situation.

Most of the analyzed variables have shown curves with a similar shape to the experimental ones. Therefore, the representations of the physical phenomena are correct for a qualitative point of view. The development of a data base with comparison of experiment and ISIS simulation to quantify the uncertainty would be desirable for a simpler application of the approach proposed by NUREG-1934. More research is needed in order to achieve this data base.

The power dependence of the outputs related with the most important inputs as presented by NUREG-1934 [3] were revised and it was found that the majority of the variables follow this approach. There was a good agreement in the THF, the temperature in the walls and the temperatures in the gases. Nevertheless, the species concentration seems to be the exception.

Two real cases were studied using the same method described in the NUREG-1934 [3]. The goals for these cases were the continuity of operation and the objectives were that at least one of the safety related equipment (pumps) in the rooms survives a fire. The criteria used were linked with the temperature in the gases near the cables used for power the pumps and the radiation heat flux in these cables. For the case I, the outcomes are shown in Table 49. The results were negative (the critical temperature was higher than the temperature of the criteria) for all the cases without automatic deluge system hence two different approaches for improving the fire safety were analyzed. To cover the cables with intumescent paint or with a material of low thermal conductivity, in order to improve the fire resistance, was the first approach. The second approach takes into account water curtains separating the different pumps to avoid smoke and heat propagation. More research is needed in order to have better understanding of the solution proposed. For the case II, the outcomes are depicted in Table 50 and all of these were positive, meaning that the temperatures and radiant heat fluxes were under the failure criteria for all the analyzed scenarios.

Ventilation	Fire source	Automatic deluge system (Activation time <160s)	HRR peak [kW]	Pump situation			Ventilation	Outcome (At least one pump do not fail)
				P1	P2	P3		
The ventilation is not working	Pump 1	On	1138.4	Fail	No Fail	No Fail	Off	No Fail
		Off	1485	Fail	Fail	Fail	Off	Fail
	Pump 2	On	1138.4	No Fail	Fail	Fail	Off	No Fail
		Off	1485	Fail	Fail	Fail	Off	Fail
	Pump 3	On	1138.4	No Fail	Fail	Fail	Off	No Fail
		Off	1485	Fail	Fail	Fail	Off	Fail
The ventilation is working at 7000m³/h	Pump 1	On	1138	Fail	No Fail	No Fail	Fail	No Fail
		Off	1478	Fail	Fail	Fail	Fail	Fail
	Pump 2	On	1138	No Fail	Fail	Fail	Fail	No Fail
		Off	1478	Fail	Fail	Fail	Fail	Fail
	Pump 3	On	1138	No Fail	Fail	Fail	Fail	No Fail
		Off	1478	Fail	Fail	Fail	Fail	Fail
The ventilation is working at the highest rate (28000m³/h +7000m³/h)	Pump 1	On	1138	Fail	No Fail	No Fail	Fail	No Fail
		Off	1487	Fail	Fail	Fail	Fail	Fail
	Pump 2	On	1138	No Fail	Fail	Fail	Fail	No Fail
		Off	1487	Fail	Fail	Fail	Fail	Fail
	Pump 3	On	1138	No Fail	Fail	Fail	Fail	No Fail
		Off	1487	Fail	Fail	Fail	Fail	Fail

** For this scenarios the deluge system is considered manually operated or not operated at all. It is assumed that the deluge system manually operated is not fast enough to change the HRR curve.*

Table 49: Summary of the outcomes of the scenarios for real case I

Ventilation	Fire source	HRR peak [kW]	Pump situation		Ventilation	Outcome
			P1	P2		
The ventilation is off	Pump 1	369	No Fail	Fail	Off	No Fail
	Pump 2	369	No Fail	Fail	off	No Fail
The ventilation is on	Pump 1	369	No fail	Fail	off	No Fail
	Pump 2	369	No Fail	Fail	off	No fail

Table 50: Summary of the outcomes of the scenarios for real case II

10. Acknowledgements

I would like to express thanks to my beloved wife Claudia for the infinite help and support. I am very thanked to my parents, sister and friends who have supported me at the distance.

I want to thank to the IMFSE for this amazing opportunity; in particular to the supervisor of this thesis, Professor Bart Merci, and to Professor Jose Luis Torero for the inspiration. I would also like to show appreciation to Elise Meerburg and all teachers of the University of Edinburgh, Lund University and Gent University.

I wish to be grateful with my classmate from whom I have learnt a lot, particularly Setareh Ebrahimzadeh for her help with suppression systems and peer reviewing, Feng Xu for helping me with ISIS and Nick Bartlet for the comments in my report.

I desire to acknowledge BEL V for the proposal and the space to work, especially to Frederick Bonte, from whom I have learnt a lot. I also want to thank to Michel Gettemans, Chantal Mommaert Vincent Sauveniere, Stéphane Leyns, Marika Roobaert, and Olivier Destin.

I want to thank to the National Institute of industrial Technology (INTI) of Argentina for the support, especially to my partners of the division Fire Technology.

11. References

1. **G.H. Yeoh and K.K. Yuen**, Computational fluid dynamics in fire safety engineering: theory, modelling and practice. **Elsevier, Amsterdam, 2009.**

2. **SFPE**, SFPE Handbook of Fire Protection Engineering – Third edition. **National Fire Protection Association, Quincy, 2002.**

3. **NUREG-1934, EPRI 1019195**, Nuclear Power Plant Fire Modelling Application Guide. U.S. Nuclear Regulatory Commission, Office of Nuclear Regulatory Research (RES), Rockville, MD, 2007, and Electric Power Research Institute (EPRI), Palo Alto, CA.

4. **NUREG-1824, EPRI 1011999**, Verification and Validation of Selected Fire Models for Nuclear Power Plant Applications. U.S. Nuclear Regulatory Commission, Office of Nuclear Regulatory Research (RES), Rockville, MD, 2007, and Electric Power Research Institute (EPRI), Palo Alto, CA.

5. **Enclosure Fire Dynamics**, Björn Karlsson and James G. Quintiere, ISBN 0-8493-1300-7. 2000.

6. **ISIS 2.3.2 - Physical Modelling in ISIS**. IRSN, CPAM/SEMIC-2009-459/DL Ind.2. 2009

7. **ISIS 3.0.0 - Physical Modelling in ISIS**. IRSN, DPAM-SEMIC-2011-054 Ind.3. 2011.

8. **Validation of the ISIS CFD code for fire simulations**, IRSN, DPAM/SEMIC-2008-167. 2008.

9. **Engineering Guide to Performance-Based Fire Protection**, SPFE, 2nd ed. 2007.

10. **PRISME SOURCE Program – Analysis report**, H. Pretel, DPAM/SEREA-2005-015 – PRISME-200604 rev.1.

11. **ISIS 3.0.0: validation**. IRSN, DPAM-SEMIC-2011-223 Ind. 3

12. **ISIS 3.0.0: tutorial**. IRSN, DPAM-SEMIC-2011-331 Ind.3

13. **ISIS 3.0.0: verification tests**. IRSN, DPAM-SEMIC-2011-329 Ind.2

14. **Validation of Zone and Field Models to Support Fire Hazard Analysis and Fire PSA review of Fire Scenarios encountered in Nuclear Power Plants.** Frederick Bonte, Ugent, 2010-2011

15. **NUREG-1805,** Fire Dynamics Tools (FDT^{s}) Quantitative Fire Hazard Analysis Methods for the U.S. Nuclear Regulatory Commission Fire Protection Inspection Program. **U.S. Nuclear Regulatory Commission, Office of Nuclear Regulatory Research (RES), Rockville, MD, 2004**

16. **NUREG/CR-6850, EPRI 1019259**, Fire Probabilistic Risk Assessment Methods Enhancements. U.S. Nuclear Regulatory Commission, Office of Nuclear Regulatory

Research (RES), Rockville, MD, 2010, and Electric Power Research Institute (EPRI), Palo Alto, CA.

17. **NUREG/CR-6905, NIST SP 1013-1**, Report of Experimental Results for the International Fire Model Benchmarking and Validation Exercise # 3. Nuclear Regulatory Commission, Office of Nuclear Regulatory Research (RES), Rockville, MD, 2004

18. **Ventilation effects on compartment fire characterization**. M. J. Peatross and C. L. Beyler. Hughes Associates, inc, USA

19. **ISIS 3.0.1, IRSN**, web page: https://gforge.irsn.fr/gf/project/isis.

20. **PRISME SOURCE - Tests in DIVA -Test Report**, H. PRETREL. DPAM/SEREA-2005-052 - PRISME-2006-03. Revision 1

21. **CFAST 6.2.0, NIST, Web page: cfast.nist.gov/**

22. **NFPA 13**: standard for the installation of sprinkler systems. NFPA, 2007.

23. **Test report U 96 055**, Institute for Construction Materials, Massive Construction and Fire Protection, Technical University of Braunschweig. 1996.

24. **Experimental Studies on Thermal and Smoke Blockage by water Curtains**. W.K Chow, Elaine Y. L. Ma. American Institute of Aeronautics and Astronautics. San Francisco, California, 2006.

25. **The use of water mist in attenuating thermal radiation from pool fire**. Setareh Ebraimzadeh. Master thesis, University of Malaya. 2009

26. **Analysis of wall-function approaches using two-equation turbulence models**. X. albets-Chico, C.D.Pérez-Segarra, A. Oliva, J.Bredberg. International Journal of Heat and Mass Transfer 51 (2008).

27. **NUREG-1924**, Electric Raceway Fire Barrier Systems in U.S. Nuclear Power Plants. Nuclear Regulatory Commission, Office of Nuclear Regulatory Research (RES), Rockville, MD, 2010.